Bioorganic Chemistry 116 (2021) 105297

Contents lists available at ScienceDirect

Bioorganic Chemistry

journal homepage: www.elsevier.com/locate/bioorg

A new class of cytotoxic agents targets tubulin and disrupts microtubule dynamics

Ayad A. Al-Hamashi [a,1], Radhika Koranne [b,1], Samkeliso Dlamini [a], Abdulateef Alqahtani [a], Endri Karaj [a], Maisha S. Rashid [b], Joseph R. Knoff [c], Matthew Dunworth [d], Mary Kay H. Pflum [c], Robert A. Casero Jr [d], Lalith Perera [e], William R. Taylor [b,*], L.M. Viranga Tillekeratne [a,*]

[a] Department of Medicinal and Biological Chemistry, College of Pharmacy and Pharmaceutical Sciences, The University of Toledo, 2801, W. Bancroft Street, Toledo, OH-43606, USA
[b] Department of Biological Sciences, College of Natural Sciences and Mathematics, The University of Toledo, 2801, W. Bancroft Street, Toledo, OH-43606, USA
[c] Department of Chemistry, Wayne State University, 5101 Cass Avenue, Detroit, MI 48202, USA
[d] The Sidney Kimmel Comprehensive Cancer Center, The Johns Hopkins University School of Medicine, Bunting/Blaustein Cancer Research Building 1 1650 Orleans Street - Room 551, Baltimore, MD 21231, USA
[e] Laboratory of Genome Integrity and Structural Biology, National Institute of Environmental Health Sciences, National Institutes of Health, Department of Health and Human Services, Research Triangle Park, NC 27709, USA

ARTICLE INFO

Keywords:
Antimitotic agents
Anticancer agents
Mitotic spindle
Chalcones
Mitotic arrest

ABSTRACT

Despite the advances in treatment strategies, cancer is still the second leading cause of death in the USA. A majority of the currently used cancer drugs have limitations in their clinical use due to poor selectivity, toxic side effects and multiple drug resistance, warranting the development of new anticancer drugs of different mechanisms of action. Here we describe the design, synthesis and initial biological evaluation of a new class of antimitotic agents that modulate tubulin polymerization. Structurally, these compounds are chalcone mimics containing a 1-(1H-imidazol-2-yl)ethan-1-one moiety, which was initially introduced to act as a metal-binding group and inhibit histone deacetylase enzymes. Although several analogues selectively inhibited purified HDAC8 with IC_{50} values in low micromolar range, tissue culture studies suggest that HDAC inhibition is not a major mechanism responsible for cytotoxicity. The compounds demonstrated cell growth inhibition with GI_{50} values of upper nanomolar to low micromolar potency with significant selectively for cancer over normal cells. Interestingly, several compounds arrested HeLaM cells in mitosis and seem to target tubulin to cause mitotic arrest. For example, when combined with inhibitors of Aurora B kinase, they led to dramatic disassembly of the mitotic spindle. In-vitro tubulin polymerization studies showed that the compounds reduced the rate of polymerization of microtubules during the elongation phase and lowered the amount of polymerized tubulin during the plateau phase. Finally, in silico docking studies identified binding of **IPE-7** to the colchicine site with similar affinity as the test compound D64131. These compounds represent a new antimitotic pharmacophore with limited HDAC inhibitory activity.

1. Introduction

Every year ~500,000 people die from cancer in the United States. [1] Despite significant advances in prevention, detection and treatment over the last few decades, the five-year survival rate of some cancers is still very low. [2] Since many cancers are only detected after metastasis has occurred, systemic treatments including small molecule chemotherapeutic agents are a main component of cancer treatment. [3] However, development of multiple drug resistance and undesirable side effects arising from off-target effects limit the clinical utility of the currently available cancer drugs. Cancer cells are characterized by high rates of proliferation; therefore, drugs that target various steps in the cell cycle are common in a therapeutic setting. Antimitotics, drugs that disrupt progression through mitosis, include a diversity of molecules currently in clinical use. Classical antimitotics are compounds that bind directly to tubulin to either stabilize polymerized microtubules or inhibit tubulin

* Corresponding authors.
E-mail addresses: william.tayor2@utoledo.edu (W.R. Taylor), ltillek@utnet.utoledo.edu (L.M.V. Tillekeratne).
[1] A.A.A (Design and synthesis) and RK (biological assay) contributed equally to this work.

https://doi.org/10.1016/j.bioorg.2021.105297
Received 16 July 2021; Received in revised form 3 August 2021; Accepted 17 August 2021
Available online 30 August 2021

polymerization. [4,5] Defects in the mitotic spindle induced by these compounds cause a prolonged mitotic arrest that triggers apoptotic cell death. [6,7] This mitotic arrest is caused by the mitotic checkpoint, a multilayer signaling pathway that delays anaphase until all chromosomes are properly attached to the spindle. [8,9] The clinical success of antimitotics like paclitaxel suggests that targeting mitosis is a viable approach to develop new anti-cancer drugs.

In this report, we describe the fortuitous discovery of a novel class of antimitotic compounds with selective toxicity towards a wide range of cancer cell lines while continuing our efforts to develop potent and selective HDAC inhibitors, [10]. This approach was motivated by the fact that clinically used HDAC inhibitors such as vorinostat (SAHA), romidepsin (FK228), [11,12] belinostat (PXD101), [13] and panobinostat [14] suffer from undesirable side effects, which can be attributed to off-target effects of the promiscuous hydroxamic acid metal-binding group shared by most of them. [15] Replacing the hydroxamic acid group with alternative metal-binding groups such as benzamides has produced promising results leading to more selective inhibitors [16,17]. The 1-(1H-imidazol-2-yl)ethan-1-one moiety was introduced as a metal-binding group for potential HDAC inhibitory effect. The zinc-ion binding ability of imidazole has been reported [18]. The ketone moiety was introduced to provide an additional coordinating site for metal chelation. Structurally, these compounds are chalcone mimics. Chalcones are privileged structure scaffolds in medicinal chemistry and it should be noted that many chalcone mimics with antimitotic activity have been reported [19–22].

Consistent with our original aim, the compounds were capable of inhibiting purified HDACs with some analogues showing selective inhibition of purified HDAC8 with IC_{50} values in low micromolar range. However, Western blot studies revealed that the acetylation of histone H3, tubulin and structural maintenance of chromosomes 3 (SMC3) protein was unchanged in HCT116 cells treated with the compounds. Despite this limited HDACi activity in cells, these new compounds showed cell growth inhibitory activity with single digit micromolar GI_{50} values in the National Cancer Institute (NCI) 60 human tumor cell line screen. Interestingly, several compounds arrested HeLaM cells in mitosis and seem to target tubulin to cause mitotic arrest. For example, when combined with inhibitors of Aurora B, our compounds display a striking ability to destabilize the mitotic spindle. In addition, these compounds reduce the rate of tubulin polymerization both in cells and of purified tubulin. Overall, these studies suggest that although the compounds possess limited in vitro HDAC inhibitory activity, their cytotoxicity is explained by disruption of microtubule dynamics leading to a lethal mitotic arrest.

2. Results and Discussion

The compounds synthesized are shown Table 1.

2.1. Chemistry

A general synthetic strategy as shown in the retrosynthetic analysis in Scheme 1 was used for the synthesis of all the analogues, except **IPE-27**. They can be synthesized by aldol reaction of *N*-tosyl imidazole ketone **1** with aldehydes **2**. The aldehydes **2** can be obtained by Heck coupling of bromoester **7** with styrene **8**, followed by ester hydrolysis, amide formation, and oxidative cleavage of olefinic double bond of the amide **4**. The aldehyde **23** can also be obtained by direct palladium-catalyzed carbonylation of the bromoester **7,** followed by ester hydrolysis and amide formation. However, this reaction gave low yields.

The imidazole ketone **1** was prepared as shown in Scheme 2A. 1-*H*-imidazole-2-caroxaldehyde **9** was tosylated to produce aldehyde **3**, which was then treated with MeMgBr, followed by Dess-Martin periodinane oxidation to afford the *N*-tosyl imidazole ketone **1** (Scheme 2A).

The synthesis of the aldehydes **2** began with palladium catalyzed Heck coupling between the bromoester **7** and styrene **8** to produce the

Table 1
Analogues synthesized and their effect on percentage mean growth of NCI sixty human tumor cell line panel at 10 μM.

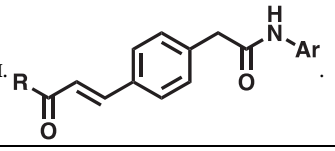

Compound	R	Ar	Mean % growth at 10 μM
IPE-1			45.33
IPE-2			70.02
IPE-3		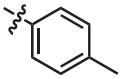	41.34
IPE-4		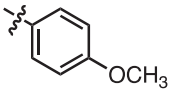	66.84
IPE-5		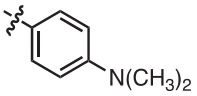	52.06
IPE-6		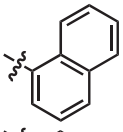	76.31
IPE-7		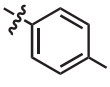	27.48
IPE-8		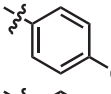	21.10
IPE-9		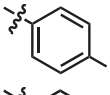	17.88
IPE-10		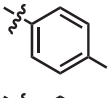	64.07
IPE-11		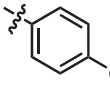	23.48
IPE-12		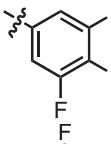	51.10
IPE-13		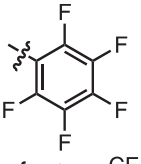	91.77
IPE-14		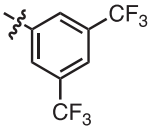	77.21
IPE-15		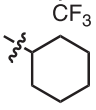	57.67
IPE-16			15.90

(*continued on next page*)

Table 1 (*continued*)

Compound	R	Ar	Mean % growth at 10 μM
IPE-17			19.33
IPE-18		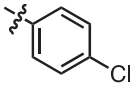	19.91
IPE-19		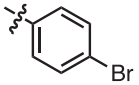	33.11
IPE-20	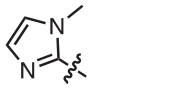	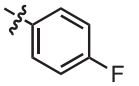	54.69
IPE-21	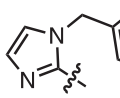	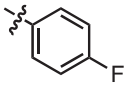	29.20
IPE-22	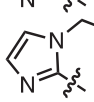	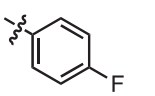	−18.79
IPE-23	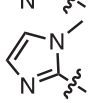	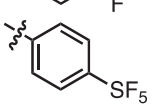	12.97
IPE-24	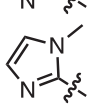	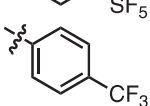	22.66
IPE-25	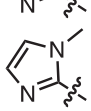	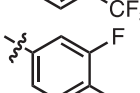	61.43
IPE-26		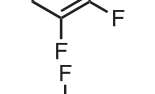	68.98
IPE-27		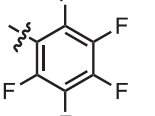	53.49
IPE-28	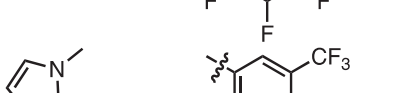		92.81
IPE-29	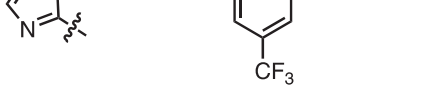		98.67
TPE-30			84.29
PPE-31		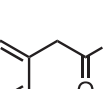	99.14
HPE-32			85.87

Table 1 (*continued*)

Compound	R	Ar	Mean % growth at 10 μM
HPE-33	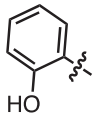		91.98
HPE-34	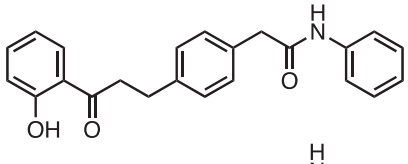		89.56
HPE-35	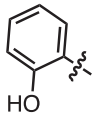	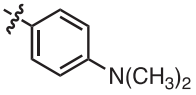	85.87
HPE-36	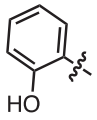	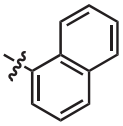	96.15

ester **11**, which was saponified and subjected to EDC coupling with different amines to produce the amides **4**. They were subjected to oxidative cleavage using osmium tetroxide and sodium periodate to produce aldehydes **2** (Scheme 2B).

With both aldehydes **2** and ketone **1** in hand, aldol coupling and tosyl group removal were carried out in one step by heating with piperidine to produce the final products **IPE-1** -**IPE-14** in 50–70% yield. Palladium-catalyzed hydrogenation of **IPE-1** gave **IPE-28** (Scheme 2C). Cyclopropanation of the olefinic double bond of **IPE-18** afforded the cyclopropyl derivative **IPE-29**. The *N*-alkyl imidazole derivatives were made by reacting the non-alkylated imidazole analogues with the corresponding alkyl halide in the presence of potassium carbonate in DMF to produce **IPE-15**–**26** (Scheme 2C). Some of the *N*-methyl imidazole analogues were prepared using *N*-methylimidazole ketone instead of the *N*-tosyl imidazole ketone **1** in the aldol reaction. *N*-methyl imidazole ketone was prepared as reported earlier.[23]

An alternative approach was used in the synthesis of analogue **IPE-27** (Scheme 3). Commercially available 4-hydroxymethylphenylacetic acid **12** was converted to the amide **13** using DEPBT as the coupling agent. It was oxidized to the aldehyde **14** with Dess-Martin periodinane and then subjected to aldol coupling as before to obtain **IPE-27**.

To determine the importance of the imidazole moiety as the ZBG, we replaced it with other isosteric aromatic and heteroaromatic rings, thiazole, phenol and pyrimidine. The thiazole and pyrimidine analogues were synthesized by aldol coupling of the aldehyde **2** with the corresponding thiazole and pyrimidine ketones as in Scheme 1. The phenol analogues were synthesized by a slightly different approach as shown in Scheme 4. Palladium-catalyzed carbonylation of ethyl 2-(4-bromophenyl)-acetate **7** using paraformaldehyde produced the aldehyde **15**. It was subjected to base-initiated aldol reaction with 2-hydroxy acetophenone **16**, followed by acidification, to afford a mixture of the α,β-unsaturated carboxylic acid **17a** and the β-hydroxyketone **17b** (Scheme 4), which were separated. Amide coupling of these acids with the respective aromatic amines **19a-c** in the presence of EDC produced the amides **HPE-32**, **HPE-35**, **HPE-36** and **HPE-34**. Palladium-catalyzed hydrogenation of **HPE-32** gave **HPE-33**.

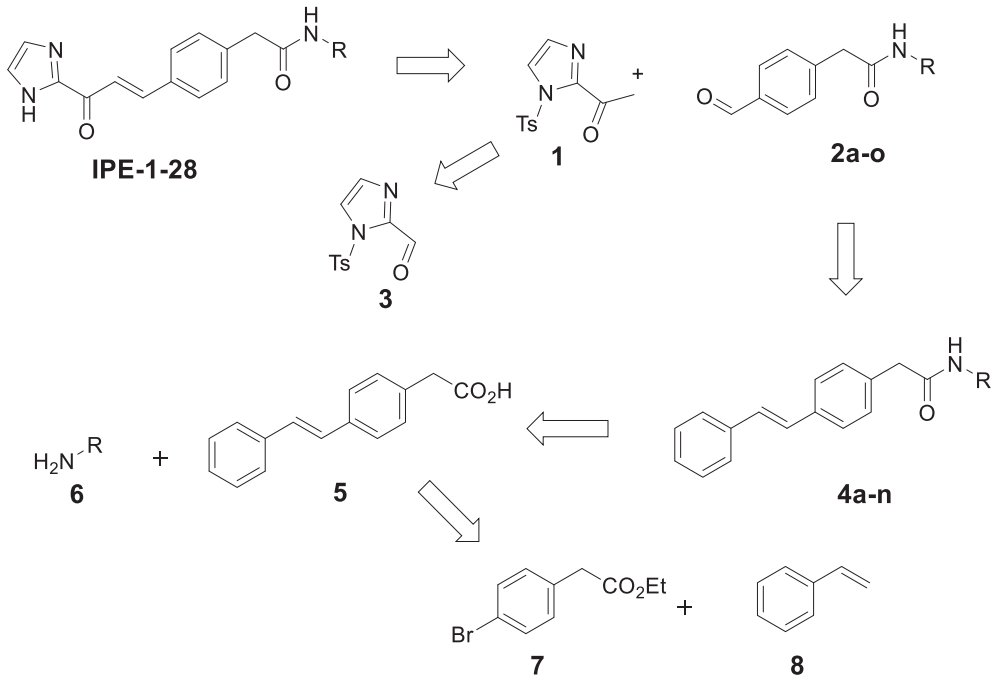

Scheme 1. Retrosynthesis of **IPE** analogues.

2.2. Biology

Preliminary screening for antiproliferative activity of several selected analogues on the human adenocarcinoma cell line HCT 116 was carried out by the MTS reduction assay using SAHA as the positive control. The cells were treated with different concentrations of the test compounds ranging from 0.01 μM to 100 μM for 96 h. All the compounds inhibited the growth of HCT 116 cells with GI_{50} values in single digit micromolar range (**IPE-3:** 6.85 μM**, IPE-7:** 6.95 μM, **IPE-8:** 5.14 μM, **IPE-16:** 5.91 μM, **IPE-19:** 6.56 μM) (Fig. 1)

In order to assess the potential HDAC enzyme inhibition activity, selected analogues were tested at 100 μM against purified HDAC isoforms (Figure S1). This analysis included all of class I (HDAC1, 2, 3, and 8) and the well-studied class IIb protein, HDAC6. Of the compounds tested, **IPE-25** was the most potent against all isoforms, with each isoform showing less than 20% activity remaining (Figure S1). **IPE-7** and **IPE-8** also showed similar pan inhibition, but with less potency, displaying 20–80% activity remaining (Figure S1). Interestingly, compounds **IPE-24**, **IPE-26**, **IPE-29**, **IPE-27**, and **IPE-22** inhibited HDAC8 with 20–60% activity remaining, but with little effect on the other isoforms, suggesting possible HDAC8 selectivity when tested against the purified enzymes (Figure S1). Finally, compounds **IPE-26** and **IPE-18** showed only modest HDAC inhibition.

Next, the dose dependence (IC_{50}) of HDAC inhibition was determined for several analogues. **IPE-25** and **IPE-7** were assessed against all isoforms (Table S3/Figure S3 and Table S4/Figure S4, respectively), given the potency in the preliminary screen. In addition, **IPE-22, IPE-24**, **IPE-26**, **IPE-27**, and **IPE-29** were tested only against HDAC8 (Table S2 and Figure S2), given the potency observed at 100 μM. The FDA-approved HDAC inhibitor SAHA (Vorinostat) was also tested for comparison. **IPE-25** displayed low micromolar inhibition against all isoforms, consistent with pan inhibition (Table 2). The remaining inhibitors tested against HDAC8 also showed low micromolar potency. Given the poor $>$ 200 μM potency against the other HDAC isoforms, the compounds showed a range of 13–67-fold selectivity for HDAC8 compared to the other isoforms. The most potent and HDAC8-selective compound was **IPE-22**, which had at least a 67-fold selectivity towards HDAC8 with an IC_{50} of 3.0 $\pm$ 0.2 μM (Table 2). The dose dependence data showed that most compounds displayed HDAC8-selectivity, with **IPE-25** and **IPE-7** distinguishing themselves as pan HDAC inhibitors in in vitro studies using purified enzymes.

2.3. HDAC inhibition in cells

Most HDACs exist in multimolecular complexes in cells; effectiveness of HDACi against purified enzymes cannot always be extrapolated to behavior in cells. Therefore, colorectal cancer cells HCT116 were treated with selected analogues **IPE-7**, **IPE-16**, and **IPE-19** for 24 h, followed by Western blotting to assess histone H3 acetylation and tubulin acetylation as a measure of cellular HDAC activity. Surprisingly, no increase in global histone acetylation or tubulin acetylation was observed in treated cells exposed to any of the compounds at the highest concentration of 25 μM (Fig. 2a). In contrast, global acetylation of histone H3 and tubulin was dramatically increased in cells exposed to the HDAC inhibitors SAHA or MS275. This result was particularly surprising with **IPE-7** which, by inhibiting HDAC1, 2 and 3 (Table 2), would be expected to increase histone H3 acetylation in cells.

Several of the compounds selectively inhibited purified HDAC8 (Table S2). Some studies suggest that HDAC8 does not deacetylate histone H3 or tubulin [24] and although this might explain the reason for not observing changes in these substrates, it is also possible that the compounds have no HDAC 8 inhibitory activity in cellular environment where HDAC enzymes exist in multimolecular complexes. Next, we applied Western blotting to measure acetylation of SMC3, a protein reported to be an HDAC8 substrate.[25] We observed an increase in SMC3 acetylation in cells exposed to PCI34051, an HDAC8 selective inhibitor, but only after treatment with high concentrations (25 μM). **IPE-7** and **IPE-8** had no effect on SMC3 acetylation (Fig. 2b; our unpublished data) suggesting that HCAC8 is not a major target in cells. Next, we generated HDAC8-null HCT116 cells using CRISPR-Cas9-mediated genome editing (Fig. 3a). In cytotoxicity assays, HDAC8-null cells were slightly more resistant to **IPE-7** and PCI34051 compared to control HCT116 cells (Fig. 3b). On the other hand, both parental and HDAC8-null cells were killed by 10 μM **IPE-7** (Fig. 3b). Taken together, these results suggest that **IPE-7** and related compounds have only limited activity against HDACs in cells and that additional targets must contribute to cytotoxicity.

Cell biological analysis suggested that HDACs were likely not a major

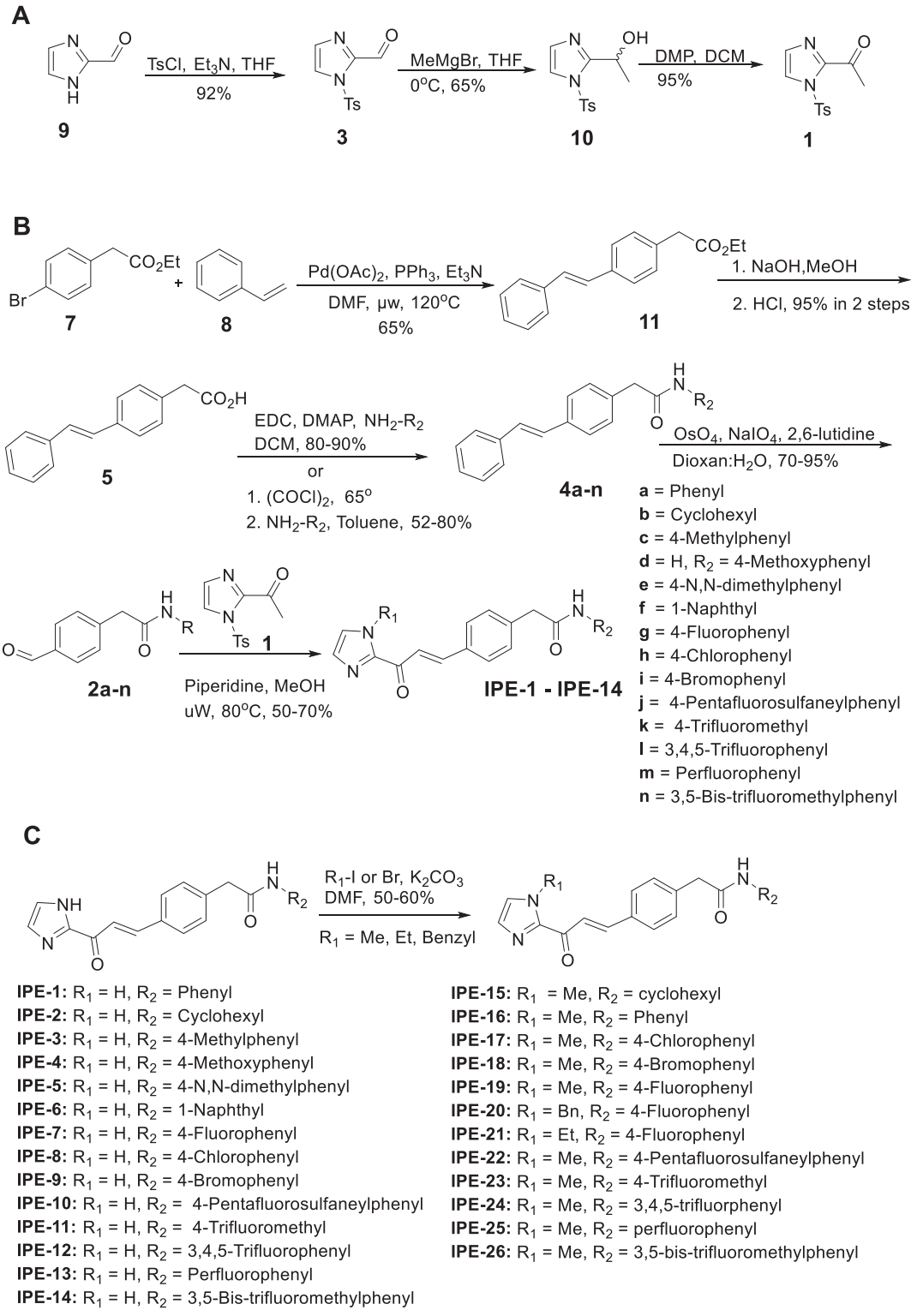

IPE-1: R_1 = H, R_2 = Phenyl
IPE-2: R_1 = H, R_2 = Cyclohexyl
IPE-3: R_1 = H, R_2 = 4-Methylphenyl
IPE-4: R_1 = H, R_2 = 4-Methoxyphenyl
IPE-5: R_1 = H, R_2 = 4-N,N-dimethylphenyl
IPE-6: R_1 = H, R_2 = 1-Naphthyl
IPE-7: R_1 = H, R_2 = 4-Fluorophenyl
IPE-8: R_1 = H, R_2 = 4-Chlorophenyl
IPE-9: R_1 = H, R_2 = 4-Bromophenyl
IPE-10: R_1 = H, R_2 = 4-Pentafluorosulfaneylphenyl
IPE-11: R_1 = H, R_2 = 4-Trifluoromethyl
IPE-12: R_1 = H, R_2 = 3,4,5-Trifluorophenyl
IPE-13: R_1 = H, R_2 = Perfluorophenyl
IPE-14: R_1 = H, R_2 = 3,5-Bis-trifluoromethylphenyl
IPE-15: R_1 = Me, R_2 = cyclohexyl
IPE-16: R_1 = Me, R_2 = Phenyl
IPE-17: R_1 = Me, R_2 = 4-Chlorophenyl
IPE-18: R_1 = Me, R_2 = 4-Bromophenyl
IPE-19: R_1 = Me, R_2 = 4-Fluorophenyl
IPE-20: R_1 = Bn, R_2 = 4-Fluorophenyl
IPE-21: R_1 = Et, R_2 = 4-Fluorophenyl
IPE-22: R_1 = Me, R_2 = 4-Pentafluorosulfaneylphenyl
IPE-23: R_1 = Me, R_2 = 4-Trifluoromethyl
IPE-24: R_1 = Me, R_2 = 3,4,5-trifluorphenyl
IPE-25: R_1 = Me, R_2 = perfluorophenyl
IPE-26: R_1 = Me, R_2 = 3,5-bis-trifluoromethylphenyl

10

Scheme 2. General approach for **IPE** synthesis.

target of the compounds we designed. However, these compounds were capable of killing a variety of cancer cells. Furthermore, normal RPE cells were less sensitive to killing by these compounds than cancer cells such as HelaM (Fig. 4). Cell survival was expressed as a percentage of the corresponding DMSO treated cells. In the case of both **IPE-7** and **IPE-22**, HeLaM cells had 2–3 fold lower IC_{50} compared to RPE cells, indicating the selectivity of these analogues for transformed cancer cells. Therefore, we expanded our toxicity studies and determined detailed SAR.

All the synthesized compounds were screened for cancer cell growth inhibitory activity in the NCI sixty human tumor cell line panel. The compounds were first tested at a single dose of 10 μM.[26] The mean growth percent observed at 10 μM for each analogue is shown in Table 1

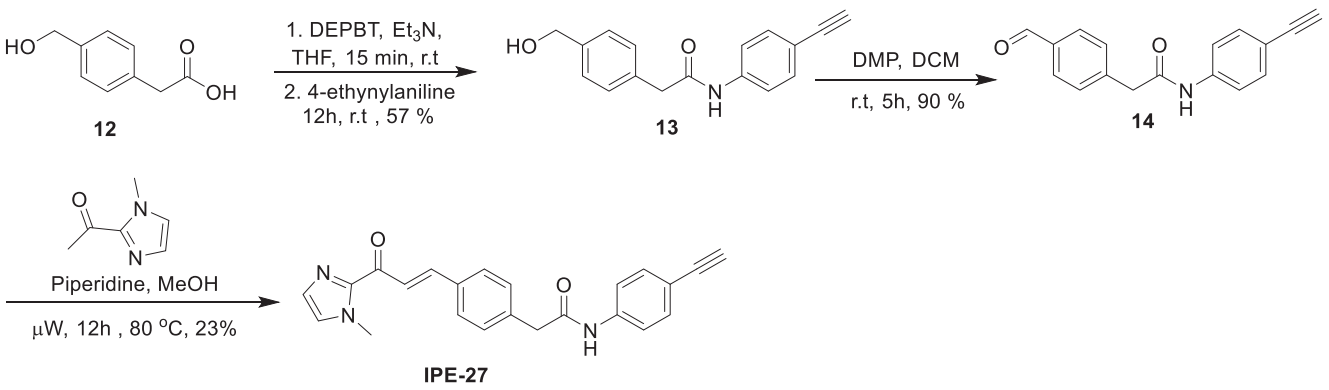

Scheme 3. Synthesis of **IPE-27**.

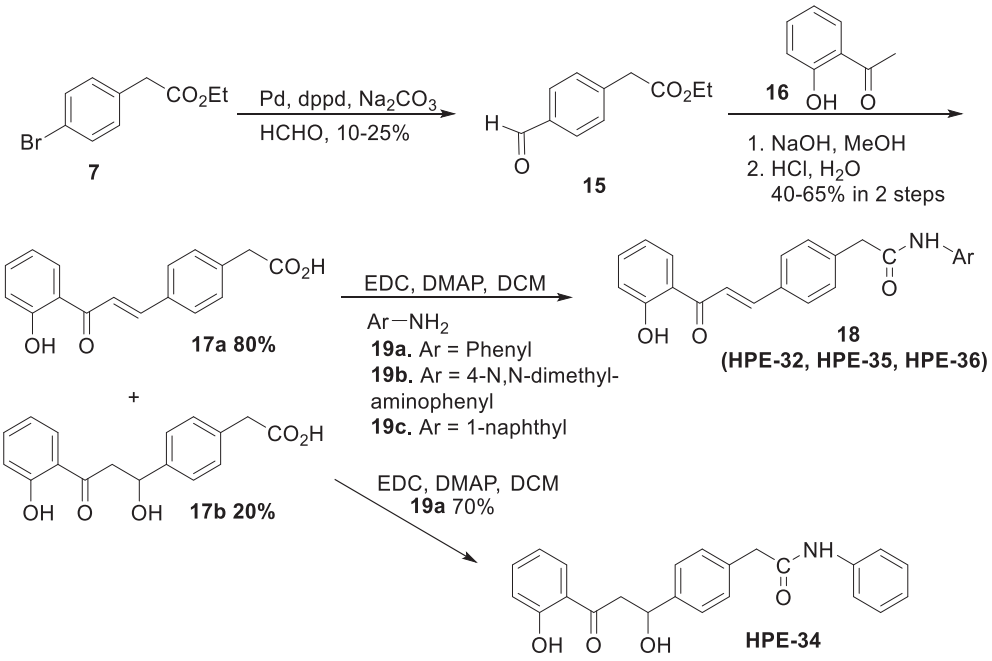

Scheme 4. Synthesis of **HPE-32 – HPE-36**.

and the growth percent of each cell line is shown in Figure S5. In general, most of the analogues with aromatic cap groups were found to show significant growth inhibition activity. The nature of the cap group seemed to have a profound effect on activity. Analogue **IPE-1** with an unsubstituted aniline moiety as cap group showed over 50% growth inhibition, whereas the corresponding cyclohexylamine analogue (**IPE-2**) was almost completely inactive. Analogue **IPE-6** with a bulkier naphthylamine moiety too was less active than the aniline analogue. What was most noteworthy from the SAR study was that the presence of electron donating groups such as methyl (**IPE-3**), methoxy (**IPE-4**) and N,*N*-dimethyl (**IPE-5**) at the 4- position of the aniline moiety did not have a significant effect on activity, whereas electron withdrawing and hydrophobic groups such as, fluorine (**IPE-7**), chlorine (**IPE-8**), bromine (**IPE-9**) and trifluoromethyl (**IPE-11**) at the para position were found to increase activity significantly. However, fluorine substituents at 3,4,5 positions did not have a significant effect on activity in the unsubstituted imidazole analogue **IPE-12** but were found to increase activity in the corresponding *N*-methylimidazole analogue **IPE-24**. Similarly, the pentafluoro analogue **IPE-13** was less active than the unsubstituted aniline analogue **IPE-1**, but the corresponding *N*-methyl analogue **IPE-22** was found to cause 100% growth inhibition at 10 μM. Trifluoromethyl substituents at 3 and 5-positions of the phenyl ring, unlike in the corresponding 4-substituted analogue, had a negative effect on activity in both unsubstituted imidazole and *N*-methylimidazole analogues. *N*-alkylation of the imidazole ring had no significant effect on activity. In general, the compounds seemed to have a higher growth inhibitory effect on leukemia cell lines, and most of colonic and CNS cancers. On the other hand, they showed weak growth inhibition activity on melanoma and renal cancer cell lines. The presence of an olefinic double bond in the linker was found to be crucial for activity as saturated analogue **IPE-28** and the cyclopropyl derivative **IPE-29** were virtually inactive. The presence of an alkynyl substituent at 4 position of the phenyl cap group as in **IPE-27** made no contribution to activity. The presence of an imidazole ring was found to be essential as replacing it with thiazole (**TPE-30**), pyrimidine (**PPE-32**) and phenol (**HPE-34 – HPE-38**) groups gave inactive analogues.

Selected analogues (**IPE-7 – IPE-9**, **IPE-11, IPE-12, IPE-16, IPE-17, IPE-19**, and **IPE-21 – IPE-24)** were further tested in the NCI dose response assay (Fig. 5). Most of the compounds inhibited the growth of multiple cell lines in a single digit micromolar range GI_{50} values. Interestingly, most of the leukemia cell lines and some of the colon cancer cell lines in general appeared to be more sensitive to these compounds. Most strikingly, analogues **IPE-22** and **IPE-24** inhibited the growth of all leukemia cell lines with upper nanomolar GI_{50} values,

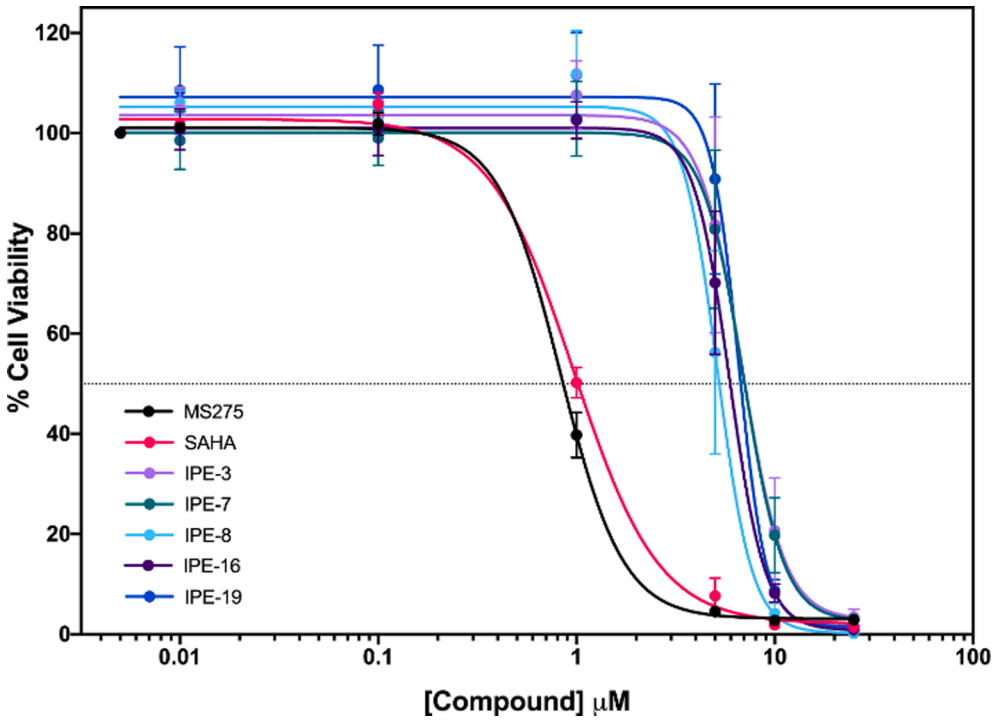

Fig. 1. Growth inhibition of HCT116 colorectal carcinoma cells treated with selected representative analogues. Cells were treated for 96 h with increasing concentrations of compounds from 10 nM to 100 μM. Data points represent the average of three biological replicates with error bars indicating the SEM. Curves were fit to the log(compound) vs. response and were calculated using a variable Hill slope model.

Table 2
IC_{50} values for SAHA and synthesized compounds.

Compound ID	IC_{50} Value (μM)*				
	HDAC1	HDAC2	HDAC3	HDAC6	HDAC8
SAHA	0.033 ± 0.001	0.096 ± 0.01	0.020 ± 0.001	0.033 ± 0.003	0.54 ± 0.01
IPE-7	1.8 ± 0.1	2.1 ± 0.2	1.8 ± 0.1	2.0 ± 0.2	1.4 ± 0.1
IPE-8	>100	>100	N.D.	>100	N.D.
IPE-18	>100	>100	>100	>100	>100
IPE-22	>200	>200	>200	>200	3.0 ± 0.2
IPE-24	>200	>200	>200	>200	13 ± 1
IPE-25	12 ± 1	8.9 ± 0.6	16 ± 1.0	8.6 ± 4.9	9.0 ± 0.5
IPE-26	>200	>100	>200	>100	15 ± 1
IPE-27	>100	>100	>100	>100	12 ± 1
IPE-29	>200	>200	>200	>200	8.5 ± 0.9

* >100 or > 200 indicates>50% HDAC activity was observed at 100 or 200 μM concentrations. Recombinant HDAC isoforms were pre-incubated with serial dilutions of the inhibitors before deacetylase activity was monitored by chemiluminescence signal intensity. The activity after inhibition was then plotted and fit to a sigmoidal curve to calculate the IC_{50} values. Higher concentrations were not tested due to solubility issues. N.D. = Not Determined

while analogue **IPE-9** inhibited the growth of all but two of the cell lines each in the leukemia and colon cancer cell line panels with submicromolar GI_{50} values. As the compounds have cell growth inhibitory activity, but limited HDAC inhibitory activity, it is likely that cells are killed by binding to additional higher affinity target(s).

2.4. Antimitotic effects of IPE compounds

We checked effects of IPEs on asynchronously growing HeLa cells by phase contrast time lapse microscopy. Images were taken at 12 min interval. Control/ DMSO treated cells start rounding up as they enter mitosis. They then divide into two daughter cells within an hour (pointed by white arrows in top panel of Fig. 6a). Strikingly, HeLaM cells exposed to **IPE** analogues showed a strong mitotic arrest lasting for 10–12 h (indicated by white arrows in bottom panel in Fig. 6a and supplemental movies A and B).

Mitosis is a complex process controlled by a feedback mechanism called the spindle assembly checkpoint (SAC). The SAC arrests cells in mitosis until all chromosomes are bi-oriented on metaphase plate. The molecular mechanism of the SAC involves activity of mitotic checkpoint complex (MCC) composed of BubR1, cdc20, Bub3 and Mad2. This complex prevents the action of the anaphase promoting complex/ cyclosome (APC/C), an E3 ubiquitin ligase that must be active for cells to exit mitosis. MCC is generated when defects occur in the attachment of chromosomes to spindle microtubules. Therefore, drugs like taxol that disrupt microtubule dynamics lead to the accumulation of MCC, inhibition of APC/C and failure to exit mitosis. Furthermore, the ensuing prolonged mitotic block that occurs upon alterations in spindle microtubule dynamics can activate apoptotic cell death. Thus, as long as the SAC is active the cell will not proceed to anaphase.[8] We observed that after a prolonged mitotic arrest induced by IPEs, the cells either underwent apoptosis or exited without cytokinesis. Previous studies have linked aberrant mitosis to inhibition of HDACs..[27–30] We checked if other commercially available pan- or specific HDAC inhibitors (i.e. inhibitors of metal binding enzymes) would cause mitotic arrest. PCI34051 and SAHA showed lengthened mitoses of 1.5 h and 3 h, respectively, but this mitotic arrest was not to the same extent as caused by **IPE** analogues. Other commercially available pan- or specific HDAC inhibitors did not cause such arrest (Fig. 6b). We did not observe any severe effect on interphase cells by phase contrast microscopy. Next, we observed the effects of the compounds on cell cycle distribution of HeLaM cells by measuring DNA content by flow cytometry. Asynchronous HeLaM cells were treated with DMSO, SAHA, Tubastatin A or **IPE** analogues and then harvested for flow-cytometry analysis at 24 h, 48 h or 72 h post treatment. SAHA caused an increase in the subG1 population compared to DMSO (72 hr: 37% vs 14%, respectively), indicating induction of cell death. subG1 cells were increased even more in cells exposed to either **IPE-7** or **IPE-8** (72 hr: 58% and 59% respectively)

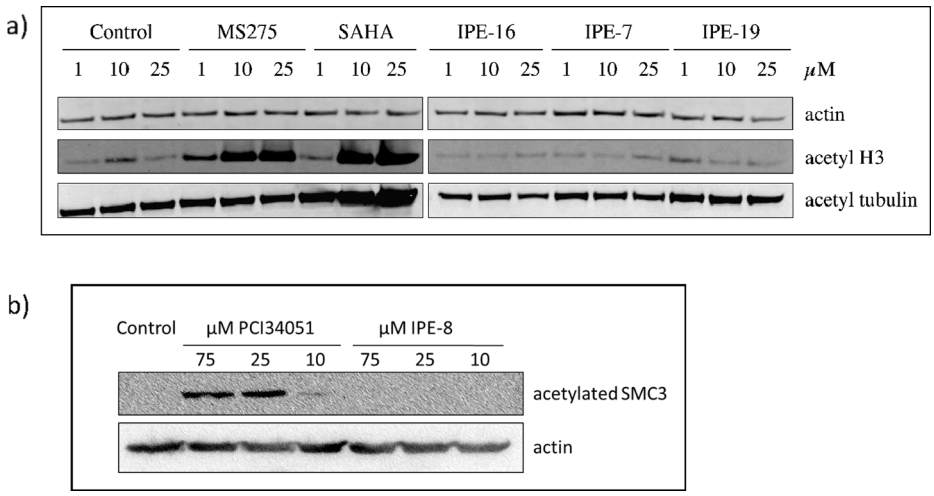

Fig. 2. Western blot analysis a) Levels of acetyl-histone H3 and acetyl-tubulin were analyzed in HCT116 cells treated with **IPE-7**, **IPE-16**, and **IPE-19** at 1, 10, and 25 μM. Cells were treated for 24 hrs, after which total cellular proteins were isolated and analysis was completed. No increase in global histone H3 and tubulin acetylation was observed. b) Acetylation of SMC3 was analyzed in HeLaM cells after overnight treatment with **IPE-8** or PCI34051.

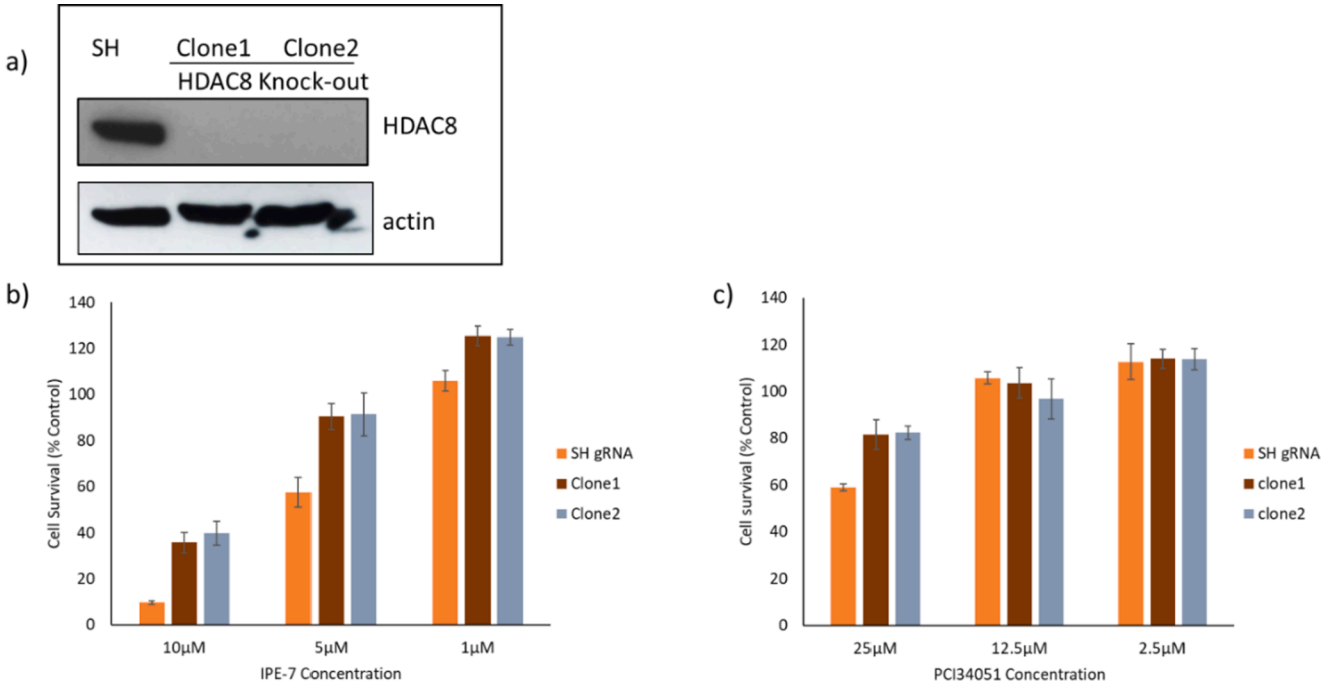

Fig. 3. Effect of HDAC8 knockout on **IPE-7** sensitivity. a) HDC8 was knocked out in HCT116 using CRISPR-Cas9, b) and c) the cells were treated with **IPE-7** or PCI34051. Knocking out HDAC8 rescued **IPE-7** mediated cell death.

(Fig. 6c). Tubastatin A had little effect on subG1 under these conditions. These experiments provide additional evidence for the toxic effects of these novel compounds. Next, we excluded subG1 cells and applied modeling software to estimate cell cycle distribution of live cells. **IPE-7** and **IPE-8** induced accumulation of cells with a G2/M content of DNA, an effect which was most evident at 48 h after treatment (Fig. 6c). Whereas 10% of DMSO, 8.2% of SAHA, and 12% of Tubastatin-treated cells were in G2/M, we observed 36% of **IPE-7** and 33% of **IPE-8**-treated cells in G2/M. This redistribution into G2/M by flow cytometry corroborates our earlier observations showing mitotic arrest upon **IPE** treatment. Interestingly post G2(polyploid) population almost doubled after treatment with **IPE**s. Increase in post G2 population indicates that the cells that escaped mitosis without division reentered the cell-cycle.

Compounds that block cells in mitosis often do so by triggering the SAC, a feedback mechanism that ensures that mitosis is completed only after all chromosomes have aligned on the metaphase plate. For example, taxanes directly disrupt spindle function, triggering SAC-dependent mitotic arrest. Aurora B, a part of chromosome passenger complex (CPC), is required for chromosome bi-orientation and their correct segregation. Along with Aurora B, CPC consists of INCENP, Borealin and Survivin. The CPC accumulates at the centromeres where it destabilizes erroneous kinetochore-microtubule attachments allowing accurate bipolar attachment of chromosomes to spindle. By destabilizing incorrect attachments Aurora B keeps the SAC active until all chromosomes align at metaphase plate. [9] To test whether IPEs trigger the SAC to cause mitotic arrest, we used an inhibitor of Aurora B (ZM447439) kinase. ZM447439 significantly reduced the mitotic arrest caused by exposure to **IPE.** To confirm these results we also used an inhibitor of

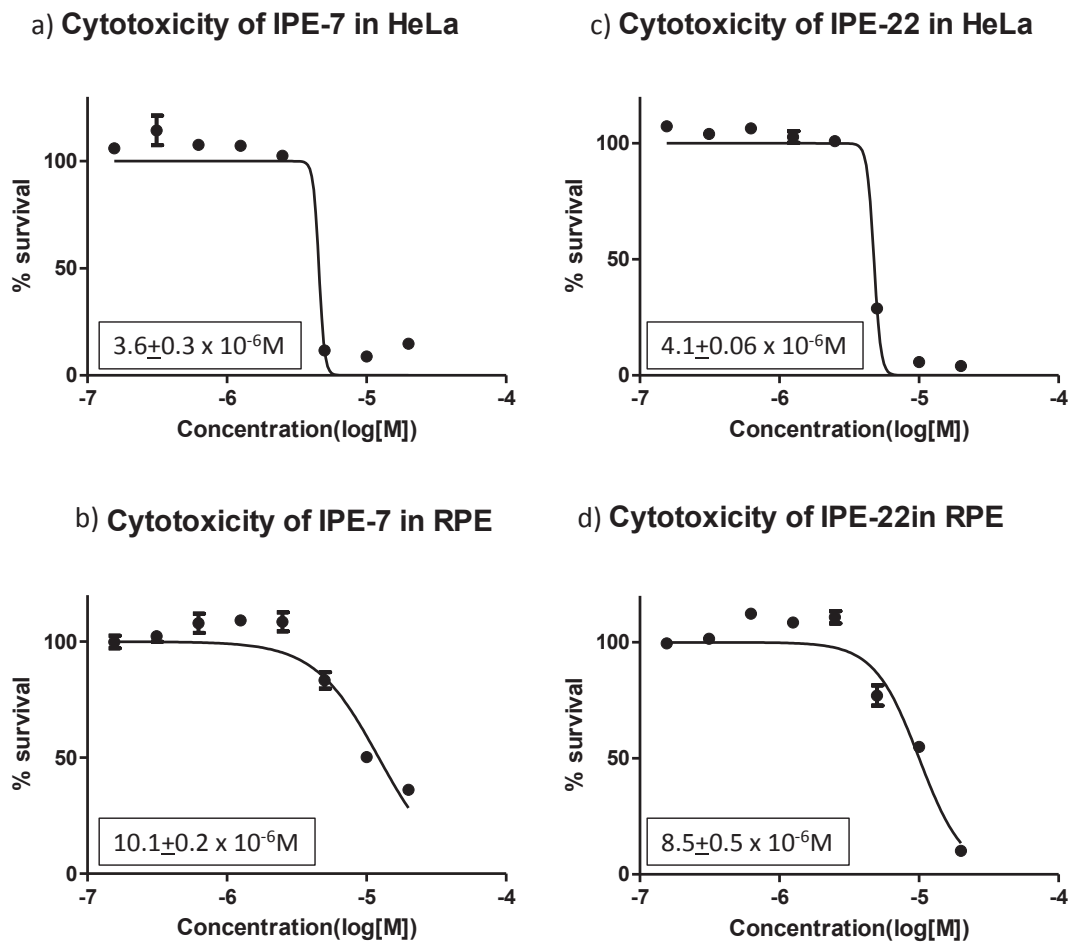

Fig. 4. Cytotoxicity of **IPE-7** and **IPE-22** was checked in malignant transformed HeLaM (a and c) and RPE (b and d) cells. Both compounds were at-least 2-fold more cytotoxic to HeLaM cells as compared to normal RPE cells. IC50s are shown in the inset.

Mps1 (reversine). Mps1 is a kinase that activates Aurora B and thus, also control the SAC. [31] Reversine also overrode the SAC suggesting that **IPE**s do activate the SAC (Fig. 7). A known spindle toxin, paclitaxel, was used as a positive control in this experiment.

Since **IPE** compounds triggered the SAC, we tested whether they affected the overall morphology of the mitotic spindle. Single treatment with several of the analogues at 10 μM had no major effect on spindle morphology (our unpublished data). However, when combined with ZM447439, we observed dramatic reorganization of the spindle. For these experiments, cells were treated with the compounds for 30 min followed by treatment with MG132 (20 μM), a proteasome inhibitor that prevents mitotic exit. Next, ZM447439 (2.5 μM) was added and immunofluorescence with antibodies to tubulin used to assess the mitotic spindle. Upon initial examination, combining the compounds with ZM447439 led to a disorganized mass of microtubules that we call "spindle collapse" (examples shown in Fig. 8). To investigate this phenomenon, mitotic cell phenotypes were quantified in a blinded manner and the spindles were categorized into 4 phenotypes: normal bipolar, monopolar, multipolar and collapsed spindles. At-least 100 mitotic cells were counted for each treatment. **IPEs** were examined in parallel to well characterized HDAC inhibitors Tubastatin A, SAHA and the HDAC8 inhibitor PCI34051.

Upon treatment with **IPE** analogues, HDACi, or ZM447439 alone did not induce monopolar or multipolar spindle or spindle collapse with the majority of cells having normal bipolar spindles as in DMSO treated cells. However, co-treatment of **IPE** and ZM447439 caused spindle collapse (3% in DMSO + MG132 + ZM447439 vs 97% in **IPE-7** + MG132 + ZM447439). Individual microtubules disappeared and only clumps of tubulin with scattered chromosomes could be seen in the cytoplasm, suggesting that co-treatment with compound and ZM abolished spindle structure and function. Representative images of these aberrant spindles are shown in Fig. 8c and Supplemental Movies C and D. This phenotype was reproduced with other analogues, viz**. IPE-16** and **IPE-22**. Data for **IPE-7** is shown in all 3 graphs in Fig. 8, and for **IPE-8** and **IPE-22** in graphs 1 and graph 3, respectively. Surprisingly, combining either Tubastatin A, SAHA or PCI34051 with ZM447439 did not produce the same aberrant spindle as that of **IPE** + ZM447439 (Fig. 8). Combining the compounds with Hesperidin also induced spindle collapse suggesting that the Aurora B paralogue is more important in this response (Fig. 8 Graph 3).

The spindle collapse morphology could be explained by depolymerization of microtubules in the presence of both **IPE** and Aurora inhibitors However, this could not be observed in static images from fixed cells. To address this idea, we observed tubulin dynamics in live cells by time-lapse fluorescence microscopy. For this purpose, we generated a HeLaM cell line expressing fluorescently tagged α-tubulin. As in the previous experiment, cells were treated with DMSO or analogues, followed by MG132 in 30 min. Thirty min after MG132, ZM447439 was added and images were taken every 5 min on SP8 Leica confocal microscope. As expected, control (DMSO + MG132) or analogue + MG132 treated cells showed normal bipolar spindles throughout the duration of imaging. However, cells treated with analogue + MG132 + ZM447439 showed rapid disappearance of spindle microtubules within an hour of Aurora B inhibition (Fig. 9) and Supplemental Movies E,F and G), explaining the "collapse" morphology observed earlier.

Aurora B regulates microtubule dynamic via its effects on the kinesin

Cancer Panel	Cell Line	IPE-7	IPE-8	IPE-9	IPE-11	IPE-12	IPE-16	IPE-17	IPE-19	IPE-21	IPE-22	IPE-23	IPE-24
Leukemia	CCRF-CEM	1.68	1.1	0.76	1.55	2.8	2.37	1.5	2	4.34	0.54	0.66	ND
	HL-60(TB)	1.66	3.8	2.78	2	4.3	1.57	4.8	1.6	3.18	0.62	1.8	0.71
	K-562	1.3	ND	0.745	1.2	2.3	1.07	ND	0.82	2.06	0.55	0.61	0.8
	MOLT-4	5.74	1.8	4	2.3	4.8	4.3	1.7	2.32	5.28	0.58	1.17	0.84
	RPMI-8226	1.27	0.86	7	0.78	0.66	1.45	0.96	1.02	2.28	0.52	0.87	0.8
	SR	1.11	0.8	0.6	0.84	2.2	1.16	0.8	0.51	0.53	0.53	0.72	0.86
Non-Small Cell Lung	A549/ATCC	6.94	6.9	6	6.4	4.1	6.6	11.5	6.43	4.16	3.3	3.8	1.6
	EKVX	7.46	5.7	4.6	5.6	8.4	6.28	15.6	5.5	3.59	2.8	3.1	3.5
	HOP-62	2.64	3.2	2.5	4.8	3.7	3.75	2.2	4.68	3.92	2.6	16.7	1.2
	HOP-92	9.11	5.7	6.7	4.9	3.5	6.63	25	4.51	3.32	1.1	2.4	2.6
	NCI-H226	9.85	7.5	3.3	6.1	4.8	8.59	7.4	8.57	3.61	3	4.2	3.4
	NCI-H23	1.91	3	2.2	3.4	3.8	3.24	2	3.04	4.25	2.4	3.28	2.1
	NCI-322M	3.35	4	3.7	4.7	4.3	2.57	4	2.07	3.49	2.1	2.6	1.8
	NCI-460	1.72	3.4	2.8	3.6	3.3	2.32	1.6	1.8	2.64	2.3	3	1.5
	NCI-H522	3.38	2.6	2.8	4.9	3.5	3.2	4.85	3.34	3.92	3.4	3.35	2.6
Colon	COLO 205	4.54	3	2.6	5.4	4	3.77	9.4	4.39	4.29	3	3.2	2.5
	HCC-2998	5.43	3.7	2.5	4	3.6	4.42	3.4	3.78	5.1	2.9	2.9	2.5
	HCT-116	1.89	0.85	0.85	0.69	2	1.68	1.3	0.99	1.84	0.82	2.4	1.2
	HCT15	1.15	0.88	0.78	1	2.4	1.25	1	1.29	1.93	0.88	1.4	1
	HT29	1.15	0.89	0.73	1.1	0.86	2.4	0.89	2.27	5.64	3.2	4	0.86
	KM12	2.1	1.3	0.86	1.1	2.8	3.39	1.5	1.62	3.06	2.1	3.2	1.6
	SW-620	1.43	1.4	0.87	1.35	1.9	2.75	1.25	1.97	4.29	1	4.2	1.5
CNS	SF-268	5.1	1.65	1.8	3	5.3	3.75	1.24	2.89	3.81	1.9	3	1.8
	SF-295	4.74	3.33	2.1	4.1	6.8	5.44	7.4	4.55	4.41	2.2	2.6	6.6
	SF-539	0.84	3.33	1.5	4.5	3.6	2.43	6.4	3.59	2.93	1	2.2	1.5
	SNB-19	1.58	2.32	2.5	2.8	4.1	1.9	1.8	2.74	3.58	2.2	2.5	2.9
	SNB-75	11.1	3.6	2.4	4	2	25	1.9	3.74	2.81	1.8	2.5	0.87
	U251	1.2	1	0.7	1.2	0.99	1.57	1.1	1.4	1.88	0.9	1.9	0.84
Melanoma	LOX IMVI	1.07	0.87	0.89	0.47	1.6	1.03	1.1	0.71	0.56	1.2	2.2	1
	MALME-3M	7.86	6.2	3.1	5.2	4.3	5.93	14.2	5.28	16.7	3	4	3.6
	M14	5.98	ND	3.1	2.6	4.1	4.55	ND	3.23	3.02	3.1	3.7	3.7
	MDA-MB-435	4.07	4.1	3.7	2.9	4.2	4.3	9.15	4.25	4.58	4	3.9	3.4
	SK-MEL-2	7.47	5.5	16.7	7.1	5.2	5.06	25	7.01	6.26	3.6	5	4.22
	SK-MEL-28	6.26	4.8	3.1	5.3	4.2	5.69	25	4.47	4.92	2.8	2.9	3.65
	SK-MEL-5	6.06	6.2	5.8	5.5	4.2	4.18	14.4	4.45	5.74	3	3.8	3.25
	UACC-257	8.67	7.2	6.6	7.2	4.5	6.98	25	6.99	14	4.3	8	3.6
	UACC-62	5.92	4	2.8	4.5	3.7	4.13	6.5	3.51	2.83	2.9	3.2	2.1
Ovarian	IGROV1	2.66	3.6	2.4	3.8	3.3	2.11	5.3	2.93	4.63	2.6	4.4	1.4
	OVCAR-3	1.7	1.1	0.85	1.1	2.8	1.87	1	0.96	3.92	2.2	3	1.36
	OVCAR-4	9.14	4.1	3.4	5.1	4.8	4.12	2.2	5.68	3.31	2.3	3.1	2.25
	OVCAR-5	2.6	3.3	2.5	4.9	4.6	4.19	10	4.36	4.97	2.1	2.4	3.6
	OVCAR-8	5.08	3.6	4	8	5.6	6.44	3.5	5.71	4.86	4.9	4.9	1.3
	NCI/ADR-RES	7.18	5	4.6	9	7.3	7.54	2.2	4.24	5.37	3.5	4.3	1
	SK-OV-3	9.38	9.7	8.2	7.7	7	9.3	8.8	9.81	6.97	3.9	6.6	5.6
Renal	786-0	1.37	1.1	0.95	1.4	3.1	2.67	1.6	1.37	4.36	0.78	1.8	2.44
	A498	8.93	5.5	4.7	4.7	4.3	6.08	25	5.56	3.73	3.1	4.2	3.6
	ACHN	4.82	4	2.7	6.3	3.9	5.24	15	5.74	3.95	2.5	3	4.5
	CAKI-1	ND	4.9	2.9	4.4	3.7	ND	13.5	3.14	5.08	2.7	3.5	2.3
	RXF 393	3.44	3	2.4	3.75	3.1	3.86	3	3.89	3.39	2.7	2.7	0.94
	SN12C	2.93	2.4	2.6	1.9	4.3	3.84	3	1.62	3.71	2.9	4.3	1.4
	TK-10	7.89	5.4	4.3	6.6	4.5	7.44	1.23	10.5	6.01	4	5	4.3
	UO-31	2.64	1.7	1.8	2.4	3.4	2.77	2.3	1.72	2.65	2.2	2.5	1.7
Prostatic	PC-3	2.8	2.4	2.5	2.8	3.8	3.29	1.4	1.99	7.06	0.53	1	1.26
	DU-145	1.19	1.7	1.1	2.1	3.4	1.1	1.4	1.24	4.45	2.2	3	1.67
Breast	MCF7	0.99	0.74	0.57	0.85	2.4	1.13	0.89	1.04	2.52	0.62	1	1.36
	MDA-MB-231/ATCC	1.83	4.3	4	2.8	6.5	2.37	5.2	2.96	3.36	2.9	4	4
	HS 578T	23.3	18.8	8	5.9	7.3	1.42	15.7	1.5	5.36	4.9	6.1	10.8
	BT-549	2.73	3.5	1.55	2.1	3.4	2.95	3.5	1.32	2.94	2.5	2.6	1.15
	T-47D	3.33	3.2	3.8	4	2.9	5.23	4.3	8.34	3.8	3.1	6	1.3
	MDA-MB-468	0.97	1.7	1.4	1.8	1.1	1.71	1	1.72	1.99	2.5	2.1	0.64

Fig. 5. The half maximal cell growth inhibition concentration (GI_{50}) (μM) for representative **IPEs** in the NCI 60 cancer cell lines. *ND = No Data.

MCAK. Aurora B phosphorylates MCAK thereby inhibiting its depolymerizing activity. [32] However, treatment with Aurora B inhibitors alone does not cause spindle collapse (Fig. 8). It is possible that regulation of MCAK by Aurora B may contribute to our phenotype, yet it is clear that a second event is required (triggered by our compounds). Also, single treatment with our compounds did not cause spindle collapse suggesting that the effects may be more subtle or related to dynamic changes in microtubules. To investigate this idea, we analyzed tubulin dynamics using a cold treatment approach. Cold treatment induced microtubule depolymerization allowing the rate of repolymerization to be observed by rewarming cells to 37 °C. [33] HeLaM cells expressing fluorescently tagged α-tubulin were treated with DMSO or **IPE-7** for 30 min at 37 °C. They were then incubated at 4 °C for 30 min before rewarming. After rewarming, cells were fixed at specific time points and observed by wide-field fluorescence microscopy. In the majority of the control cells, bipolar spindle was formed after 8 min of rewarming (Fig. 10a). To quantify this phenotype, we repeated the experiment a total of 4 times, and collected images of between 10 and 30 cells per experiment per condition (total DMSO n = 72, **IPE-7**n = 73). Images were assessed in a blinded manner and scored as either normal or abnormal spindle (examples are shown in Fig. 10a). No significant differences were observed at either 0 min or 20 min post rewarming.

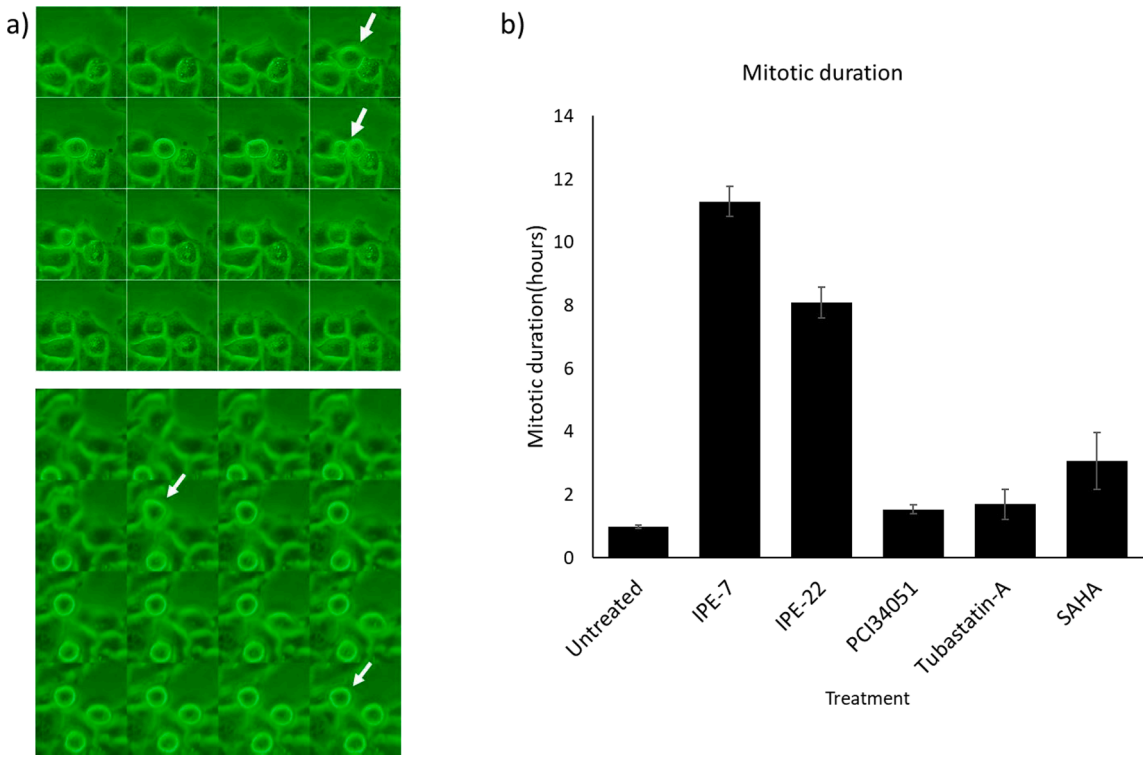

Fig. 6. Compounds arrest HeLaM cells in mitosis. a): asynchronous HeLaM cells were treated with DMSO or **IPE**, images were taken every 12 min on a phase contrast microscope. The arrows indicate mitotic cells. b) Mitotic duration was calculated for every treatment and is displayed in the bar graph. c) Asynchronous HeLaM cells were treated with indicated inhibitors and cells were harvested at 24 h, 48 h and 72 h post-treatment for cell cycle analysis using flow cytometry. Graphs for Cell count vs. PI intensity for each of the treatments are displayed. After treatment with **IPE-7** and **IPE-8,** there is clear increase in G2/M i.e. 4 N peak and post G2 population (i.e. > 4 N) confirming mitotic arrest and mitotic exit without division into two daughter cells. Also, cell death as seen in increased subG1 population.

However, at 8 min post-rewarming, we observed significantly more abnormal spindles in **IPE-7**-treated samples than control (Fig. 10b). As a second method of quantitation, again using blinded images at the 8 min time-point, we used ImageJ to trace spindle outline and quantify spindle morphology (Fig. 10c). **IPE-7**-treated cells had spindles that occupied significantly smaller area compared to control cells. These analyses suggest that **IPE-7** delays spindle assembly during recovery after cold shock (Fig. 10d).

Spindle toxins that interfere with microtubule dynamics usually cause mitotic arrest. Based on antimitotic effects, collapsed spindle phenotype with inhibition of Aurora B and delayed tubulin polymerization after cold shock, we predicted that tubulin may be directly targeted by **IPE**s. Hence, we measured the effect of **IPE** on polymerization of purified tubulin by spectrophotometry. Light scattering was measured every 30 s upon warming purified tubulin to 37 °C. The Vmax slope during the exponential phase was measured in mOD/min. 10 μM Taxol, which stabilizes microtubules, was used as a positive control and showed a higher V_{max} than DMSO. [34] (Fig. 11a and b). In contrast, **IPE-7** delayed tubulin polymerization. This effect was observed in dose-dependent manner as tubulin polymerization was slowed down significantly in both 10 and 50 μM **IPE-7** as compared to DMSO (Vmax 10mOD/min in DMSO vs 5.5mOD/min in 10 μM **IPE-7** and 4.5 mOD/min in 50 μM **IPE-7**). After warming samples to 37 °C for an hour, the spectrometer was set to cool to ~15 °C. Spectrophotometry was continued during this cooling phase to monitor microtubule depolymerization. Depolymerization was accelerated in 50 μM **IPE-7** compared to the DMSO-treated sample (Fig. 11 c and d). As a second way to visualize the extent of polymerization we graphed the rate of change in absorbance (change in absorbance for each time point versus time). **IPE-7** reduced the amplitude of this change in absorbance compared to DMSO, again pointing to a reduction in the rate of polymerization (Fig. 11e and f). These results suggest that **IPE-7** destabilizes microtubules at 37 °C and accelerates depolymerization upon cooling.

Evidence so far suggests that our compounds affect microtubule dynamics by targeting tubulin. In order to further validate this observation, we carried out molecular docking studies of **IPE-7** on the surface of β-tubulin, specifically targeting the colchicine binding site. The occupation of this site by colchicine or various other molecules gives rise to a curved αβ-tubulin dimer that inhibits formation of microtubule assembly. [35,36]

Experimentally, it has been established that colchicine binds to tubulin-β at the tubulin-α interacting interface. Most crystal structures used in the studies of colchicine binding site inhibition contained two units of αβ-tubulin heterodimers with Guanosine triphosphate (GTP) bound to tubulin-α and both Guanosine diphosphate (GDP) and 2-(*N*-Morpholino)-ethanesulfonic acid (MES) bound to tubulin-β in addition to the occupation of an inhibitor at the colchicine binding site. The recently evaluated D64131-bound αβ-tubulin dimer crystal structure [37] was chosen as the primary system on which various other potential docking sites were also tested. The colchicine binding site (occupied by D64131) containing β-tubulin was selected as the target protein for **IPE-7** docking and in addition to the sites used by GDP, MES, and D64131, two other sites predicted by the OpenEye software were used for primary docking (See Fig. 12a). The **IPE-7** binding scores on these sites were given in Table S5a along with the score of the native ligand D64131 (or D3L as labeled in the pdb) for comparison. **IPE-7** at the colchicine binding site exhibited the best binding score with a site simply above it (Site Y) also showing a similar score. This score was in par with the native inhibitor D64131 co-crystallized with β-tubulin. The other three sites showed relatively weaker docking scores. Also, the docking scores for **IPE-7** remained relatively unchanged for most β-tubulin targets from various other crystal structures at the colchicine binding site

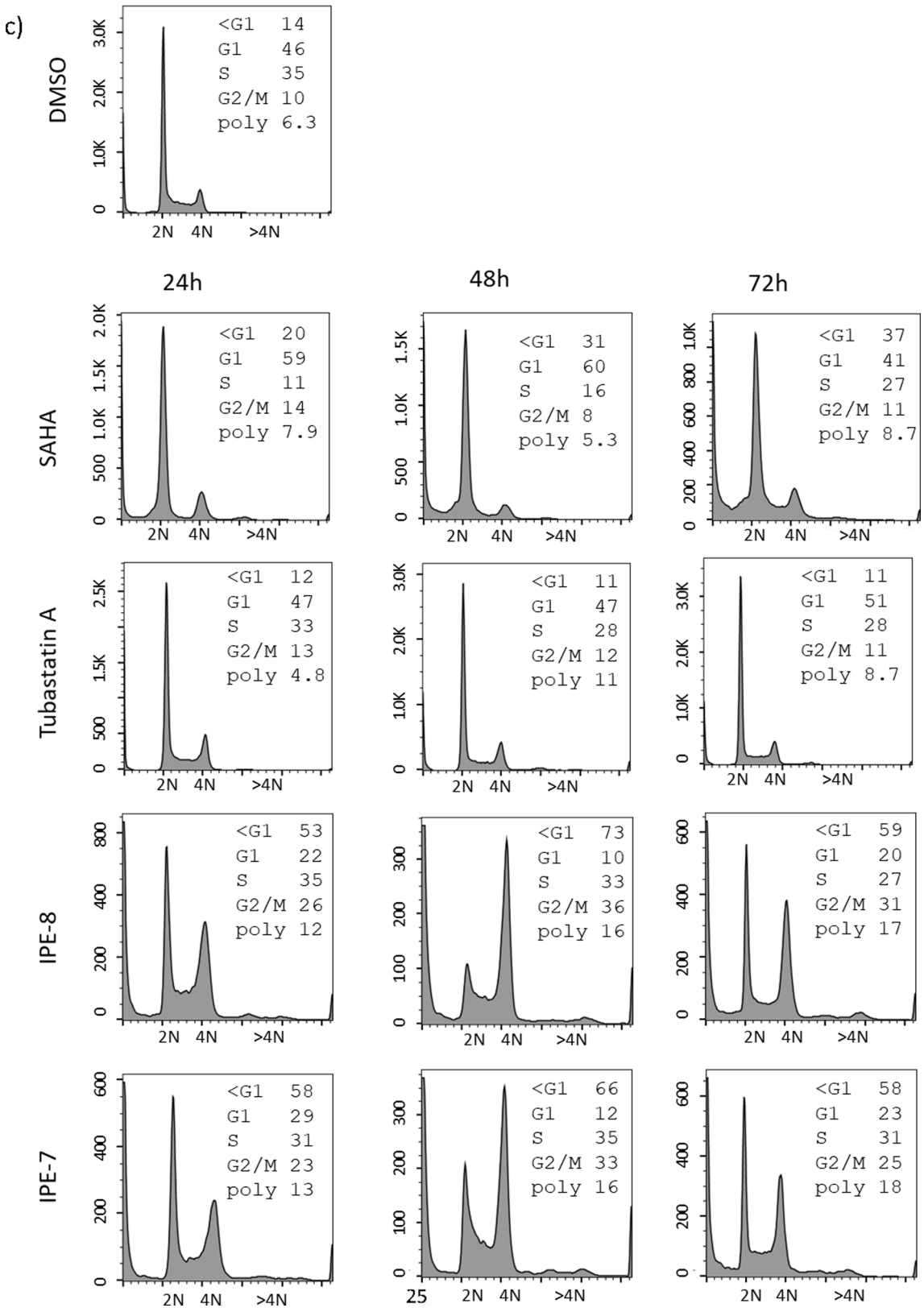

Fig. 6. (*continued*).

(Table S5b). A slightly reduced binding score was observed when **IPE-7** was docked at the taxane binding site. However, this score was relatively higher than that estimated for Taxol when the co-crystallized ligand was occupying the binding site. The best docking poses for **IPE-7** at the colchicine and taxane binding sites as well as the contacting residues of β-tubulin are also shown in Fig. 12.

2.5. Conclusion

We designed chalcone mimetics containing 1-(1H-imidazol-2-yl)

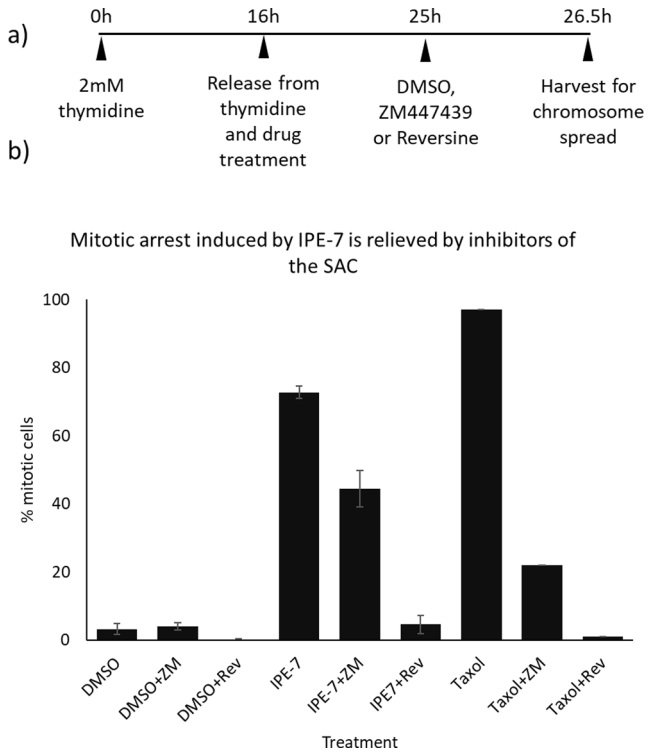

Fig. 7. Compounds activate the SAC in HeLaM cells a) HeLaM cells were synchronized in S phase by a single thymidine block. They were released from thymidine into **IPE-7** (10 μM) or DMSO or paclitaxel (1 μM). 9 h post thymidine release cells were treated with ZM447439 or reversine for 90 min and fixed. At-least 200 cells per treatment were counted from chromosome spreads in blinded manner. b) Treatment with **IPE-7** arrested cells in mitosis. Mitotic arrest was relieved by ZM447438 (ZM) or reversine (Rev).

ethan-1-one moiety as the ZBG for potential HDAC inhibition. All compounds were prepared using a convergent synthetic approach. They showed cancer cell growth inhibition with a low micromolar potency. Imidazole moiety was found to be crucial for cytotoxic activity, as replacing it with thiazole, pyrimidine, or phenolic moieties caused total loss of cytotoxic activity. The olefin moiety in the linker is also essential for the cytotoxic activity, as hydrogenation of this double bond or conversion to a cyclopropyl moiety abolished the antiproliferative activity. The double bond, although is part of an α,β-unsaturated system, the Michel acceptor properties of this moiety is likely attenuated by electron donation from the imidazole ring. This is consistent with the fact that the compounds are not general toxins as some of the analogues, which differ only in the nature of the cap group, are not active. In fact, the nature of the cap group moiety was found to have a profound effect on cancer cell growth inhibition activity. Replacing the aniline moiety of the cap group with a cyclohexyl group or a bulky naphthyl moiety reduced antiproliferative activity; on the other hand, halogen atoms or trifluoromethyl group at *para*-position improved in vitro performance. Some of the analogues showed very distinctive cancer cell growth inhibition selectivity. Almost all leukemia cell lines, and most of the colon cancer cell lines were found to be particularly sensitive to these compounds. On the other hand, compounds exhibited low growth inhibitory activity on melanoma, renal cancer cell lines and normal RPE cells. Although the molecules contained a 1-(1H-imidazol-2-yl)ethan-1-one moiety as a metal-binding group for HDAC inhibition, Western blot analysis showed no increased global H3, tubulin or SMC3 acetylation in treated cells. Their most striking characteristic was mitotic arrest due to activation of the SAC. Also, spindle collapse when combined with an Aurora B inhibitor suggested a potential interaction with tubulin. Indeed, **IPE-7** delayed spindle assembly after rewarming cells and reduced the rate of polymerization of purified tubulin. Molecular docking studies identified an interaction of **IPE-7** with tubulin. Consistent with this observation, **IPE-7** reduced the polymerization of purified tubulin indicating a potential direct interaction. Interestingly, 10 μM **IPE** on its own does not affect the overall appearance of the mitotic spindle as assessed by immunofluorescence microscopy even though mitotic arrest is robust at this concentration. We hypothesize that subtle changes in tubulin polymerization dynamics at this concentration may preclude effective kinetochore-microtubule attachments leading to activation of the spindle assembly checkpoint. These compounds represent a new class of antimitotic compounds that impact the function of the spindle. Other groups have designed dual inhibitors of HDACs and tubulin with potential as anti-cancer agents. [38–40] Given the inhibitory activity of our compounds against purified HDACs, it is possible that with further refinement this class of molecules may yield effective dual HDAC/tubulin inhibitors, however this has not yet been achieved in our case. It is important to note that while this ZBG was chosen to target HDACs, it is possible that these compounds might bind other zinc-containing proteins as do other zinc-binding groups, including hydroxamic acid; [41] this possibility was not directly tested. Chemical biology studies to directly identify intracellular targets using molecular probes are currently underway.

3. Experimental.

3.1. Material and Methods.

All chemicals and solvents were purchased from commercial suppliers and used without further purification, unless stated otherwise. Anhydrous tetrahydrofuran and diethyl ether were freshly distilled from sodium and benzophenone before use. ^{1}H and ^{13}C NMR spectra were carried out on Brucker Avance 600 MHz, INOVA 600 MHz and Varian VXRS 400 MHz NMR spectrometers in deuterated solvents using residual undeuterated solvents as internal standard. High-resolution mass spectra (HRMS) were recorded on a Waters Synapt high definition mass spectrometer (HDMS) equipped with nano-ESI source. Melting points were determined using a Fisher-Johns melting point apparatus. Crude products were purified by flash chromatography on silica gel (40–63 μ) from Sorbent Technologies and on a Teledyne ISCO CombiFlash Companion chromatography system on RediSep prepacked silica cartridges. Thin layer chromatography (TLC) plates (20 cm × 20 cm) were purchased from Sorbent Technologies (catalog #4115126) and were viewed under Model UVG-54 mineral light lamp UV-254 nm. Uniplates (1000 μm) purchased from Analtech Inc. were used for preparative thin layer chromatography. A Shimadzu Prominence HPLC with an LCT20AT solvent delivery system coupled to a Shimadzu Prominence SPD 20AV Dual wavelength UV/vis absorbance Detector, a Shimadzu C18 column (1.9 m, 2.1 mm × 50 m) and HPLC grade solvents (methanol, 1% formic acid and water) and a Waters 1525 binary pump HPLC system with Waters 2487 dual wavelength absorbance detector on a symmetry C18 column (5μ, 4.6 mm × 150 m)) were used to determine the purity of compounds by HPLC. A Biotage initiator was used for all microwave reactions in recommended vials of 10 mL and 20 mL capacity. Structural integrity and purity of the test compounds were determined by a combination of ^{1}H and ^{13}C NMR, HRMS and HPLC and the purity of all test compounds were found to be > 95%.

3.2. Synthesis of 1H-imidazole ketones.

3.2.1. 1-Tosyl-1H-imidazole-2-carbaldehyde (3).

To a stirred solution of 1H-imidazole-2-carbaldehyde **9** (1.92 g, 20 mmol, 1 equiv) in dichloromethane (40 mL) were added tosyl chloride (4.2 g, 22 mmol, 1.1 equiv), triethylamine (4.05 g, 40 mmol, 2 equiv), and DMAP (244 mg, 2 mmol, 0.1 equiv). The reaction mixture was stirred overnight at room temperature. The solvent was evaporated under reduced pressure. The residue was purified by column chromatography on silica gel in 40% ethyl acetate in hexanes to give **3** as an off-

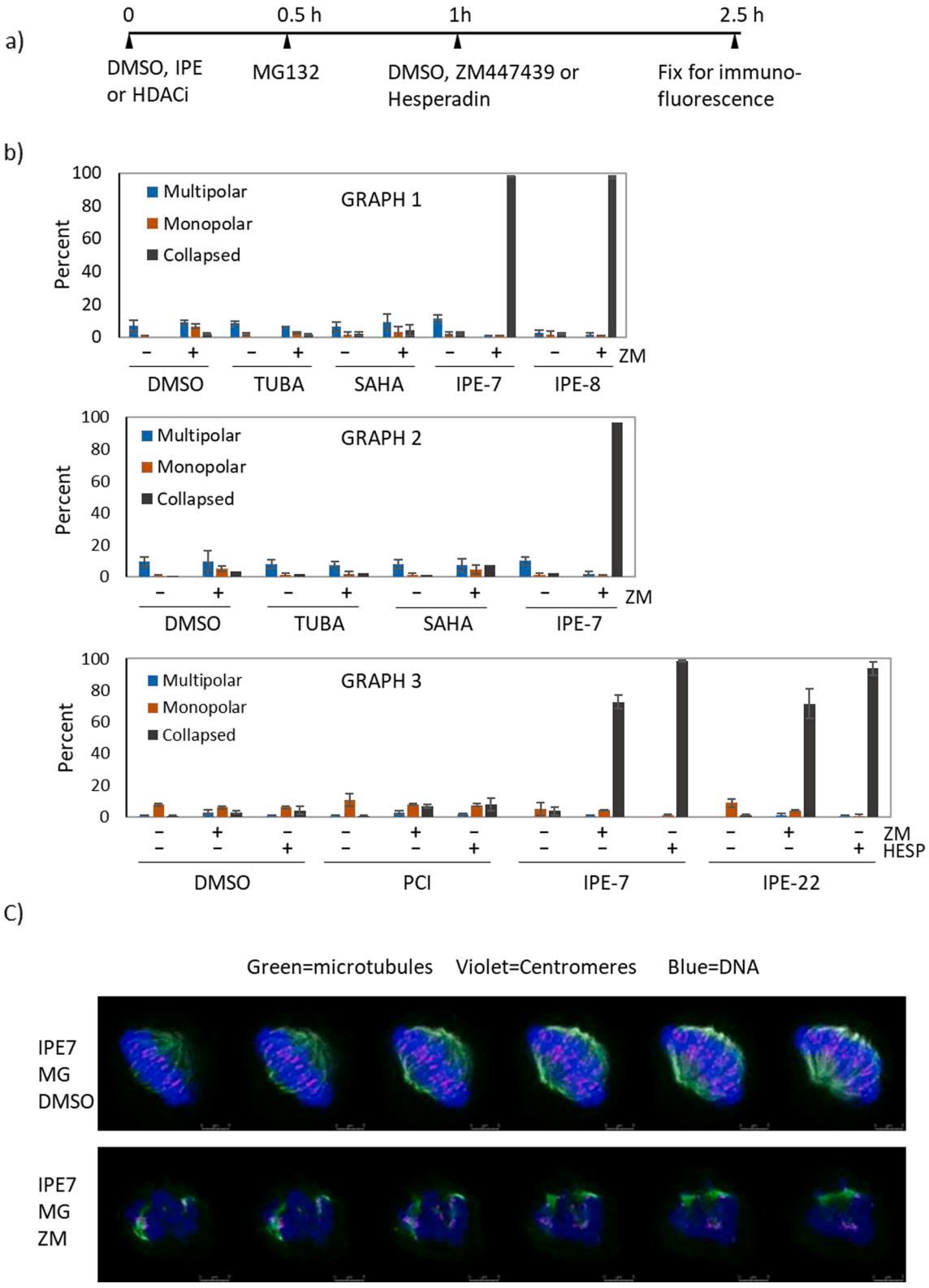

Fig. 8. Spindle collapse in cells exposed to analogues in combination with Aurora B inhibition. a) HeLaM cells were treated with **IPE-7** or **IPE-8** or **IPE-22** (10 μM) or DMSO, followed by treatment with 20 μM MG132 (MG) to arrest their cell cycle progression. They were then treated with 2.5 μM ZM447439 (ZM) or Hesparadine (Hesp) for 90 min. b) Spindle phenotypes were quantified in blinded manner. In graph 3, the Aurora B inhibitor Hesperadin was used instead of ZM447439. For ease of presentation, normal spindles are omitted from the graphs c) Representative images of normal bipolar (**IPE-7**, MG, DMSO) and collapsed spindles (**IPE**, MG, ZM). Six z-planes from two confocal scans are shown.

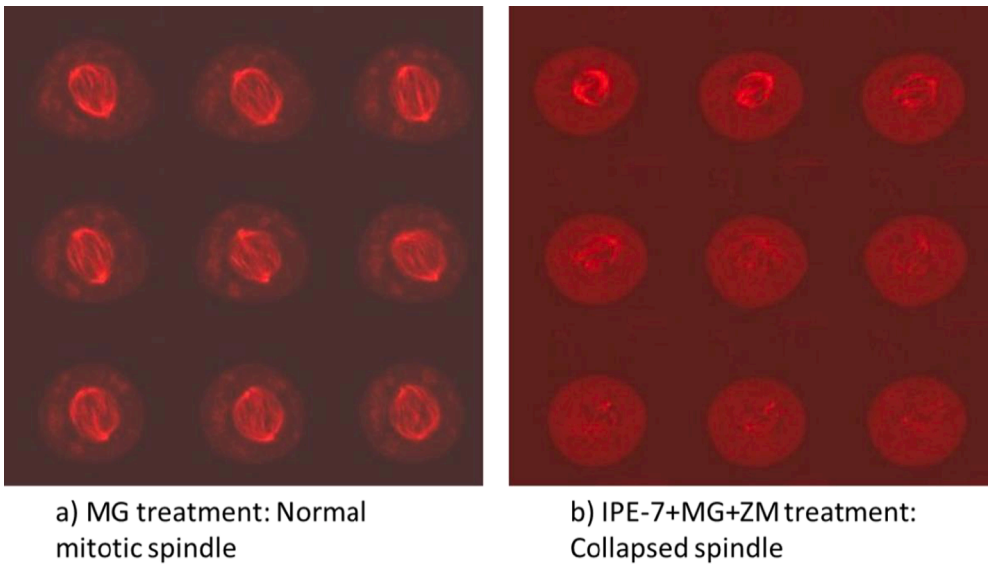

Fig. 9. Co-treatment with IPE-7 + ZM447439 leads to collapsed mitotic spindle: HeLaM cells were treated with IPE-7 or DMSO (30 min) followed by MG132 (MG) for 30 min. Images were captured on Leica confocal microscope immediately after addition of ZM447439 (ZM).

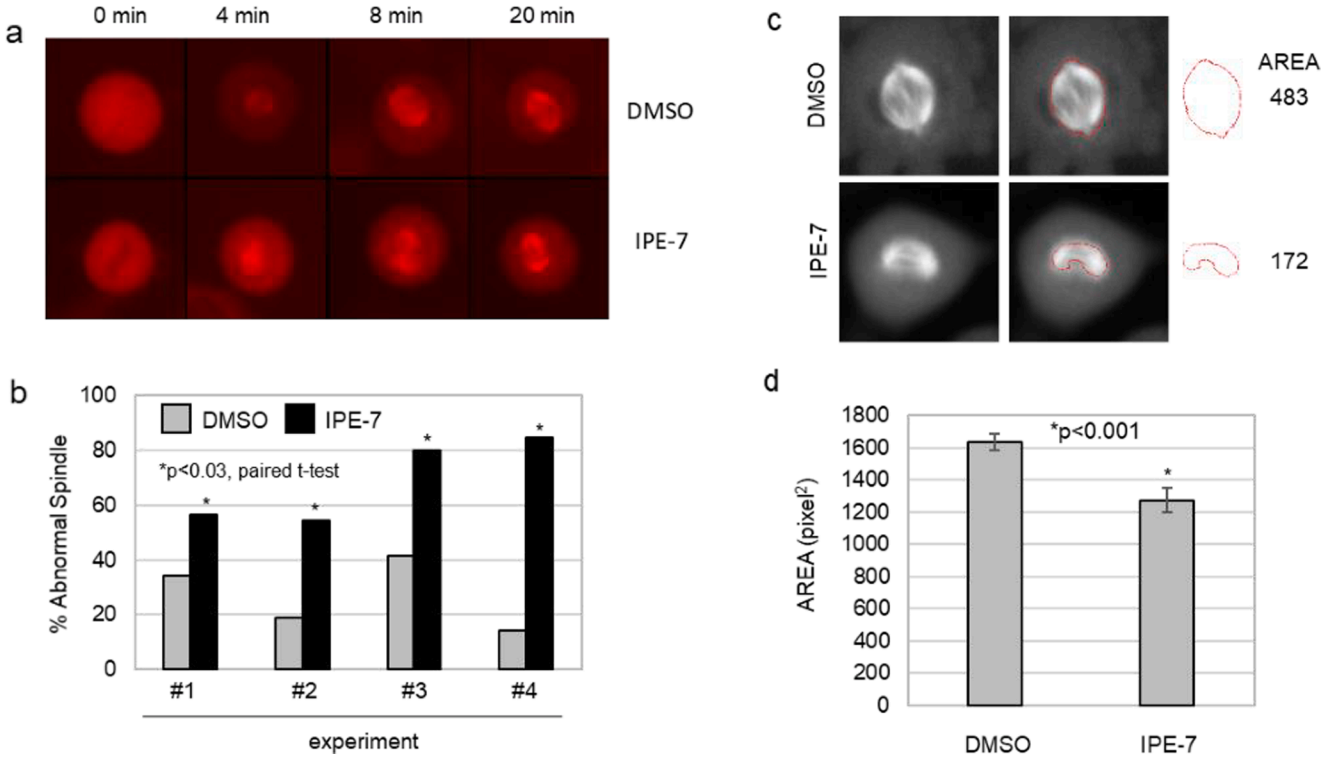

Fig. 10. Treatment with **IPE-7**delays spindle reassembly after recovery from cold shock: HeLaM cells expressing mcherry-α-tubulin fusion were exposed to either DMSO or **IPE-7** for 30 min at 37 °C. Cells were then incubated at 4 °C for 30 min followed by rewarming at 37 °C. Cells were fixed and images collected at 0, 4, 8 or 20 post-rewarming. (a) Examples of fluorescent images of control and **IPE-7**-treated cells at the indicated time points. (b) Visual assessment of blinded images. Spindles were scored as either normal or abnormal and percent abnormal is shown. p-value using a paired *t*-test is indicated. (c) Examples of spindle morphology detection using the threshold feature and object identification features of ImageJ. Examples of normal and abnormal spindles in DMSO and **IPE-7**-treated cells respectively are shown. (d) Area of spindles identified using ImageJ. Average and standard errors along with p-value from a student's *t*-test are shown.

white powder (3.8 g, 76%); mp 155 °C. ^{1}H NMR (600 MHz, $CDCl_3$) δ 9.81 (s, 1H), 8.02 (d, $J = 8.4$ Hz, 2H), 7.86 (s, 1H), 7.39 (d, $J = 8.5$ Hz, 2H), 7.33 (d, $J = 1.3$ Hz, 1H), 2.47 (s, 3H). ^{13}C NMR (151 MHz, $CDCl_3$) δ 178.71, 146.88, 143.55, 133.68, 130.54, 130.03, 128.93, 124.65, 21.84.

3.2.2. 1-(1-Tosyl-1H-imidazol-2-yl)ethan-1-ol (10).

To a stirred solution of 1-tosyl-1H-imidazole-2-carbaldehyde **3** (1.1 g, 4.4 mmol, 1 equiv) in tetrahydrofuran (15 mL) at −78 °C was added methyl magnesium bromide (8.8 mL of 1.0 M solution in butyl ether, 8.8 mmol, 2 equiv). The reaction mixture was stirred for 1 h at −78 °C. After adding saturated ammonium chloride (10 mL), the reaction mixture was extracted with ethyl acetate (20 mL). The organic layer was separated, and the water layer was extracted with ethyl acetate (3 × 10 mL). The combined organic extract was washed with brine and dried over

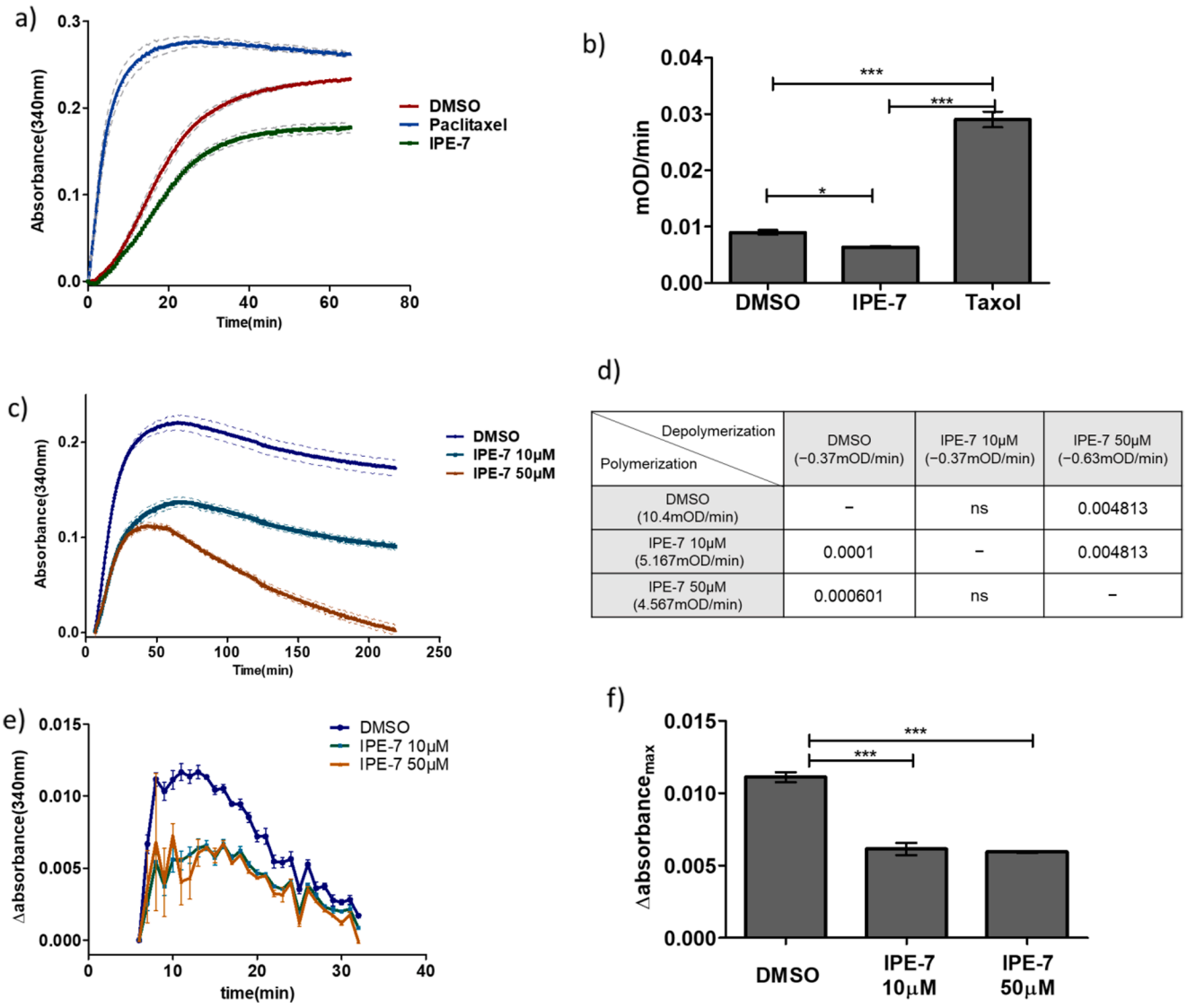

Fig. 11. IPE-7 affects in-vitro tubulin polymerization: Polymerization of tubulin heterodimers, purified from porcine brain, into microtubules was measured as increase in absorbance at 340 nm at 37 °C. Data points are mean absorbance from 3 experiments. a) **IPE-7** destabilized microtubules and b) reduced Vmax. Vmax is expressed as mOD/min in exponential phase of polymerization. c) **IPE**s affected tubulin dynamics in dose dependent manner. d) p values for tubulin polymerization and depolymerization. e) and f) As **IPE-7** destabilized microtubules, efficiency of tubulin polymerization was reduced as seen by lower amplitude for Δabsorbance vs time.

anhydrous sodium sulfate and the solvent was evaporated under reduced pressure. The residue was purified by column chromatography on silica gel in ethyl acetate/hexanes (30–60%) to give **10** as a yellow oil (750 mg, 65%), recovered starting material (190 mg, 18%); mp 199–200 °C. ^{1}H NMR (400 MHz, $CDCl_3$) δ 7.77 (d, J = 8.3 Hz, 2H), 7.31 (dd, J = 18.8, 4.9 Hz, 3H), 6.89 (d, J = 1.5 Hz, 1H), 5.20 (q, J = 6.5 Hz, 1H), 2.36 (s, 3H), 1.51 (d, J = 6.5 Hz, 3H). ^{13}C NMR (151 MHz, $CDCl_3$) δ 151.90, 146.40, 134.98, 130.43, 128.19, 127.38, 119.89, 63.00, 22.25, 21.76. HRMS: (ESI) calcd for $C_{12}H_{14}N_2O_3S$ $[M + H]^+$ 267.0803; found, 267.0797.

3.2.3. *1-(1-Tosyl-1H-imidazol-2-yl)ethan-1-one (1).*

To a stirred solution of 1-(1-tosyl-1H-imidazol-2-yl)ethan-1-ol **10** (535 mg, 2 mmol, 1 equiv) in dichloromethane (25 mL) at 0 °C was added Dess-Martin Periodinane (1.02 g, 2.4 mmol, 1.2 equiv). The reaction mixture was stirred for 4 h at room temperature, filtered through a pad of celite, and concentrated in *vacuo*. The residue was purified by column chromatography on silica gel in ethyl acetate/hexanes (5–20%) to give **1** as an off-white powder (528 mg, 100%); mp 103–104 °C. ^{1}H NMR (400 MHz, $CDCl_3$) δ 7.98 (t, J = 8.1 Hz, 6H), 7.87 (d, J = 1.3 Hz, 3H), 7.36 (d, J = 8.1 Hz, 7H), 7.18 (d, J = 1.3 Hz, 3H), 2.58 (s, 9H), 2.44 (s, 9H). ^{13}C NMR (151 MHz, $CDCl_3$) δ 187.71, 146.14, 143.96, 134.25, 129.98, 129.62, 129.10, 128.43, 127.41, 124.99, 44.64, 27.23, 21.82.

3.2.4. *Ethyl (E)-2-(4-styrylphenyl)acetate (11).*

To a solution of ethyl 2-(4-bromophenyl)acetate **7** (2.4 g, 10 mmol, 1 equiv) in dimethylformamide (10 mL) in a microwave vial was added styrene **8** (1.041 g, 30 mmol, 3 equiv), palladium acetate (80 mg, 3 mol %), triphenyl phosphine (160 mg, 6 mol%), and trimethylamine (2.024 mL, 20 mmol, 2 equiv). The reaction mixture was heated in a microwave synthesizer for 6 h at 120 °C. It was allowed to cool to room temperature. The resulting suspension was filtered and the filtrate was concentrated under reduced pressure. The residue was purified by column chromatography on silica gel in ethyl acetate/hexanes (1–3%) to afford **11** as a white powder (1.73 g, 65%); mp 72 °C. ^{1}H NMR (400 MHz, $CDCl_3$) δ 7.55 – 7.44 (m, 2H), 7.36 (t, J = 7.6 Hz, 1H), 7.28 (dd, J = 6.3, 4.4 Hz, 1H), 7.10 (d, J = 8.7 Hz, 1H), 4.22 – 4.07 (m, 1H), 3.62 (s, 1H), 1.26 (td, J = 7.1, 3.2 Hz, 1H). ^{13}C NMR (151 MHz, CDCl*3*) δ 171.55, 137.30,

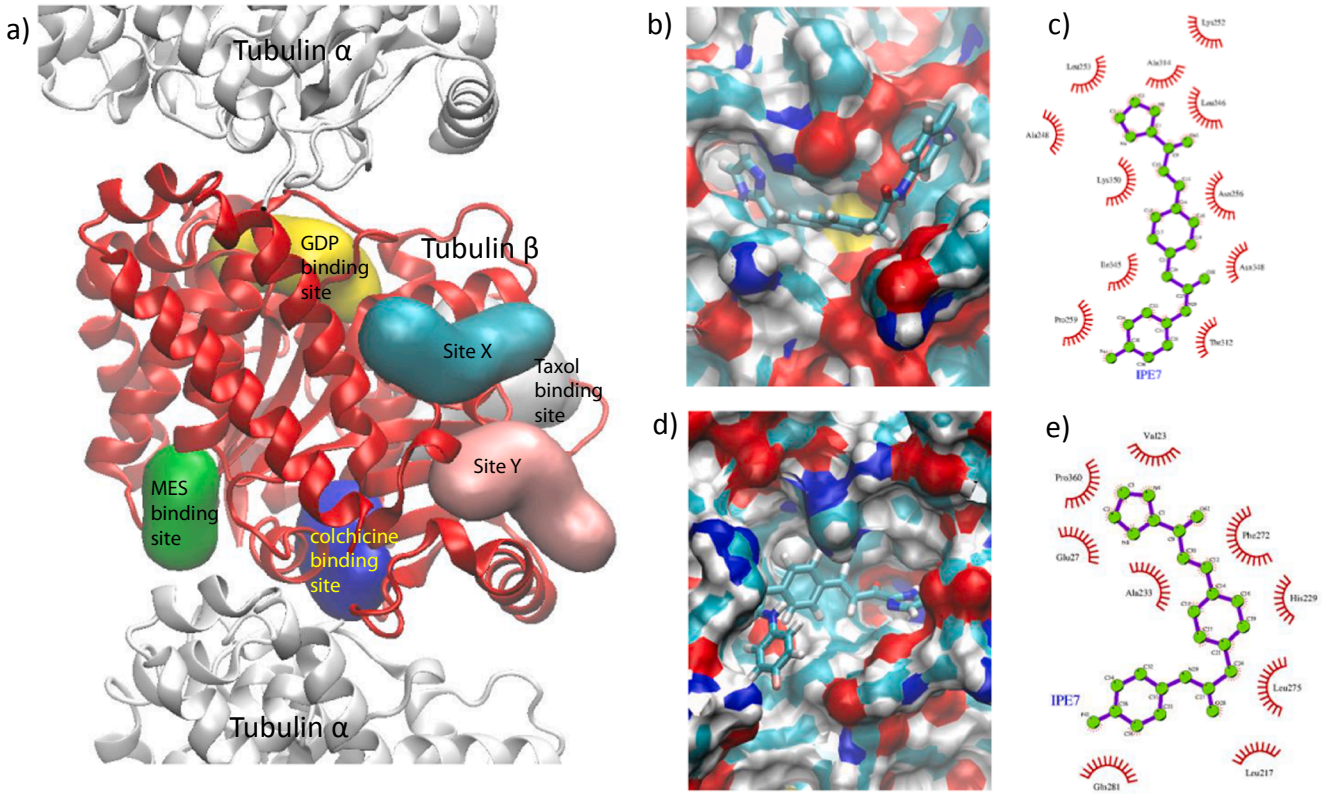

Fig. 12. (a) Various ligand binding sites used in the present study for **IPE-7** docking on the surface of β-tubulin (represented by the red ribbon). In the selected pdb structure (pdb ID: 6k9v), two units of α- and β-tubulin were present and the neighboring α-tubulin molecules are shown in white ribbons. (b) **IPE-7** docked at the colchicine binding site. (c) the colchicine binding site residues of β-tubulin that are in contact with **IPE-7**. (d) **IPE-7** docked at the taxane binding site. (e) the taxane binding site residues that are in contact with **IPE-7.**

136.21, 133.52, 129.61, 128.70, 128.64, 128.26, 127.64, 126.69, 126.51, 60.95, 41.21, 14.21. HRMS: (ESI) calcd for $C_{18}H_{18}O_2$ $[M + H]^+$ 267.1385; found, 267.1374.

3.2.5. (E)-2-(4-Styrylphenyl)acetic acid (5).

To a stirred solution of ethyl (*E*)-2-(4-styrylphenyl)acetate **11** (1.5 g, 6.25 mmol, 1 equiv) in methanol (15 mL) at 0 °C was added sodium hydroxide (375 mg, 9.4 mmole, 1.5 equiv). The reaction mixture was stirred at room temperature for 6 h, and acidified with hydrochloric acid. The solid product was collected by filtration and dried to afford **5** as a white powder (1.35 g, 91%) ; mp 195 °C. ^{1}H NMR (400 MHz, CDCl3) δ 7.49 (q, J = 8.7 Hz, 2H), 7.36 (t, J = 7.5 Hz, 1H), 7.27 (dd, J = 12.0, 6.9 Hz, 2H), 7.10 (s, 1H), 3.67 (s, 1H). ^{13}C NMR (151 MHz, CDCl3) δ 137.24, 136.55, 132.59, 129.73, 128.87, 128.71, 128.13, 127.70, 126.78, 126.53, 40.51.

3.3. General procedure for the synthesis of amides (4a-n).

To a stirred solution of (*E*)-2-(4-styrylphenyl)acetic acid **5** (1 equiv) in dichloromethane (20 mL) were added 1-ethyl-3-(3-dimethylaminopropyl)carbodiimide (1.5 equiv), DMAP (0.1 equiv), and the corresponding amines (1.5 equiv). The reaction mixture was stirred at room temperature overnight. Water (10 mL) was added, the organic layer was separated, and the water layer was extracted with dichloromethane (3 × 10 mL). The combined organic extract was washed with brine and dried over anhydrous sodium sulfate, and the solvent was evaporated under reduced pressure. The residue was purified by column chromatography on silica gel in ethyl acetate/hexanes (10–30 %) to give amides **4a-n.**

3.3.1. (E)-N-Phenyl-2-(4-styrylphenyl)acetamide (4a).

White powder (70%); mp 70 °C. ^{1}H NMR (400 MHz, CDCl3) δ 7.53 (dd, J = 15.7, 7.4 Hz, 11*H*), 7.46 (t, J = 8.1 Hz, 3H), 7.42 (d, J = 7.9 Hz, 4H), 7.40 – 7.27 (m, 17H), 7.19 – 7.01 (m, 14H), 3.82 – 3.63 (m, 7H). ^{13}C NMR (151 MHz, CDCl3) δ 168.93, 137.56, 137.10, 136.90, 133.57, 130.01, 129.95, 129.26, 128.98, 128.89, 128.75, 127.97, 127.86, 127.85, 127.55, 127.33, 127.08, 126.58, 124.53, 119.84, 119.80, 44.64. HRMS: (ESI) calcd for $C_{22}H_{19}NO$ $[M + H]^+$ 314.1545; found, 314.1552.

3.3.2. (E)-N-Cyclohexyl-2-(4-styrylphenyl)acetamide (4b).

Cream solid (50%); mp. 130 °C. ^{1}H NMR (600 MHz, $CDCl_3$) δ 7.50 (d, J = 6.6 Hz, 1H), 7.36 (d, J = 7.3 Hz, 1H), 7.24 (d, J = 5.7 Hz, 1H), 7.11 (s, 1H), 3.74 (s, 1H), 3.54 (s, 1H), 2.18 (s, 4H), 1.82 (s, 1H), 1.60 (s, 1H), 1.31 (s, 1H), 1.09 (d, J = 11.5 Hz, 1H), 1.01 (d, J = 9.7 Hz, 1H ppm. ^{13}C NMR (151 MHz, $CDCl_3$) δ 169.87, 137.18, 136.41, 134.43, 129.77, 128.93, 128.74, 128.03, 127.76, 127.08, 126.53, 48.23, 43.79, 32.95, 25.46, 24.74 ppm. HRMS calcd for $C_{22}H_{25}NO$: 320.1936, found: 320.2024

3.3.3. (E)-2-(4-styrylphenyl)-N-(p-tolyl)acetamide (4c).

White solid (80%); mp. 220 °C. ^{1}H NMR (600 MHz, $CDCl_3$) δ 7.55 (dd, J = 12.0, 7.7 Hz, 1H), 7.38 (t, J = 7.4 Hz, 1H), 7.34 (d, J = 7.6 Hz, 1H), 7.32 – 7.28 (m, 1H), 7.14 (d, J = 3.6 Hz, 1H), 7.09 (d, J = 7.7 Hz, 1H), 6.99 (s, 1H), 3.75 (s, 1H), 2.30 (s, 1H), 1.57 (s, 1H) ppm. ^{13}C NMR (151 MHz, $CDCl_3$) δ 168.81, 137.12, 136.84, 135.0, 134.18, 133.70, 129.96, 129.45, 129.22, 128.75, 127.86, 127.31, 126.57, 119.91, 44.59, 20.87 ppm.

3.3.4. (E)-N-(4-Methoxyphenyl)-2-(4-styrylphenyl)acetamide (4d).

White powder (77%); mp 202–203 °C. ^{1}H NMR (400 MHz, $CDCl_3$) δ 7.54 (t, J = 8.3 Hz, 4H), 7.41 – 7.28 (m, 7H), 7.13 (d, J = 1.5 Hz, 2H),

6.94 (s, 1H), 6.85 – 6.79 (m, 2H), 3.77 (s, 3H), 3.74 (s, 2H). ^{13}C NMR (151 MHz, $CDCl_3$) δ 168.80, 156.57, 137.11, 136.85, 133.74, 130.64, 129.96, 129.23, 128.75, 127.88, 127.84, 127.31, 126.57, 121.79, 114.09, 55.48, 44.45. HRMS: (ESI) calcd for $C_{23}H_{21}NO_2$ $[M + H]^+$ 344.1651; found, 344.1682.

3.3.5. (E)-N-(4-(Dimethylamino)phenyl)-2-(4-styrylphenyl)acetamide (4e).

Off-white powder (73%); mp 229 °C. ^{1}H NMR (600 MHz, CDC_{l3}) δ 9.81 (s, 1H), 8.02 (d, J = 8.4 Hz, 2H), 7.86 (s, 1H), 7.39 (d, J = 8.5 Hz, 2H), 7.33 (d, J = 1.3 Hz, 1H), 2.47 (s, 3H). ^{13}C NMR (151 MHz, $CDCl_3$) δ 168.72, 137.15, 136.72, 134.00, 129.97, 129.13, 128.74, 127.95, 127.80, 127.25, 126.57, 121.84, 44.44. HRMS: (ESI) calcd for $C_{24}H_{24}N_2O$ $[M + H]^+$ 357.1967; found, 357.1967.

3.3.6. (E)-N-(Naphthalen-1-yl)-2-(4-styrylphenyl)acetamide (4f).

Yellow powder (73%); mp 206 °C. ^{1}H NMR (600 MHz, $CDCl_3$) δ 7.94 (d, J = 7.5 Hz, 1H), 7.80 (d, J = 8.0 Hz, 1H), 7.64 (d, J = 8.2 Hz, 1H), 7.61 (d, J = 8.1 Hz, 2H), 7.52 (d, J = 7.5 Hz, 2H), 7.43 (dd, J = 13.3, 5.8 Hz, 4H), 7.36 (ddd, J = 26.6, 15.4, 5.9 Hz, 5H), 7.26 (t, J = 6.7 Hz, 1H), 7.14 (d, J = 3.2 Hz, 2H), 3.89 (s, 2H). ^{13}C NMR (151 MHz, $CDCl_3$) δ 169.44, 137.15, 137.05, 134.02, 133.80, 131.93, 130.16, 129.41, 128.80, 128.78, 127.91, 127.80, 127.53, 126.83, 126.60, 126.39, 125.93, 125.82, 125.76, 120.36, 119.99, 44.67. HRMS: (ESI) calcd for $C_{26}H_{21}NO$ $[M + H]^+$ 364.1701; found, 364.1712.

3.3.7. (E)-N-(4-Fluorophenyl)-2-(4-styrylphenyl)acetamide (4g).

White powder (72%); mp 223 °C. ^{1}H NMR (400 MHz, $CDCl_3$) δ 7.60 – 7.48 (m, 4H), 7.42 – 7.35 (m, 4H), 7.35 – 7.31 (m, 2H), 7.29 (d, J = 7.4 Hz, 1H), 7.13 (d, J = 2.3 Hz, 2H), 7.02 (d, J = 7.6 Hz, 1H), 6.97 (dd, J = 12.0, 5.4 Hz, 2H), 3.75 (s, 2H). ^{13}C NMR (151 MHz, $CDCl_3$) δ 168.94, 159.49 (d, J = 244.0 Hz), δ 137.02 (d, J = 12.4 Hz), 136.97, 133.47 (d, J = 14.4 Hz), 129.95, 129.34, 128.77, 127.84 (d, J = 14.6 Hz), 127.37, 126.58, 121.72 (d, J = 8.2 Hz), 115.63 (d, J = 22.8 Hz), 44.46. HRMS: (ESI) calcd for $C_{22}H_{18}FNO$ $[M + H]^+$ 332.1451; found, 332.1463.

3.4. General procedure for the synthesis of amides (25h-i).

A mixture of 2-(4-styrylphenyl)acetic acid **5** (2.0 equiv) and excess oxalyl chloride was refluxed at 65 ^{0}C for 2 h. After removing oxalyl chloride on rotary evaporator, corresponding amines (2.0 equiv) and anhydrous toluene (5.0 mL) were added via syringe and the reaction mixture was stirred overnight. The reaction was monitored by TLC (50% ethyl acetate/hexanes). The reaction was quenched with water (10 mL) and extracted with DCM (3 × 20 mL). The organic extract was dried over anhydrous sodium sulfate and DCM was removed on rotary evaporator to obtain a brown solid. It was chromatographed on silica gel in 20–50% ethyl acetate /hexanes to yield amides **25h-i**.

3.4.1. (E)-N-(4-Chlorophenyl)-2-(4-styrylphenyl)acetamide (4h).

Light brown solid (0.5 g, 44%); mp. 210 °C. ^{1}H NMR (600 MHz, $CDCl_3$) δ 7.55 (dd, J = 17.0, 7.8 Hz, 1H), 7.38 (dd, J = 8.1, 5.1 Hz, 1H), 7.34 (d, J = 7.9 Hz, 1H), 7.30 (d, J = 7.5 Hz, 1H), 7.28 – 7.23 (m, 4H), 7.14 (d, J = 5.8 Hz, 1H), 7.04 (s, 1H), 3.76 (s, 1H), 1.59 (s, 3H) ppm. ^{13}C NMR (151 MHz, $CDCl_3$) δ 169.04, 159.42, 140.88, 136.99, 136.29, 133.44, 129.93, 129.37, 128.85, 127.85, 127.32, 126.57, 125.15, 124.08, 121.04, 118.65, 110.84, 106.54, 55.92, 44.50, 43.17, 39.97, 36.50, 35.17, 25.42, 15.52 ppm. HRMS calcd for $C_{22}H_{18}ClNO$: 348.1076, found: 348.1152.

3.4.2. (E)-N-(4-Bromophenyl)-2-(4-styrylphenyl)acetamide (4i).

White powder (283 mg, 83%); mp 220–221 °C. ^{1}H NMR (600 MHz, $CDCl_3$) δ 7.52 (dd, J = 16.4, 7.7 Hz, 4H), 7.39 – 7.33 (m, 4H), 7.30 (dd, J = 8.5, 3.6 Hz, 4H), 7.26 (t, J = 6.8 Hz, 1H), 7.10 (d, J = 5.7 Hz, 2H), 7.03 (s, 1H), 3.72 (s, 2H). ^{13}C NMR (151 MHz, $CDCl_3$) δ 168.92, 137.04, 136.64, 133.24, 131.93, 129.94, 129.39, 128.77, 127.90, 127.77, 127.39, 126.59, 121.32, 117.09, 44.59. HRMS: (ESI) calcd for $C_{22}H_{18}BrNO$ $[M + H]^+$ 392.0650; found, 392.0652.

3.4.3. (E)-N-(4-Pentafluorosulfaneyl)-2-(4-styrylphenyl)acetamide (4j).

White powder (283 mg, 74%); mp 212–214 °C. ^{1}H NMR (400 MHz, $CDCl_3$) δ 7.66 (d, J = 9.1 Hz, 2H), 7.55 (dd, J = 11.8, 8.7 Hz, 6H), 7.34 (ddd, J = 20.8, 13.8, 7.3 Hz, 6H), 7.13 (d, J = 3.2 Hz, 2H), 3.78 (s, 2H). ^{13}C NMR (151 MHz, $CDCl_3$) δ 169.22, 140.19, 137.18, 136.99, 132.87, 129.90, 129.51, 128.78, 127.95, 127.69, 127.45, 126.97 (d, J = 4.4 Hz), 126.60, 118.90, 44.60. HRMS: (ESI) calcd for $C_{22}H_{18}F_5NOS$ $[M + H]^+$ 440.1108; found, 440.1113.

3.4.4. (E)-2-(4-Styrylphenyl)-N-(4-(trifluoromethyl)phenyl)acetamide (4k).

Light brown solid; mp. 235 °C. ^{1}H NMR (600 MHz, $CDCl_3$) δ 7.60 – 7.52 (m, 1H), 7.44 (s, 1H), 7.39 (t, J = 7.7 Hz, 1H), 7.35 (d, J = 8.0 Hz, 1H), 7.19 – 7.13 (m, 1H), 7.10 (d, J = 11.6 Hz, 1H), 3.79 (s, 1H) ppm. ^{13}C NMR (151 MHz, $CDCl_3$) δ 169.13, 140.58, 137.14, 137.02, 133.01, 129.93, 129.48, 128.78, 127.93, 127.73, 127.44, 126.60, 126.26, 126.24, 119.30, 44.66 ppm. HRMS calcd for $C_{23}H_{19}F_3NO$: 382.1418, found: 382.1089.

3.5. General procedure for the oxidative cleavage using OsO_4 for the synthesis of aldehydes (2a-n).

To a solution of **4a-n** (1 equiv) in dioxane:water (2:1) were added 2,6-lutidine (2 equiv), OsO_4 (2.5 wt% in 2-methyl-2-propanol, 2 mol%), and NaIO4 (4 equiv). The reaction mixture was stirred at room temperature overnight. Water and dichloromethane were added. The organic layer was separated, and the water layer was extracted with dichloromethane.The combined organic extract was washed with brine and dried over anhydrous sodium sulfate, and the solvent was evaporated under *vacuo*. The residue was purified by column chromatography on silica gel in ethyl acetate/hexanes (30–50%) to produce **2a-n.**

3.5.1. 2-(4-Formylphenyl)-N-phenylacetamide (2a).

White powder (93%); mp 183–185 °C. ^{1}H NMR (400 MHz, $CDCl_3$) δ 10.03 (s, 1H), 7.91 (d, J = 8.0 Hz, 2H), 7.54 (d, J = 8.0 Hz, 2H), 7.44 (d, J = 8.0 Hz, 2H), 7.30 (t, J = 7.9 Hz, 2H), 7.11 (t, J = 7.4 Hz, 2H), 3.82 (s, 2H). ^{13}C NMR (151 MHz, CDCl3) δ 191.74, 167.72, 141.25, 137.37, 135.66, 130.44, 130.17, 129.07, 124.78, 119.87, 44.79. HRMS: (ESI) calcd for $C_{15}H_{13}NO_2$ $[M + H]^+$ 240.1025; found, 240.1031.

3.5.2. N-Cyclohexyl-2-(4-formylphenyl)acetamide (2b).

White solid (40%); mp. 160 °C. ^{1}H NMR (600 MHz, $CDCl_3$) δ 10.02 (s, 1H), 8.07 (d, J = 8.2 Hz, 1H), 7.88 (d, J = 8.1 Hz, 2H), 7.46 (d, J = 8.0 Hz, 2H), 7.38 (d, J = 8.1 Hz, 1H), 5.24 (s, 1H), 3.78 (s, 1H), 3.62 (s, 2H), 1.87 (d, J = 12.4 Hz, 3H), 1.71 – 1.62 (m, 7H), 1.60 (dd, J = 13.0, 3.7 Hz, 3H), 1.37 (d, J = 3.4 Hz, 1H), 1.34 (d, J = 13.4 Hz, 2H), 1.31 (s, 1H), 1.15 (s, 1H), 1.12 (d, J = 12.6 Hz, 1H), 1.08 (s, 1H), 1.05 (d, J = 11.1 Hz, 2H), 1.03 (s, 1H) ppm. ^{13}C NMR (151 MHz, $CDCl_3$) δ 191.82, 142.15, 130.76, 130.28, 129.97, 129.49, 77.24, 77.03, 76.82, 48.49, 44.06, 32.99, 25.43, 24.74 ppm. HRMS calcd for $C_{15}H_{15}NO_2$: 246.1415, found: 246.1497.

3.5.3. 2-(4-Formylphenyl)-N-(p-tolyl)acetamide (2c).

White crystals (55%); mp. 120 °C. ^{1}H NMR (600 MHz, $CDCl_3$) δ 10.02 (s, 1H), 7.88 (d, J = 8.1 Hz, 2H), 7.46 (d, J = 8.0 Hz, 2H), 3.62 (s, 3H), 1.87 (d, J = 8.9 Hz, 3H), 1.65 (d, J = 13.6 Hz, 8H), 1.59 (d, J = 13.2 Hz, 3H), 1.34 (d, J = 13.4 Hz, 3H), 1.12 (d, J = 12.6 Hz, 1H), 1.05 (d, J = 11.1 Hz, 2H) ppm. ^{13}C NMR (151 MHz, $CDCl_3$) δ 191.73, 167.57, 141.37, 135.64, 134.80, 134.48, 130.42, 130.17, 129.54, 119.97, 44.76, 20.88 ppm.

3.5.4. 2-(4-Formylphenyl)-N-(4-methoxyphenyl)acetamide (2d).

White powder (99%); mp 193 °C. ^{1}H NMR (600 MHz, $CDCl_3$) δ 10.05

(s, 1H), 7.93 (d, $J = 8.1$ Hz, 2H), 7.56 (d, $J = 8.0$ Hz, 2H), 7.39 – 7.33 (m, 2H), 7.03 (s, 1H), 6.88 – 6.79 (m, 2H), 3.82 (s, 2H), 3.80 (s, 3H). ^{13}C NMR (151 MHz, $CDCl_3$) δ 191.74, 167.60, 156.74, 141.43, 135.63, 130.42, 130.17, 121.88, 114.17, 55.49, 44.61. HRMS: (ESI) calcd for $C_{16}H_{15}NO_3$ $[M + H]^+$ 270.1130; found, 270.1141.

3.5.5. N-(4-(Dimethylamino)phenyl)-2-(4-formylphenyl)acetamide (2e).

The product was used in the next step without further purification.

3.5.6. 2-(4-Formylphenyl)-N-(naphthalen-1-yl)acetamide (2f).

White powder (95%); mp 296 °C. ^{1}H NMR (600 MHz, $CDCl_3$) δ 10.09 (s, 1H), 8.01 (d, $J = 7.9$ Hz, 2H), 7.94 (d, $J = 7.5$ Hz, 1H), 7.87 (d, $J = 7.8$ Hz, 1H), 7.72 (d, $J = 8.2$ Hz, 1H), 7.68 (d, $J = 7.9$ Hz, 2H), 7.53 – 7.40 (m, 5H), 4.01 (s, 2H). ^{13}C NMR (151 MHz, $CDCl_3$) δ 191.66, 168.26, 141.45, 135.82, 134.06, 131.65, 130.64, 130.33, 128.90, 126.98, 126.52, 126.24, 126.07, 125.71, 120.93, 119.95, 44.83. HRMS: (ESI) calcd for $C_{19}H_{15}NO_2$ $[M + H]^+$ 290.1181; found, 290.1186.

3.5.7. N-(4-Fluorophenyl)-2-(4-formylphenyl)acetamide (2g).

Yellow powder (99%); mp 183–184 °C. ^{1}H NMR (600 MHz, $CDCl_3$) δ 10.05 (s, 1H), 7.93 (d, $J = 8.1$ Hz, 2H), 7.53 (dd, $J = 16.6$, 6.4 Hz, 2H), 7.47 – 7.38 (m, 2H), 7.17 (s, 1H), 7.06 – 6.98 (m, 2H), 3.83 (s, 2H). ^{13}C NMR (151 MHz, $CDCl_3$) δ 191.74, 167.77, 159.59 (d, $J = 244.1$ Hz), 141.14, 135.68, 133.35, 133.34, 130.31 (d, $J = 44.0$ Hz), 121.82 (d, $J = 8.0$ Hz), 115.74 (d, $J = 22.4$ Hz), 77.25, 77.04, 76.83, 44.59. HRMS: (ESI) calcd for $C_{15}H_{12}FNO_2$ $[M + H]^+$ 258.0930; found, 258.0934.

3.5.8. N-(4-Chlorophenyl)-2-(4-formylphenyl)acetamide (2h).

Cream solid (76%); mp. 195 °C. ^{1}H NMR (600 MHz, $CDCl_3$) δ 10.01 (s, 1H), 7.90 (d, $J = 8.0$ Hz, 1H), 7.50 (d, $J = 8.0$ Hz, 1H), 7.38 (d, $J = 8.8$ Hz, 1H), 7.02 (s, 1H), 3.79 (s, 1H), 1.53 (s, 1H) ppm. ^{13}C NMR (151 MHz, $CDCl_3$) δ 191.67, 167.71, 140.94, 135.93, 135.74, 130.47, 130.16, 129.78, 129.09, 121.10, 44.71 ppm.

3.5.9. N-(4-Bromophenyl)-2-(4-formylphenyl)acetamide (2i).

Yellow powder (96 mg, 89%); mp 193–196 °C. ^{1}H NMR (600 MHz, $CDCl_3$) δ 10.06 (s, 1H), 7.94 (d, $J = 8.1$ Hz, 2H), 7.55 (d, $J = 8.0$ Hz, 2H), 7.44 (d, $J = 8.9$ Hz, 2H), 7.37 (d, $J = 8.9$ Hz, 2H), 7.09 (s, $J = 8.4$ Hz, 1H), 3.83 (s, 2H). ^{13}C NMR (151 MHz, $CDCl_3$) δ 191.66, 167.70, 140.90, 136.45, 135.75, 132.04, 130.47, 130.16, 121.39, 117.39, 44.73. HRMS: (ESI) calcd for $C_{15}H_{12}BrNO_2$ $[M + H]^+$ 318.0130; found, 318.0135.

3.5.10. N-(4-pentafluorosulfaneyl)-2-(4-formylphenyl)acetamide (2j).

Yellow powder (121 mg, 98%); mp 191–193 °C. ^{1}H NMR (600 MHz, $CDCl_3$) δ 10.05 (s, 1H), 7.94 (d, $J = 8.1$ Hz, 2H), 7.71 (t, $J = 6.0$ Hz, 2H), 7.59 (d, $J = 8.9$ Hz, 2H), 7.54 (d, $J = 8.0$ Hz, 2H), 7.36 (s, 1H), 3.86 (s, 2H). ^{13}C NMR (151 MHz, $CDCl_3$) δ 191.67, 168.03, 140.55, 140.03, 135.81, 130.50, 130.15, 127.13 – 127.05 (m), 119.00, 44.70. HRMS: (ESI) calcd for $C_{15}H_{12}F_5NO_2S$ $[M + H]^+$ 366.0587; found, 366.0591.

3.5.11. 2-(4-Formylphenyl)-N-(4-(trifluoromethyl)phenyl)acetamide (2k).

Cream solid (46%); mp. 170 °C. ^{1}H NMR (400 MHz, $CDCl_3$) δ 10.05 (s, 1H), 7.94 (d, $J = 8.1$ Hz, 2H), 7.56 (dd, $J = 15.5$, 5.2 Hz, 6H), 3.86 (s, 2H), 1.56 (s, 2H) ppm. ^{13}C NMR (151 MHz, $CDCl_3$) δ 191.62, 140.64, 130.51, 130.17, 126.37, 126.34, 119.39, 44.79 ppm. HRMS calcd for $C_{16}H_{13}F_3NO_2$: 308.0898, found: 308.0907.

3.5.12. N-(4-Ethynylphenyl)-2-(4-formylphenyl)acetamide (2o).

To a stirred solution of 2-(4-(hydroxymethyl)phenyl)acetic acid (166 mg, 1 mmol, 1 equiv.) in THF (3 mL), was added DEPBT (600 mg, 2 mmol, 2 equiv.), followed by the addition of Et_3N (0.28 mL, 2 mmol, 2 equiv.). The resulting mixture was stirred at room temperature for 15 min. 4-ethynylaniline (117 mg, 1 mmol, 1 equiv.) was added and the reaction mixture was stirred overnight at room temperature. The reaction was quenched by the addition of brine and extracted with EtOAc. The combined organic extract was dried over anhydrous Na_2SO_4, filtered and concentrated under reduced pressure. The crude product was purified by column chromatography on silica in EtOAc/DCM to obtain N-(4-ethynylphenyl)-2-(4-hydroxymethyl)phenyl)acetamide as a pure product (151 mg, 57%) as a white solid. ^{1}H NMR (600 MHz, DMSO) δ 10.32 (s, 1H), 7.64 – 7.59 (m, 2H), 7.42 – 7.39 (m, 2H), 7.29 – 7.24 (m, 4H), 5.14 (br, 1H), 4.47 (s, 2H), 4.09 (s, 1H), 3.63 (s, 2H). ^{13}C NMR (151 MHz, DMSO) δ 169.94, 141.33, 140.23, 134.49, 132.84, 129.28, 126.96, 119.35, 116.52, 84.02, 80.34, 63.14, 43.51.

To a stirred solution of N-(4-ethynylphenyl)-2-(4-(hydroxymethyl) phenyl)acetamide (60 mg, 0.22 mmol, 1 equiv.) in anhydrous DCM (3 mL) was added DMP (140 mg, 0.33 mmol, 1.5 equiv) . The resulting mixture was stirred at room temperature for 5 h. The crude product was purified by column chromatography on silica in EtOAc/ hexanes (0 –〉 50 EtOAc) to obtain the pure product (52 mg, 90 %) as a white solid. ^{1}H NMR (600 MHz, DMSO) δ 10.44 (s, 1H), 9.99 (s, 1H), 7.88 (d, $J = 8.1$ Hz, 2H), 7.62 (d, $J = 8.7$ Hz, 2H), 7.56 (d, $J = 8.1$ Hz, 2H), 7.43 (d, $J = 8.6$ Hz, 2H), 4.10 (s, 1H), 3.81 (s, 2H). ^{13}C NMR (151 MHz, DMSO) δ 193.24 (s), 169.03, 143.24, 140.06, 135.28, 132.88, 130.53, 130.05, 119.43, 116.71, 83.98 , 80.40, 43.76.

3.6. General procedure for the aldol reaction using piperidine for the synthesis of final products (IPE-1–IPE-14).

To a mixture of aldehyde **2** (1 equiv) and methyl ketone **1** (1.2 equiv) in methanol in a microwave vial was added piperidine (4 equiv). The reaction mixture was heated in a microwave synthesizer for 4 h at 90 °C. The solvent was removed under reduced pressure, and the residue was purified by column chromatography on silica gel in ethyl acetate/hexanes to obtain the final products (50–75%).

3.6.1. (E)-2-(4-(3-(1H-Imidazol-2-yl)-3-oxoprop-1-en-1-yl)phenyl)-N-phenylacetamide (IPE-1).

Off-white powder (45%); mp 211–214 °C. ^{1}H NMR (600 MHz, acetone-d_6) δ 9.40 (s, 1H), 8.00 – 7.92 (m, 1H), 7.89 – 7.81 (m, 1H), 7.74 (d, $J = 8.0$ Hz, 2H), 7.64 (d, $J = 7.9$ Hz, 2H), 7.47 (d, $J = 9.4$ Hz, 3H), 7.26 (t, $J = 7.8$ Hz, 3H), 7.02 (t, $J = 7.3$ Hz, 1H), 3.75 (s, 2H). ^{13}C NMR (151 MHz, acetone-d_6) δ 178.60, 168.43, 168.34, 146.29, 142.79, 139.47, 139.38, 138.89, 133.52, 130.99, 130.92, 129.98, 129.10, 128.65, 128.62, 126.95, 123.34, 121.53, 121.30, 119.19, 119.10, 43.68, 43.64. HRMS: (ESI) calcd for $C_{20}H_{17}N_3O_2$ $[M + H]^+$ 332.1399; found, 332.1401.

3.6.2. (E)-2-(4-(3-(1H-Imidazol-2-yl)-3-oxoprop-1-en-1-yl)phenyl)-N-cyclohexylacetamide (IPE-2).

Cream solid (25%); mp. 208.5 ^{0}C. ^{1}H NMR (600 MHz, $CDCl_3$) δ 11.86 (t, $J = 11.0$ Hz, 1H), 11.66 (d, $J = 8.2$ Hz, 1H), 11.39 – 11.31 (m, 2H), 7.27 (dt, $J = 3.3$, 1.6 Hz, 3H), 5.81 (d, $J = 9.6$ Hz, 1H), 5.71 (dd, $J = 10.3$, 3.2 Hz, 1H), 5.59 (d, $J = 12.8$ Hz, 1H), 5.37 – 5.12 (m, 4H) ppm. ^{13}C NMR (151 MHz, $CDCl_3$) δ 179.30, 169.31, 146.19, 144.25, 138.09, 133.76, 129.95, 129.42, 121.21, 77.25, 77.04, 76.82, 48.37, 43.91, 32.95, 29.72, 25.44, 24.72 ppm. HRMS calcd for $C_{20}H_{23}N_3O_2$: 338.1868, found: 338.1881.

3.6.3. (E)-2-(4-(3-(1H-Imidazol-2-yl)-3-oxoprop-1-en-1-yl)phenyl)-N-(p-tolyl)acetamide (IPE-3).

Cream solid (22%); mp. 218.5 ^{0}C. ^{1}H NMR (600 MHz, CD_3OD) δ 7.86 (q, $J = 15.9$ Hz, 1H), 7.69 (d, $J = 8.1$ Hz, 1H), 7.42 (d, $J = 8.1$ Hz, 1H), 7.38 (d, $J = 8.4$ Hz, 1H), 7.07 (d, $J = 8.2$ Hz, 1H), 3.26 (s, 9H), 2.25 (s, 2H) ppm. ^{13}C NMR (151 MHz, CD_3OD) δ 178.62, 170.08, 145.98, 143.91, 143.81, 143.74, 138.77, 135.81, 133.70, 133.47, 129.67, 129.45, 128.94, 128.79, 128.70, 128.51, 120.70, 120.63, 120.53, 120.08, 120.03, 119.86, 48.02, 47.88, 47.73, 47.59, 47.45, 47.31, 47.17, 43.09, 19.51, 19.47 ppm. HRMS calcd for $C_{21}H_{19}N_3O_2$: 346.1555, found: 346.1573.

3.6.4. (E)-2-(4-(3-(1H-imidazol-2-yl)-3-oxoprop-1-en-1-yl)phenyl)-N-(4-methoxyphenyl)acetamide (IPE-4).

White powder (30%); mp 224–226 °C. ^{1}H NMR (400 MHz, CD_3OD) δ 7.97 – 7.82 (m, 2H), 7.73 (d, J = 8.2 Hz, 2H), 7.44 (dt, J = 5.4, 4.7 Hz, 5H), 7.29 (s, 1H), 6.91 – 6.81 (m, 2H), 3.76 (s, 3H), 3.71 (s, 2H). ^{13}C NMR (151 MHz, CD_3OD) δ 178.63, 169.99, 156.62, 143.85, 138.83, 133.46, 131.33, 129.55, 128.62, 121.69, 120.60, 113.54, 54.42, 42.99. HRMS: (ESI) calcd for $C_{21}H_{19}N_3O_3$ $[M + H]^+$ 362.1505; found, 362.1515.

3.6.5. (E)-2-(4-(3-(1H-imidazol-2-yl)-3-oxoprop-1-en-1-yl)phenyl)-N-(4-(dimethylamino)phenyl)acetamid (IPE-5).

Yellow powder (30%); mp 221 °C. ^{1}H NMR (600 MHz, CD_3OD) δ 7.92 (q, J = 15.9 Hz, 1H), 7.74 (dd, J = 20.6, 5.3 Hz, 1H), 7.48 (d, J = 8.1 Hz, 1H), 7.43 – 7.34 (m, 2H), 6.80 (d, J = 9.0 Hz, 1H), 3.73 (s, 2H), 2.92 (s, 3H). ^{13}C NMR (151 MHz, CD_3OD) δ 178.62, 169.86, 145.96, 143.87, 138.96, 133.43, 129.53, 128.61, 121.56, 120.59, 113.27, 42.99, 40.11. HRMS: (ESI) calcd for $C_{22}H_{22}N_4O_2$ $[M + H]^+$ 375.1821; found, 375.1811.

3.6.6. (E)-2-(4-(3-(1H-imidazol-2-yl)-3-oxoprop-1-en-1-yl)phenyl)-N-(naphthalen-1-yl)acetamide (IPE-6).

Yellow powder (55%); mp 229–230 °C. ^{1}H NMR (600 MHz, DMSO-d_6) δ 10.22 (s, 2H), 8.06 (d, J = 8.0 Hz, 3H), 8.00 – 7.91 (m, 6H), 7.86 (dd, J = 13.8, 9.1 Hz, 3H), 7.81 (d, J = 8.0 Hz, 4H), 7.78 (d, J = 8.1 Hz, 2H), 7.67 (t, J = 10.9 Hz, 3H), 7.60 – 7.46 (m, 15H), 7.28 (s, 2H), 3.89 (s, 4H). ^{13}C NMR (151 MHz, DMSO-d_6) δ 178.94, 169.89, 146.29, 143.26, 139.69, 134.16, 133.82, 133.33, 130.42, 129.21, 128.65, 128.18, 126.53, 126.38, 126.03, 125.85, 123.02, 122.23, 121.92, 43.20. HRMS: (ESI) calcd for $C_{24}H_{19}N_3O_2$ $[M + H]^+$ 382.1556; found, 382.1568.

3.6.7. (E)-2-(4-(3-(1H-Imidazol-2-yl)-3-oxoprop-1-en-1-yl)phenyl)-N-(4-fluorophenyl)acetamide (IPE-7).

White powder (30%); mp 224–226 °C. ^{1}H NMR (400 MHz, CD_3OD) δ 7.95 – 7.83 (m, 2H), 7.72 (d, J = 8.2 Hz, 2H), 7.58 – 7.53 (m, 2H), 7.45 (d, J = 8.2 Hz, 2H), 7.29 (s, 1H), 7.07 – 7.00 (m, 2H), 3.72 (s, 2H). ^{13}C NMR (151 MHz, CD_3OD) δ 178.62, 170.16, 159.33 (d, J = 242.0 Hz), 145.96, 143.80, 138.59, 134.63, 133.51, 129.57, 128.62, 121.73 (d, J = 7.7 Hz), 120.64, 114.88 (d, J = 22.6 Hz), 43.00. HRMS: (ESI) calcd for $C_{20}H_{16}FN_3O_2$ $[M + H]^+$ 350.1305; found, 350.1310.

3.6.8. (E)-2-(-4(3-(1H-imidazol-2-yl)-3-oxoprop-1-en-1-yl)phenyl)-N-(4-chlorophenyl)acetamide (IPE-8).

Cream solid (51%); mp. 244 ^{0}C. ^{1}H NMR (600 MHz, CD_3OD) δ 7.92 – 7.84 (m, 1H), 7.72 (d, J = 8.2 Hz, 1H), 7.57 – 7.54 (m, 1H), 7.44 (d, J = 8.2 Hz, 1H), 7.35 (s, 1H), 7.29 – 7.26 (m, 1H), 3.71 (d, J = 10.5 Hz, 1H), 3.35 – 3.32 (m, 1H), 1.32 – 1.25 (m, 2H) ppm. ^{13}C NMR (151 MHz, CD_3OD) δ 143.78, 138.49, 129.59, 128.72, 128.61, 128.40, 121.13, 120.67, 43.08 ppm. HRMS calcd for $C_{20}H_{16}ClN_3O_2$: 366.1009, found: 366.1037.

3.6.9. (E)-2-(-4(3-(1H-imidazol-2-yl)-3-oxoprop-1-en-1-yl)phenyl)-N-(4-bromophenyl)acetamide (IPE-9).

Yellow powder (41 mg, 41%); mp 209–212 °C. ^{1}H NMR (600 MHz, CD_3OD) δ 7.91 (q, J = 15.9 Hz, 2H), 7.74 (d, J = 8.2 Hz, 2H), 7.56 – 7.52 (m, 2H), 7.48 – 7.42 (m, 5H), 7.35 (s, J = 7.5 Hz, 1H), 3.75 (s, 2H). ^{13}C NMR (151 MHz, CD_3OD) δ 178.61, 170.23, 145.97, 143.77, 138.46, 137.79, 133.54, 131.42, 129.59, 128.61, 121.43, 120.68, 116.19, 43.10. HRMS: (ESI) calcd for $C_{20}H_{16}BrN_3O_2$ $[M + H]^+$ 410.0504; found, 410.0508.

3.6.10. (E)-2-(-4(3-(1H-imidazol-2-yl)-3-oxoprop-1-en-1-yl)phenyl)-N-(4-pentafluorosulfaneyl)acetamide (IPE-10).

White powder (34 mg, 30%); mp 196–197 °C. ^{1}H NMR (600 MHz, CD_3OD) δ 7.92 (q, J = 15.9 Hz, 2H), 7.82 – 7.72 (m, 7H), 7.48 (d, J = 8.1 Hz, 2H), 7.42 (d, J = 16.4 Hz, 1H), 7.32 (s, 1H), 3.80 (s, 2H). ^{13}C NMR (151 MHz, CD_3OD) δ 178.62, 170.54, 146.00, 143.75, 141.76, 138.18, 133.60, 129.65, 128.62, 126.54, 120.72, 118.88, 43.10. HRMS: (ESI) calcd for $C_{20}H_{16}F_5N_3O_2S$ $[M + H]^+$ 458.0962; found, 458.0974.

3.6.11. (E)-2-(4-(3-(1H-Imidazole-2-yl)-3-oxoprop-1-en-1-yl)phenyl)-N-(4-(trifluoromethyl)phenyl)acetamide (IPE-11).

Cream solid (30%); mp. 240.5 ^{0}C. ^{1}H NMR (600 MHz, CD_3OD) δ 7.90 (q, J = 15.9 Hz, 2H), 7.78 (d, J = 8.6 Hz, 3H), 7.74 (d, J = 8.2 Hz, 3H), 7.60 (d, J = 8.7 Hz, 3H), 7.46 (d, J = 8.1 Hz, 3H), 7.42 (s, 1H), 7.29 (s, 1H), 5.50 (s, 1H), 3.78 (s, 3H), 2.01 (s, 1H) ppm. ^{13}C NMR (151 MHz, CD_3OD) δ 178.62, 178.60, 170.52, 170.50, 145.97, 143.76, 142.06, 138.29, 133.58, 130.14, 129.63, 128.62, 125.66, 125.63, 125.16, 120.70, 119.37, 43.14 ppm. HRMS calcd for $C_{21}H_{17}F_3N_3O_2$: 400.1273, found: 413.2071.

3.6.12. (E)-2-(-4(3-(1H-imidazol-2-yl)-3-oxoprop-1-en-1-yl)phenyl)-N-(3,4,5-trifluorophenyl)acetamide (IPE-12).

Brown solid (22 mg, 21.7%). TLC R_f = 0.1 (50% ethyl acetate/hexanes), mp 255 °C. ^{1}H NMR (600 MHz, MeOD) δ 7.92 (q, J = 15.9 Hz, 3H), 7.75 (d, J = 8.2 Hz, 2H), 7.43 (ddd, J = 13.4, 8.5, 5.5 Hz, 5H), 7.31 (s, 1H), 3.75 (s, 2H). ^{13}C NMR (151 MHz, MeOD) δ 178.60 (s), 170.35 (s), 151.70 – 151.55 (m), 150.07 – 149.92 (m), 145.97 (s), 143.71 (s), 138.06 (s), 133.63 (s), 130.14 (s), 129.61 (s), 128.62 (s), 121.40 (s), 120.74 (s), 103.64 (dd, J = 20.4, 5.6 Hz). HRMS calcd for $C_{20}H_{14}F_3N_3O_2$ $[M + H]^+$ 386.1116, found: 386.1120.

3.6.13. (E)-2-(-4(3-(1H-imidazol-2-yl)-3-oxoprop-1-en-1-yl)phenyl)-N-(perfluorophenyl)acetamide (IPE-13).

Brown solid (16 mg, 13.07%). TLC R_f = 0.5 (50% ethyl acetate/hexanes), mp 235 °C. ^{1}H NMR (600 MHz, CD_3OD) δ 7.90 (q, J = 15.9 Hz, 2H), 7.75 (d, J = 8.1 Hz, 2H), 7.46 (d, J = 8.0 Hz, 2H), 7.41 (s, 1H), 7.29 (s, 1H), 3.83 (s, 2H). ^{13}C NMR (151 MHz, MeOD) δ 178.61 (s), 170.87 – 170.85 (m), 146.01 – 145.94 (m), 137.75 (s), 133.73 (s), 130.59 (s), 130.23 – 130.02 (m), 129.59 (s), 128.66 (s), 128.51 (s), 120.82 (s), 41.71 (s). HRMS calcd for $C_{20}H_{12}F_5N_3O_2$ $[M + H]^+$ 422.0927 found: 422.0913.

3.6.14. (E)-2-(-4(3-(1H-imidazol-2-yl)-3-oxoprop-1-en-1-yl)phenyl)-N-(bis(3,5-trifluoromethyl)phenyl)acetamide (IPE-14).

Brown solid (16 mg, 13.07%). TLC R_f = 0.5 (50% ethyl acetate/hexanes), mp 235 °C. ^{1}H NMR (600 MHz, CD_3OD) δ 8.19 (s,2H), 7.86 (q, J = 15.9 Hz, 2H), 7.71 (d, J = 8.2 Hz, 2H), 7.61 (s, 1H), 7.43 (d, J = 8.1 Hz, 2H), 7.38 (s, 1H), 7.25 (s, 1H), 3.76 (s, 2H). ^{13}C NMR (151 MHz, MeOD) δ 178.61 (s), 170.74 (s), 145.97 (s), 143.73 (s), 140.68 (s), 137.89 (s), 131.86 (q, J = 33.3 Hz), 130.12 (s), 129.67 (s), 128.65 (s), 124.20 (s), 122.39 (s), 121.40 (s), 120.77 (s), 119.02 (s), 116.32 (s), 43.10 (s). HRMS calcd for $C_{22}H_{15}F_6N_3O_2$ $[M + H]^+$ 468.1146 found: 468.1164.

3.7. General procedure for the synthesis of the alkylated imidazole (IPE-15–IPE-26).

To a stirred solution of unalkylated imidazole based compounds (1 equiv) in dimethylformamide (0.5 mL) were added alkyl halide (1.2 equiv), and sodium carbonate (18 mg, 0.12 mmol, 2 equiv). The reaction mixture was stirred overnight at room temperature. Water (1 mL) and dichloromethane (2 mL) were added. The organic layer was separated, and the water layer was extracted with dichloromethane (3 × 2 mL). The combined organic extract was washed with brine, dried over anhydrous sodium sulfate, and the solvent was evaporated under vacuo. The residue was purified by column chromatography on silica gel in methanol/dichloromethane (0–2%), followed by reversed phase chromatography on C18 in methanol/water (20–60%) to produce the alkylated final compounds.

3.7.1. (E)-N-Cyclohexyl-2-(4-(3-(1-methyl-1H-imidazol-2-yl)-3-oxoprop-1-en-1-yl)phenyl)acetamide (IPE-15).

White crystals (6.0 mg, 38%), mp. 182.5 ^{0}C, ^{1}H NMR (600 MHz, CD_3OD) δ 8.13 (d, J = 6.7 Hz, 1H), 7.98 (d, J = 15.9 Hz, 1H), 7.79 (d, J = 15.9 Hz, 1H), 7.69 (d, J = 8.1 Hz, 2H), 7.49 (s, 1H), 7.42 – 7.35 (m, 3H), 7.21 (s, 1H), 7.09 (s, 1H), 4.09 (s, 3H), 3.69 – 3.58 (m, 1H), 3.52 (s, 2H), 1.91 – 1.59 (m, 7H), 1.42 – 1.28 (m, 3H), 1.27 – 1.14 (m, 4H) ppm. ^{13}C NMR (151 MHz, CD_3OD) δ 179.85, 171.01, 143.20, 138.98, 133.43, 129.33, 128.47, 127.91, 121.87, 48.54, 42.34, 35.33, 32.32, 25.22, 24.71 ppm. HRMS calcd for $C_{21}H_{25}N_3O_2$: 352.2025, found: 352.2038

3.7.2. (E)-2-(4-(3-(1-Methyl-1H-imidazol-2-yl)-3-oxoprop-1-en-1-yl) phenyl)-N-phenylacetamide (IPE-16).

The starting material were **IPE-1** and methyl iodide. A white powder was produced (6 mg, 60%); mp 184–186 °C. ^{1}H NMR (400 MHz, acetone-d_6) δ 9.40 (s, 1H), 8.11 (d, J = 16.1 Hz, 1H), 7.81 – 7.68 (m, 3H), 7.66 (d, J = 8.2 Hz, 2H), 7.49 (d, J = 8.1 Hz, 2H), 7.39 (d, J = 8.5 Hz, 1H), 7.28 (t, J = 7.9 Hz, 2H), 7.16 (s, 1H), 7.04 (t, J = 7.4 Hz, 1H), 4.08 (s, 3H), 3.77 (s, 2H). ^{13}C NMR (151 MHz, acetone-d_6) δ 179.74, 168.44, 143.95, 141.85, 139.47, 138.68, 133.63, 129.95, 128.97, 128.64, 128.52, 127.90, 123.34, 122.84, 119.19, 43.68, 35.45. HRMS: (ESI) calcd for $C_{21}H_{19}N_3O_2$ $[M + H]^+$ 346.1556; found, 346.1554.

3.7.3. (E)-N-(4-chlorophenyl)-2-(4-(3-(1-methyl-1H-imidazol-2-yl)-3-oxoprop-1-en-1-yl)phenyl)acetamide (IPE-17).

Cream solid (10 mg, 12%); mp. 250 °C. ^{1}H NMR (600 MHz, CD_3OD) δ 8.01 – 7.78 (m, 1H), 7.72 (d, J = 8.1 Hz, 1H), 7.59 – 7.55 (m, 1H), 7.44 (d, J = 8.1 Hz, 1H), 7.40 (s, 1H), 7.31 – 7.28 (m, 1H), 7.20 (s, 1H), 4.08 (s, 1H), 3.72 (d, J = 9.6 Hz, 1H) ppm. ^{13}C NMR (151 MHz, CD_3OD) δ 179.83, 170.25, 143.13, 143.05, 138.29, 137.31, 133.62, 129.55, 128.71, 128.55, 128.40, 128.35, 127.93, 121.99, 121.12, 43.07, 35.33 ppm. HRMS calcd for $C_{21}H_{18}ClN_3O_2$ $[M + H]^+$ 380.1165, found: 380.1170.

3.7.4. (E)-N-(4-Bromophenyl)-2-(4-(3-(1-methyl-1H-imidazol-2-yl)-3-oxoprop-1-en-1-yl)phenyl)acetamide (IPE-18).

The starting material were **IPE-9** and methyl iodide. A white powder was produced (7 mg, 60%); mp 221–223 °C. ^{1}H NMR (600 MHz, acetone-d_6) δ 9.53 (s, 1H), 8.14 (d, J = 16.2 Hz, 1H), 7.79 (dd, J = 16.3, 12.1 Hz, 3H), 7.67 (d, J = 16.1 Hz, 2H), 7.50 – 7.43 (dd, J = 12.1, 12.5 Hz, 4H), 7.39 (s, 1H), 7.18 (s, 1H), 4.11 (s, 3H), 3.78 (s, 2H). ^{13}C NMR (151 MHz, acetone-d_6) δ 179.72, 168.65, 143.95, 141.79, 138.77, 138.36, 133.70, 131.58, 129.97, 128.98, 128.54, 127.91, 122.90, 121.05, 115.21, 43.61, 35.44. ^{13}C NMR (151 MHz, acetone-d_6) δ 179.72, 168.65, 143.95, 141.79, 138.77, 138.36, 133.70, 131.58, 129.97, 128.98, 128.54, 127.91, 122.90, 121.05, 115.21, 43.61, 35.44. HRMS: (ESI) calcd for $C_{21}H_{18}BrN_3O_2$ $[M + H]^+$ 424.0661; found, 424.0668.

3.7.5. (E)-N-(4-Fluorophenyl)-2-(4-(3-(1-methyl-1H-imidazol-2-yl)-3-oxoprop-1-en-1-yl)phenyl)acetamide (IPE-19).

The starting material were **IPE-7** and methyl iodide. A white powder was produced (7.5 mg, 33%); mp 213 °C. ^{1}H NMR (600 MHz, acetone-d_6) δ 9.45 (s, 1H), 8.12 (d, J = 16.1 Hz, 1H), 7.77 (dd, J = 16.4, 12.1 Hz, 3H), 7.72 – 7.65 (m, 2H), 7.50 (d, J = 8.1 Hz, 2H), 7.42 (s, 1H), 7.18 (d, J = 0.8 Hz, 1H), 7.11 – 7.04 (m, 2H), 4.10 (s, 3H), 3.77 (s, 2H). ^{13}C NMR (151 MHz, acetone-d_6) δ 179.73, 168.37, 158.70 (d, J = 240.5 Hz),143.96, 141.80, 138.55, 135.76, 133.66, 129.95, 128.98, 128.52, 127.90, 122.87, 120.96 (d, J = 7.7 Hz), 115.06 (d, J = 22.8 Hz), 43.55, 35.44. HRMS: (ESI) calcd for C21H18FN3O2 $[M + H]^+$ 364.1461; found, 364.1468.

3.7.6. (E)-2-(4-(3-(1-Benzyl-1H-imidazol-2-yl)-3-oxoprop-1-en-1-yl) phenyl)-N-(4-fluorophenyl)acetamide (IPE-20).

The starting material were **IPE-7** and benzyl bromide. A white powder was produced (5.5 mg, 67%); mp 200–202 °C. ^{1}H NMR (600 MHz, $CDCl_3$) δ 8.14 (d, J = 16.0 Hz, 1H), 7.83 (d, J = 15.9 Hz, 1H), 7.73 (d, J = 8.0 Hz, 2H), 7.44 – 7.35 (m, 6H), 7.33 (t, J = 7.2 Hz, 1H), 7.26 (d, J = 7.4 Hz, 2H), 7.17 (s, 1H), 7.08 (s, 1H), 7.01 (t, J = 8.6 Hz, 2H), 5.78 (s, 2H), 3.78 (s, 2H). ^{13}C NMR (151 MHz, $CDCl_3$) δ 180.29, 168.38, 160.33, 158.72, 143.55, 142.62, 136.62, 136.47, 134.48, 133.46, 130.05, 129.85, 129.53, 128.93, 128.13, 127.60, 126.45, 123.34, 121.79, 121.73, 115.73, 115.59, 51.98, 44.55. HRMS: (ESI) calcd for $C_{27}H_{22}FN_3O_2$ $[M + H]^+$ 440.1774; found, 440.1771.

3.7.7. (E)-2-(4-(3-(1-Ethyl-1H-imidazol-2-yl)-3-oxoprop-1-en-1-yl) phenyl)-N-(4-fluorophenyl)acetamide (IPE-21).

The starting material were **IPE-7** and the alkyl halide is ethyl iodide. A white powder was produced (6.5 mg, 63%); mp 219–220 °C. ^{1}H NMR (400 MHz, $CDCl_3$) δ 8.11 (d, J = 16.0 Hz, 1H), 7.80 (d, J = 16.0 Hz, 1H), 7.72 (d, J = 8.0 Hz, 2H), 7.43 – 7.34 (m, 4H), 7.24 (s, 1H), 7.17 (s, 1H), 7.07 (s, 1H), 6.98 (t, J = 8.6 Hz, 2H), 4.55 (q, J = 7.2 Hz, 2H), 3.76 (s, 2H), 1.48 (t, J = 7.2 Hz, 3H). ^{13}C NMR (151 MHz, $CDCl_3$) δ 180.11, 168.39, 159.53 (d, J = 244.2 Hz), 143.40, 142.29, 136.53, 134.56, 133.45, 130.04, 129.64, 129.52, 125.73, 123.50, 121.76 (d, J = 8.1 Hz), 115.66 (d, J = 22.6 Hz), 44.56, 44.06, 29.72, 16.55. HRMS: (ESI) calcd for $C_{22}H_{20}FN_3O_2$ $[M + H]^+$ 379.1618; found, 379.1618.

3.7.8. (E)-2-(4-(3-(1-Methyl-1H-imidazol-2-yl)-3-oxoprop-1-en-1-yl) phenyl)-N-(4-(pentafluoro- λ^6-sulfanyl)phenyl)acetamide (IPE-22).

The starting material were **IPE-10** and methyl iodide. A white powder was produced (5 mg, 56%); mp 215–216 °C. ^{1}H NMR (600 MHz, acetone-d_6) δ 9.81 (s, 1H), 8.09 (d, J = 16.1 Hz, 1H), 7.85 (d, J = 8.9 Hz, 2H), 7.79 (d, J = 9.2 Hz, 2H), 7.73 (dd, J = 12.2, 8.3 Hz, 3H), 7.46 (d, J = 8.0 Hz, 2H), 7.39 (s, 1H), 7.14 (s, 1H), 4.06 (s, 3H), 3.81 (s, 2H). ^{13}C NMR (151 MHz, acetone-d_6) δ 179.71, 169.22, 143.95, 142.51, 141.74, 138.00, 133.79, 130.02, 128.99, 128.56, 127.92, 126.81, 122.96, 118.70, 43.58, 35.44. HRMS: (ESI) calcd for $C_{21}H_{18}F_5N_3O_2S$ $[M + H]^+$ 472.1118; found, 472.1119.

3.7.9. (E)-2-(4-(3-(1-methyl-1H-imidazol-2-yl)-3-oxoprop-1-en-1-yl) phenyl)-N-(4-(trifluoromethyl)phenyl)acetamide (IPE-23).

Brown solid (27 mg, 27%). TLC R_f = 0.2 (50% ethyl acetate/hexanes), mp 218 °C. ^{1}H NMR (600 MHz, $CDCl_3$) δ 8.08 (d, J = 16.0 Hz, 1H), 7.81 (d, J = 16.0 Hz, 1H), 7.70 (d, J = 8.0 Hz, 2H), 7.57 (dd, J = 24.3, 8.3 Hz, 5H), 7.41 (br, J = 12.3 Hz, 1H), 7.37 (d, J = 7.8 Hz, 2H), 7.24 (s, 1H), 7.12 (s, 1H), 4.12 (s, 3H), 3.79 (s, 2H). ^{13}C NMR (151 MHz, $CDCl_3$) δ 180.30 (s), 168.60 (s), 143.97 (s), 142.33 (s), 140.51 (s), 136.14 (s), 134.64 (s), 130.02 (s), 129.57 (s), 129.43 (s), 127.45 (s), 126.27 (q, J = 3.8 Hz), 123.36 (s), 119.34 (s), 44.73 (s), 36.44 (s).). HRMS calcd for $C_{22}H_{18}F_3N_3O_2$ $[M + H]^+$ 414.1429, found: 414.1441.

3.7.10. (E)-2-(4-(3-(1-methyl-1H-imidazol-2-yl)-3-oxoprop-1-en-1-yl) phenyl)-N-(3,4,5-trifluorophenyl)acetamide (IPE-24).

Brown solid (49 mg, 23.4%). TLC R_f = 0.1 (50% ethyl acetate/hexanes), mp 222 °C. ^{1}H NMR (600 MHz, $CDCl_3$) δ 8.09 (d, J = 16.0 Hz, 1H), 7.82 (d, J = 16.0 Hz, 1H), 7.72 (d, J = 8.1 Hz, 2H), 7.36 (d, J = 8.1 Hz, 2H), 7.25 (s, 1H), 7.18 (dt, J = 10.5, 5.3 Hz, 2H), 7.12 (s, 2H), 4.12 (s, 3H), 3.77 (s, 2H). ^{13}C NMR (151 MHz, $CDCl_3$) δ 180.19 (s), 168.56 (s), 151.98 – 151.79 (m), 150.32 – 150.15 (m), 142.39 (s), 137.58 – 137.19 (m), 135.94 (s), 134.69 (s), 133.20 – 132.93 (m), 129.99 (s), 129.59 (s), 127.43 (s), 123.38 (s), 104.19 (dd, J = 20.1, 6.0 Hz), 44.55 (s), 36.48 (s). HRMS (ESI) calcd for $C_{21}H_{16}F_3N_3O_2$ $[M + H]^+$ 400,1272, found: 400.1273.

3.7.11. (E)-2-(4-(3-(1-methyl-1H-imidazol-2-yl)-3-oxoprop-1-en-1-yl) phenyl)-N-(perfluorophenyl)acetamide (IPE-25).

Brown solid (30 mg, 13.1%). TLC R_f = 0.7 (50% ethyl acetate/hexanes), mp 248 °C. ^{1}H NMR (600 MHz, $CDCl_3$) δ 8.07 (d, 1H), 7.79 (d, J = 13.4 Hz, 1H), 7.72 (d, J = 8.1 Hz, 2H), 7.39 (d, J = 13.5 Hz, 2H), 7.22 (s, 1H), 7.11 (s, 1H), 6.87 (br, 1H), 4.11 (s, 3H), 3.86 (s, 2H). ^{13}C NMR (151 MHz, $CDCl_3$) δ 180.27 (s), 168.84 (s), 143.94 (s), 142.33 (s), 141.28 – 141.05 (m), 139.62 – 139.26 (m), 138.76 – 138.40 (m), 137.09 – 136.77

(m), 129.95 (s), 129.58 (s), 129.40 (s), 127.47 (s), 123.32 (s), 43.28 (s), 36.45 (s). HRMS (ESI) calcd for $C_{21}H_{14}F_5N_3O_2$ [M + H]$^+$ 436.1084, found: 436.1093.

3.7.12. (E)-N-(3,5-bis(trifluoromethyl)phenyl)-2-(4-(3-(1-methyl-1H-imidazol-2-yl)-3-oxoprop-1-en-1-yl)phenyl)acetamide (IPE-26).

Brown solid (30 mg, 30%). TLC R_f = 0.7 (50% ethyl acetate/hexanes), mp 215 °C. ^{1}H NMR (600 MHz, $CDCl_3$) δ 8.11 (d, J = 16.0 Hz, 1H), 7.99 (s, 2H), 7.82 (d, J = 16.0 Hz, 1H), 7.74 (d, J = 8.1 Hz, 2H), 7.59 (s, 1H), 7.56 (br, 1H), 7.38 (d, J = 8.0 Hz, 2H), 7.26 (s, 1H), 7.13 (s, 1H), 4.13 (s, 3H), 3.82 (s, 2H). ^{13}C NMR (151 MHz, $CDCl_3$) δ 168.89 (s), 138.99 (s), 135.85 (s), 134.69 (s), 132.35 (q, J = 33.5 Hz), 130.02 (s), 129.67 (s), 127.44 (s), 127.44 (s), 123.91 (s), 123.33 (s), 122.10 (s), 119.49 (s), 117.79 (s), 44.55 (s), 36.52 (s). HRMS (ESI) calcd for $C_{23}H_{17}F_6N_3O_2$ [M + H]$^+$ 482,1303, found: 482.1321.

3.7.13. (E)-N-(4-Ethynylphenyl)-2-(4-(3-(1-methyl-1H-imidazol-2-yl)-3-oxoprop-1-en-1-yl)phenyl)acetamide (IPE-27).

White solid (59 mg, 23%), m.p 242 °C ^{1}H NMR (600 MHz, DMSO) δ 10.39 (s, 1H), 8.02 (d, J = 16.1 Hz, 1H), 7.74 (m, , 3H), 7.63 (d, J = 8.7 Hz, 2H), 7.58 (s, 1H), 7.44 – 7.40 (m, 4H), 7.21 (d, J = 0.7 Hz, 1H), 4.10 (s, 1H), 4.02 (s, 3H), 3.73 (s, 2H), ^{13}C NMR (151 MHz, DMSO) δ 179.85, 169.41, 143.75, 142.51, 140.14, 139.00, 133.42, 132.87, 130.40, 129.50, 129.13, 129.09, 123.02, 119.39, 116.63, 83.99, 80.39, 43.65, 36.32. HRMS (ESI) calcd for $C_{23}H_{19}N_3O_2$ [M + H]$^+$ 370.1556, found: 370.1563.

3.7.14. 2-(4-(3-(1H-imidazol-2-yl)-3-oxopropyl)phenyl)-N-phenylacetamide (IPE-28).

A mixture of (*E*)-2-(4-(3-(1H-Imidazol-2-yl)-3-oxoprop-1-en-1-yl) phenyl)-*N*-phenylacetamide **IPE-1** (7 mg, 0.021 mmol, 1 equiv) and 5% Pd/C (10 wt%) in MeOH (1 mL) was stirred under hydrogen at 3 atm for 5 h. After disappearance of starting material (TLC), the reaction mixture was filtered through a pad of celite, concentrated in *vacuo*, and the residue was purified by column chromatography on silica gel in ethyl acetate/hexanes (30–50%) to give **IPE-28** as a white powder (5.5 mg, 79%); mp 193–195 °C. ^{1}H NMR (400 MHz, acetone-$_{d6}$) δ 9.28 (s, 1H), 7.64 (d, J = 7.6 Hz, 2H), 7.40 (s, 1H), 7.26 (dt, J = 17.9, 6.5 Hz, 6H), 7.18 (s, 1H), 7.03 (t, J = 7.4 Hz, 1H), 3.64 (s, 2H), 3.36 (dd, J = 9.4, 5.9 Hz, 2H), 3.00 (t, J = 7.6 Hz, 2H). ^{13}C NMR (151 MHz, acetone-$_{d6}$) δ 190.04, 168.99, 145.34, 139.86, 139.56, 133.59, 130.60, 129.27, 129.16, 128.60, 128.39, 126.76, 123.21, 120.89, 120.74, 119.11, 43.51, 39.02. HRMS: (ESI) calcd for $C_{20}H_{19}N_3O_2$ [M + H]$^+$ 334.1555; found, 334.1559.

3.7.15. N-(4-bromophenyl)-2-(4-(2-(1-methyl-1H-imidazole-2-carbonyl) cyclopropyl)phenyl)acetamide (IPE-29).

A mixture of (Z)-3-(4-(2-(4-bromophenyl)-2-oxoethyl)phenyl)-1-(1-methyl-1H-imidazol-2-yl)prop-2-en-1-one (43 mg , 0.0912 mmol) and palladium acetate (2 mg, 0.045 mmol, 10 mol%) were dissolved in anhydrous diethyl ether (1.5 mL) at −78 °C. A saturated solution of diazomethane in anhydrous ether (5 mL) was added dropwise. The reaction mixture was allowed to slowly warm up to room temperature and stirred at this temperature for 12 h. Water (1 mL) was added and the mixture was extracted with EtOAc (3 × 2 mL). The combined organic extract was dried over anhydrous sodium sulfate and filtered. The solvent was removed under reduced pressure, and the residue was purified by column chromatography on silica gel in ethyl acetate/hexanes (30–60%) to obtain **IPE-29** (7 mg, 16%) as a dark brown semi solid: TLC Rf = 0.6 (80% EtOAc-hexanes); ^{1}H NMR (600 MHz, acetone-$_{d6}$) δ 9.46 (s, 1H), 7.66 (m, 2H), 7.47 (m, 2H), 7.37 (s, 1H), 7.32 (d, J = 8.2 Hz, 2H), 7.22 (m, 2H), 7.09 (d, J = 0.8 Hz, 1H), 4.02 (s, 3H), 3.68 (s, 2H), 3.61 (ddd, J = 8.3, 5.4, 4.1 Hz, 1H), 2.54 (ddd, J = 9.1, 6.5, 4.1 Hz, 1H), 2.10 (s, 1H), 1.71 (ddd, J = 9.2, 5.4, 3.9 Hz, 1H), 1.52 (ddd, J = 8.3, 6.5, 3.9 Hz, 1H). ^{13}C NMR (151 MHz, acetone-d_6) δ 189.28, 169.12, 143.44, 139.41, 138.84, 133.81, 131.53, 129.27, 129.00, 127.64, 126.14, 121.02, 115.09, 76.33, 55.04, 43.43, 35.27, 18.29; HRMS: (ESI) calcd for $C_{22}H_{20}$ Br N_3O_2 [M + H]$^+$ 437.0701; found, 438.0817.

3.7.16. (E)-2-(4-(3-Oxo-3-(thiazol-2-yl)prop-1-en-1-yl)phenyl)-N-phenylacetamide (TPE-30).

To a mixture of 2-(4-formylphenyl)-*N*-phenylacetamide **2a** (30 mg, 0.125 mmol, 1 equiv) and 1-(thiazol-2-yl)ethan-1-one **15a** (19 mg, 0.15 mmol, 1.2 equiv) in methanol (4 mL) in a microwave vial was added piperidine (33 mg, 0.375 mmol, 3 equiv). The reaction mixture was heated in a microwave synthesizer for 6 h at 90 °C. The solvent was removed under reduced pressure, and the residue was purified by column chromatography on silica gel in ethyl acetate/hexanes (30–60%) to give **TPE-30** as a yellow powder (23 mg, 55%); mp 185–187 °C. ^{1}H NMR (400 MHz, CD_3OD) δ 8.12 (d, J = 3.0 Hz, 6H), 8.01 – 7.97 (m, 19H), 7.74 (d, J = 8.2 Hz, 14H), 7.58 – 7.53 (m, 15H), 7.47 (d, J = 8.2 Hz, 14H), 7.30 (t, J = 8.0 Hz, 17H), 7.09 (t, J = 7.4 Hz, 8H), 3.74 (s, 13H). ^{13}C NMR (151 MHz, CD_3OD) δ 181.50, 170.17, 168.30, 145.20, 144.65, 139.03, 138.41, 133.37, 129.64, 128.79, 128.43, 126.93, 123.96, 120.00, 119.87, 43.12. HRMS: (ESI) calcd for $C_{20}H_{16}N_2O_2S$ [M + H]$^+$ 349.1011; found, 349.1027.

3.7.17. (E)-2-(4-(3-Oxo-3-(pyrimidin-2-yl)prop-1-en-1-yl)phenyl)-N-phenylacetamide (TPE-31).

To a mixture of 2-(4-formylphenyl)-*N*-phenylacetamide **2a** (30 mg, 0.125 mmol, 1 equiv) and 1-(pyrimidin-2-yl)ethan-1-one **15b** (18 mg, 0.15 mmol, 1.2 equiv) in methanol (4 mL) in a microwave vial was added piperidine (33 mg, 0.375 mmol, 3 equiv). The reaction mixture was heated in a microwave synthesizer for 3 h at 85 °C. The solvent was removed under reduced pressure, and the residue was purified by column chromatography on silica gel in ethyl acetate/hexanes (30–80%) to give **TPE-31** as a yellow oily (24 mg, 45%). ^{1}H NMR (600 MHz, acetone-d_6) δ 9.40 (s, 1H), 9.04 (d, J = 4.8 Hz, 2H), 8.06 (d, J = 16.1 Hz, 1H), 7.86 (d, J = 16.1 Hz, 1H), 7.79 (d, J = 8.2 Hz, 2H), 7.71 (t, J = 4.8 Hz, 1H), 7.67 (d, J = 7.7 Hz, 2H), 7.52 (d, J = 8.1 Hz, 2H), 7.30 (t, J = 8.0 Hz, 2H), 7.06 (t, J = 7.4 Hz, 1H), 3.79 (s, 2H). ^{13}C NMR (151 MHz, acetone-d_6) δ 187.31, 168.36, 161.54, 157.76, 144.70, 139.47, 139.19, 133.44, 130.02, 128.74, 128.64, 123.34, 123.05, 121.94, 119.18, 43.68. HRMS: (ESI) calcd for $C_{21}H_{17}N_3O_2$ [M + H]$^+$ 344.1399; found, 344.1404.

3.7.18. (E)-2-(4-(3-(2-Hydroxyphenyl)-3-oxoprop-1-en-1-yl)phenyl)-N-phenylacetamide (HPE-32), and 2-(4-(1-Hydroxy-3-(2-hydroxyphenyl)-3-oxopropyl)phenyl)-N-phenylacetamide (HPE-34).

To a stirred solution of a mixture of (*E*)-2-(4-(3-(2-hydroxyphenyl)-3-oxoprop-1-en-1-yl)phenyl)acetic acid **17a** and 2-(4-(1-hydroxy-3-(2-hydroxyphenyl)-3-oxopropyl)phenyl)acetic acid **17b** (4:1) (65 mg, 0.17 mmol, 1 equiv) in dichloromethane (2 mL) were added 1-ethyl-3-(3-dimethylaminopropyl)carbodiimide (51 mg, 0.34 mmole, 2 equiv), DMAP (4 mg, 0.034 mmol, 0.2 equiv), and aniline **19a** (34 mg, 0.34 mmole, 2 equiv). The reaction mixture was stirred at room temperature overnight. Water (3 mL) was added, the organic layer was separated, and the water layer was extracted with dichloromethane (3 × 5 mL). The combined organic extract was washed with brine and dried over anhydrous sodium sulfate, and the solvent was evaporated under reduced pressure. The residue was purified by column chromatography on silica gel in ethyl acetate/ dichloromethane (0.5–4%) to give **HPE-32** as a yellow powder (32 mg, 70%); mp 233–235 °C. ^{1}H NMR (600 MHz, $CDCl_3$) δ 7.91 (dd, J = 8.5, 7.1 Hz, 2H), 7.67 (t, J = 12.3 Hz, 3H), 7.53 – 7.47 (m, 1H), 7.42 (dd, J = 7.4, 6.3 Hz, 4H), 7.28 (dd, J = 16.5, 8.3 Hz, 2H), 7.09 (dd, J = 14.4, 6.9 Hz, 2H), 7.03 (dd, J = 8.4, 0.8 Hz, 1H), 6.97 – 6.91 (m, 1H), 3.77 (s, 2H). ^{13}C NMR (151 MHz, $CDCl_3$) δ 193.63, 168.21, 163.64, 144.64, 137.46, 137.34, 136.55, 134.04, 130.22, 129.66, 129.39, 129.04, 124.68, 120.46, 119.98, 119.83, 118.93, 118.71, 44.68. HRMS: (ESI) calcd for $C_{23}H_{19}NO_3$ [M + H]$^+$ 358.1143; found, 358.1441. And **HPE-34** as a white powder (10 mg, 77%); mp 211–212 °C. ^{1}H NMR (600 MHz, $CDCl_3$) δ 7.99 – 7.94 (m, 1H), 7.58 –

7.52 (m, 3H), 7.46 (t, $J = 7.6$ Hz, 4H), 7.32 (t, $J = 7.9$ Hz, 2H), 7.12 (ddd, $J = 17.3$, 16.2, 9.9 Hz, 4H), 5.54 (dd, $J = 13.3$, 2.7 Hz, 1H), 3.80 (d, $J = 8.2$ Hz, 2H), 3.11 (dd, $J = 16.8$, 13.3 Hz, 1H), 2.94 (dd, $J = 16.8$, 2.9 Hz, 1H). ^{13}C NMR (151 MHz, $CDCl_3$) δ 191.83, 168.64, 161.45, 138.21, 137.52, 136.33, 135.06, 130.01, 129.02, 127.11, 127.00, 124.61, 121.78, 120.93, 119.89, 118.14, 79.22, 44.63, 44.51. HRMS: (ESI) calcd for $C_{23}H_{21}NO_4$ $[M + H]^+$ 376.1549; found, 376.1553.

3.7.19. 4-(3-(2-Hydroxyphenyl)-3-oxopropyl)phenyl)-N-(naphthalen-1-yl)acetamide (HPE-33).

A mixture of **HPE-32** (5.4 mg, 0.015 mmol, 1 equiv) was dissolved in MeOH (1 mL) and Pd/C (10 wt%) was stirred under hydrogen at 3 atm for 4 h. After disappearance of starting material (TLC), the reaction mixture was filtered through a pad of celite, concentrated in *vacuo*, and the residue was purified by column chromatography on silica gel in dichloromethane to give **HPE-33** as a white powder (4.5 mg, 85%); mp 186–187 °C. ^{1}H NMR (600 MHz, $CDCl_3$) δ 12.30 (s, 1H), 7.78 (dd, $J = 8.0$, 1.5 Hz, 1H), 7.49 (ddd, $J = 8.6$, 7.3, 1.6 Hz, 1H), 7.43 (d, $J = 7.7$ Hz, 2H), 7.34 – 7.29 (m, 6H), 7.11 (t, $J = 7.4$ Hz, 1H), 7.05 (s, 1H), 7.01 (dd, $J = 8.4$, 0.9 Hz, 1H), 6.91 (ddd, $J = 8.2$, 7.3, 1.1 Hz, 1H), 3.74 (s, 2H), 3.38 (t, $J = 7.6$ Hz, 2H), 3.12 (t, $J = 7.6$ Hz, 2H). ^{13}C NMR (151 MHz, $CDCl_3$) δ 205.18, 169.06, 162.47, 140.29, 137.57, 136.46, 132.36, 129.80, 129.35, 128.97, 124.50, 119.81, 119.26, 118.99, 118.63, 44.49, 39.82, 29.58. HRMS: (ESI) calcd for $C_{23}H_{21}NO_3$ $[M + H]^+$ 382.1419; found, 382.1422.

3.7.20. (E)-N-(4-(Dimethylamino)phenyl)-2-(4-(3-(2-hydroxyphenyl)-3-oxoprop-1-en-1-yl)phenyl)acetamide (HPE-35).

To a stirred solution of (*E*)-2-(4-(3-(2-Hydroxyphenyl)-3-oxoprop-1-en-1-yl)phenyl)acetic acid **17a** (36 mg, 0.13 mmol, 1 equiv) in dichloromethane (2 mL) were added 1-ethyl-3-(3-dimethylaminopropyl)carbodiimide (51 mg, 0.26 mmole, 2 equiv), DMAP (3 mg, 0.026 mmol, 0.2 equiv), and N_1,N_1-dimethylbenzene-1,4-diamine **19b** (35 mg, 0.26 mmole, 2 equiv). The reaction mixture was stirred at room temperature overnight. Water (3 mL) was added, the organic layer was separated, and the water layer was extracted with dichloromethane (3 × 5 mL). The combined organic extract was washed with brine and dried over anhydrous sodium sulfate, and the solvent was evaporated under reduced pressure. The residue was purified by column chromatography on silica gel in ethyl acetate/ dichloromethane (0.5–10%) to give **HPE-35** as a yellow powder (38 mg, 74%); mp 217–219 °C. ^{1}H NMR (600 MHz, $CDCl_3$) δ 7.94 – 7.87 (m, 2H), 7.70 – 7.61 (m, 3H), 7.49 (t, $J = 7.2$ Hz, 1H), 7.41 (d, $J = 8.0$ Hz, 2H), 7.26 (d, $J = 4.7$ Hz, 1H), 7.02 (d, $J = 8.3$ Hz, 1H), 6.95 (dd, $J = 13.3$, 5.3 Hz, 2H), 6.65 (t, $J = 10.7$ Hz, 2H), 3.73 (s, 2H), 2.88 (s, 6H). ^{13}C NMR (151 MHz, $CDCl_3$) δ 193.65, 168.05, 163.62, 148.25, 144.77, 137.85, 136.51, 133.84, 130.22, 129.67, 129.32, 127.14, 121.91, 120.29, 120.00, 118.92, 118.68, 112.89, 44.46, 40.86. HRMS: (ESI) calcd for $C_{25}H_{24}N_2O_3$ $[M + H]^+$ 401.1865; found, 401.1861.

3.7.21. (E)-2-(4-(3-(2-Hydroxyphenyl)-3-oxoprop-1-en-1-yl)phenyl)-N-(naphthalen-1-yl)acetamide (HPE-36).

To a stirred solution of (*E*)-2-(4-(3-(2-hydroxyphenyl)-3-oxoprop-1-en-1-yl)phenyl)acetic acid **17a** (36 mg, 0.13 mmol, 1 equiv) in dichloromethane (2 mL) were added 1-ethyl-3-(3-dimethylaminopropyl)carbodiimide (51 mg, 0.26 mmole, 2 equiv), DMAP (3 mg, 0.026 mmol, 0.2 equiv), and 1-naphthylamine **19c** (38 mg, 0.26 mmole, 2 equiv). The reaction mixture was stirred at room temperature overnight. Water (3 mL) was added, the organic layer was separated, and the water layer was extracted with dichloromethane (3 × 5 mL). The combined organic extract was washed with brine and dried over anhydrous sodium sulfate, and the solvent was evaporated under reduced pressure. The residue was purified by column chromatography on silica gel in ethyl acetate/ dichloromethane (0.5–2%) to give **HPE-36** as a yellow powder (37 mg, 76%); mp 253–254 °C. ^{1}H NMR (600 MHz, DMSO-d_6) δ 10.16 (s, 3H), 8.23 (d, $J = 8.0$ Hz, 3H), 8.02 (t, $J = 12.0$ Hz, 6H), 7.94 – 7.85 (m, 8H), 7.83 (d, $J = 15.5$ Hz, 3H), 7.73 (d, $J = 8.1$ Hz, 3H), 7.65 (d, $J = 7.3$ Hz, 3H), 7.58 – 7.48 (m, 13H), 7.45 (t, $J = 7.8$ Hz, 3H), 6.98 (t, $J = 8.9$ Hz, 6H), 3.87 (s, 6H). ^{13}C NMR (151 MHz, DMSO-d_6) δ 194.10, 169.82, 162.35, 145.20, 140.03, 136.83, 134.16, 133.85, 133.33, 131.35, 130.31, 129.77, 128.66, 128.16, 126.52, 126.35, 126.04, 125.82, 123.03, 122.19, 121.75, 121.21, 119.66, 118.22, 43.25. HRMS: (ESI) calcd for $C_{27}H_{21}NO_3$ $[M + H]^+$ 408.1560; found, 408.1579.

3.8. Microtubule polymerization assay

Turbidity-based tubulin polymerization assay kit (Cytoskeleton Inc. catalog #BK004P) was used. Tubulin was resuspended at 4 mg/ml concentration in ice-cold G-PEM buffer [80 mM PIPES, 2 mM $MgCl_2$, 0.5 mM EGTA, 1 mM GTP, 5% glycerol]. In triplicate 100 µL of 4 mg/ml tubulin was used for each treatment. **IPE** stock concentrations were adjusted to have exactly the same amount of DMSO in the final assay. Half area 96 well plate was warmed to 37 °C along with the compounds or DMSO. Immediately after addition of tubulin, light scattering was measured in temperature-controlled spectrophotometer at 340 nm every 30 s for 3.5 h. 1 h into the assay, the spectrophotometer was cooled down to measure depolymerization. Graph-pad Prism was used for data analysis.

3.9. Cell culture and cell viability Assays.

HCT116 colorectal carcinoma cells (ATCC # CCL-247) were maintained in McCoy's 5A medium (Thermo # 16600082) supplemented with 10% fetal bovine serum (Gemini Bio-Products # 100–106) at 37 °C with 5 % CO_2. For viability assays, cells were seeded in triplicate per experimental condition (3×10^3 cells/well) in 96-well plates and allowed to adhere overnight. The medium was then replaced with 100 µL of fresh medium containing the appropriate concentration of each compound or DMSO. Following incubation for 96 hrs, 20 µL of CellTiter 96 Aqueous One Solution (Promega # G3582) was added per well and plates were mixed then incubated for 2 hrs at 37 °C. Resulting absorbance was measured at 490 nm using a SpectraMax M5 (Molecular Devices). In some experiments cell viability was assessed using methylene blue staining: cells were plated at 25000/well or 5000/well in 24 or 96 well plates respectively and treated the next day. Three days post treatment cells were fixed and stained in methylene blue saturated in 50% ethanol for 30 min at RT. Plates were rinsed to wash off excessive dye. Retained dye was dissolved in 0.1 N HCl and absorbance was measured at 668 nm. Cell viability was expressed as a percentage of absorbance of control cells.

For Figs. 6-11, cells were cultured in a humidified 37 °C atmosphere containing 10% CO_2 in Dulbecco's Modified Eagle's medium (Mediatech, Inc.) supplemented with 10% calf serum (Atlanta Biologicals) and 1000 U/ml of both Penicillin and Streptomycin (Mediatech, Inc.). HeLaM cells were obtained from Ganes Sen (Cleveland Clinic) and HCT116 used for HDAC8 knockout were obtained from Bert Vogelstein (Johns Hopkins). HDAC8 Knock-out HCT-116 cell were generated by transferring plasmid coding for cas9 and dual gRNA against HDAC8. Plasmid expressing non-coding Safe Harbor (SH) gRNA was used as control. The plasmids were a generous gift from E. Chen's lab at University of Washington.[42] After antibiotic selection isolated clones were used for further experiments. For experiments to study tubulin dynamics, a plasmid coding for mCherry-α-tubulin courtesy of Dr. Song-Tao Liu, University of Toledo was transferred in HeLaM cells, and an appropriate antibiotic resistant clone showing enough fluorescence without any cytotoxic effect was selected for further experiments.

4. Western blot analysis of histone acetylation Levels.

HCT116 cells were seeded into T-25 flasks (2×10^6 cells) and allowed to adhere overnight. Medium was then replaced with 5 mL of fresh medium containing either experimental compounds or DMSO.

After incubation for 24 hrs, cell lysates were extracted using 1X RIPA buffer (Thermo # 89900) and resulting protein concentrations were determined using a BCA Protein Assay (Thermo # 23225). Reduced protein samples (25 μg/sample) were separated on a Bolt 4–12% Bis-Tris Gel (Thermo # NW04120BOX), transferred to a PVDF membrane (Bio-Rad # 1620177), and blocked using standard western blotting techniques. Primary antibodies used were acetyl-Histone H3 (Sigma # 06–599), acetyl-Tubulin Lys40 (Sigma # ABT241), and β-actin (Santa-Cruz # sc-8432). Fluorescent-conjugated secondary antibodies from Li-Cor Biosciences were used for detection and visualization was conducted using a fluorescent Odyssey scanning system (LiCor Biosciences). To detect acetylated SMC3, antibodies were obtained from EMD Millipore (MABE1073), and detection was carried out using horse radish peroxidase secondary antibodies (Biorad) and enhanced chemiluminescence reagents (Biorad). Images were obtained by exposure to film.

4.1. Inhibitor testing with HDAC Isoforms.

In a half-area 96-well white opaque plate (Corning), recombinant HDAC1 (1 μL; 3 ng/μL, BPS Bioscience), HDAC2 (1 μL; 1 ng/μL, BPS Bioscience), HDAC3 (1 μL; 30 ng/μL, BPS Bioscience), HDAC6 (1 μL; 35 ng/μL, BPS Bioscience), HDAC8 (1 μL; 70 ng/μL, BPS Bioscience), or buffer alone (1 μL) was added to HDAC-Glo™ buffer (43 μL, Promega). Serial dilutions or single concentrations of inhibitors (1 μL in DMSO, concentrations described in supplement) or DMSO alone (1 μL) were added to the enzyme solution, followed by 3 hr. incubation at room temperature. The HDAC-Glo™ reagent (5 μL), prepared per manufacturer recommendations, was added to each reaction. Luminescent signal was measured every 3 min over the course of 30 min using an M−Plex Infinite 200 Pro (Tecan). To determine IC_{50}, the luminescent signal at peak reading was first background corrected with the signal from a background control reaction where HDAC was excluded. The background corrected luminescence signal of each inhibitor-containing reaction was divided by the signal of the reaction without inhibitor for each HDAC enzyme to generate a percent deacetylase activity remaining value. IC_{50} values were calculated by fitting the percent deacetylase activity remaining as a function of inhibitor concentration to a sigmoidal dose–response curve ($y = 100/(1+(x/IC_{50})^z)$, where y = percent deacetylase activity and × = inhibitor concentration) using non-linear regression with KaleidaGraph 4.1.3 software.

4.2. Chromosome drops to determine mitotic Index.

HeLaM cells were synchronized in S-phase by a single thymidine block (2 mM thymidine treatment overnight). Then they were washed with PBS and released into **IPE**s or Paclitaxel for about 9 hrs. Then they were treated with ZM447439 for 90 min. For harvesting both attached and floating cells were collected without discarding the culture medium or PBS after wash. Cells were trypsinized and harvested in DMEM + 10 %CS and P/S, then spun down. To swell the cells, cell pellets were resuspended in 0.075 M KCl for 10 min at 37 °C and fixed with pre-chilled methanol: acetic acid (3:1 v/v). The cells were dropped onto slides and stained with DAPI (1:2000) and then rinsed three times in PBS. Following this a drop of mounting medium [1% w/v p-phenylenediamine, in 90% glycerol plus 10 mM TRIS (pH 9)] was placed on the slides and covered with coverslip. Chromosome morphology and mitotic index was determined for each sample in a blinded manner and include data from at least three experiments.

4.3. Microscopy.

For phase contrast time lapse imaging, cells were plated at ~ 70% density and were treated the next day. Cells were maintained in a sealed flask containing growth medium + drug pre-equilibrated to 10% CO2. Flasks were placed on a 37 °C heated stage on an inverted microscope. Images were captured using a × 40 microscope objective and an Olympus C740 digital camera controlled by AmScope software. Image analysis was done using ImageJ. Mitotic duration of at-least 50 cells was counted.[7] For immunofluorescence, cells were plated on sterilized coverslips. After treatments they were fixed with 2% formaldehyde in phosphate buffered saline (PBS) for 10 min, followed by permeabilization [150 mM NaCl, 10 mM Tris (pH 7.7), 0.1% Triton X-100, and 0.1% BSA] for 9 min. Fixed cells were blocked with PBS containing 0.1% BSA for 1 hr at room temperature. Cells were then stained with antibodies to α-tubulin (Sigma-Aldrich), and human anti-centromere antibodies (ACA). Antibodies were visualized by incubating samples with Alexafluor-conjugated secondary antibodies (Invitrogen). DNA was visualized by staining with Hoechst 33342. Phenotypes were counted in blinded manner. Representative images were captured on SP8 Leica Confocal microscope. For mCherry-α-tubulin time lapse imaging, cells were plated on 35 mm culture dish with glass bottom at about 70% confluence. They were treated the next day. Images were captured SP8 Leica confocal microscope right after addition of ZM447439 at the interval of 5 min. During imaging, cells were maintained in 37 °C humidified chamber and in Ham's F-12 medium with additional 20 mM HEPES (pH 7.4) and 10% calf serum.

4.4. Flow Cytometry.

Five hundred thousand HeLaM cells were plated on 7 cm dishes and treated with the compounds the next day. After 24 h, 48 h, or 72 h of treatment, all cells (floating and attached) were collected by trypsinization and centrifugation. Cells were then fixed by pre-chilled 70% ethanol (final concentration). Fixed cells were collected by centrifugation and resuspended in PBS. Then they were treated with RNase H (10μg/ml) for 30 min at 37 °C. Cells were again collected by centrifugation and resuspended in PBS + 2% FBS + propidium iodide. Cells were analyzed using BD LSR Fortessa FACScanner and FloJo software. Twenty thousand cells were analyzed for each treatment.

4.5. Molecular Docking.

In order to further validate this observation, we carried out molecular docking studies using the crystal structure of tubulin in complex with inhibitor D64131 (pdb ID: 6k9v) as receptor configuration. This structure contained two α-tubulin and two β-tubulin molecules with Guanosine triphosphate (GTP) bound to α-tubulin and Guanosine diphosphate (GDP) and 2-(*N*-morpholino)-ethenesulfonic acid (MES) bound to β-tubulin in addition to D64131 bound at the colchicine binding site of β-tubulin. All ligand binding sites of β-tubulin were tested for **IPE-7** binding and the sites were prepared for docking using the Make_Receptor module (Release 3.5.0.4) of the OpenEye software package (OpenEye Scientific Software, Inc., Santa Fe, NM, U.S.A.) with the help of bound ligand in defining the binding cavity while docking studies were carried out using either the Hybrid or Fred module (Release 3.5.0.4). Additional sites (Site X and Site Y in Fig. 12) were defined by searching potential ligand binding sites on β-tubulin with the help of the Make_Receptor module. All possible conformations of **IPE-7** were constructed with Omega2 module (Release 4.0.0.4) and the scorings were done using the default ChemGauss4 scoring function used by the Hybrid/Fred modules. This scoring function is based on the shape of the ligand, hydrogen bonding between ligand and receptor, hydrogen bonding interactions with implicit solvent, and metal-chelator interactions.

In addition, multiple other X-ray crystal structures with the colchicine binding site of β-tubulin occupied by various inhibitors were subjected to the docking study for further evaluation of the binding of **IPE-7** to this side and for the comparison of **IPE-7** binding scores with those co-crystallized ligands of β-tubulin. Additionally, the taxol-bound β-tubulin (pdb ID:6wvr) was used to evaluate the possibility of **IPE-7** binding at the taxol binding site

Declaration of Competing Interest

The authors declare that they have no known competing financial interests or personal relationships that could have appeared to influence the work reported in this paper.

Acknowledgements

This research is supported by NIH grants R15CA213185 to L.M.V.T, grant R15GM120712 to W.R.T, grants GM131821 and GM121061 to MKHP and grant Z01 ES043010 of the intramural research program of the National Institute of Environmental Health Sciences to L.P. The authors thank the Developmental Therapeutics Program of the National Cancer Institute, Bethesda, MD, USA for performing cytotoxicity studies in the human tumor cell lines screes and Gloria Basil for help with time-lapse imaging.

Appendix A. Supplementary data

Supplementary data to this article can be found online at https://doi.org/10.1016/j.bioorg.2021.105297.

References.

[1] (Accessed Feb 16 (2021) (n.d.). https://www.cancer.gov.
[2] D. Mahalingam, A. Mita, M.M. Mita, S.T. Nawrocki, F.J. Giles, Targeted therapy for advanced non-small cell lung cancers: historical perspective, current practices, and future development, Curr Probl Cancer. 33 (2) (2009) 73–111, https://doi.org/10.1016/j.currproblcancer.2009.03.001.
[3] M. Röcken, Early Tumor Dissemination, But Late Metastasis: Insights Into Tumor Dormancy, J. Clin. Invest. 120 (6) (2010) 1800–1803, https://doi.org/10.1172/JCI43424.
[4] I. Arnal, R.H. Wade, How Does Taxol Stabilize Microtubules? Curr. Biol. 5 (8) (1995) 900–908, https://doi.org/10.1016/S0960-9822(95)00180-1.
[5] D.R. Matson, P.T. Stukenberg, Cdt1 Throws Kinetochore-Microtubule Attachments for a Loop, Nat. Cell Biol. 14 (6) (2012) 561–563, https://doi.org/10.1038/ncb2513.
[6] C.H. Topham, S.S. Taylor, Mitosis and Apoptosis: How is The Balance Set? Curr. Opin. Cell Biol. 25 (6) (2013) 780–785, https://doi.org/10.1016/j.ceb.2013.07.003.
[7] M.E. Bekier, R. Fischbach, J. Lee, W.R. Taylor, Length of Mitotic Arrest Induced by Microtubule-Stabilizing Drugs Determines Cell Death After Mitotic Exit, Mol. Cancer Ther. 8 (6) (2009) 1646–1654, https://doi.org/10.1158/1535-7163.MCT-08-1084.
[8] A.P. Joglekar, A cell biological perspective on past, present and future investigations of the spindle assembly checkpoint, Biology (Basel). 5 (2016) 1–19, https://doi.org/10.3390/biology5040044.
[9] E.A. Foley, T.M. Kapoor, Microtubule Attachment and Spindle Assembly Checkpoint Signalling at The Kinetochore, Nat. Rev. Mol. Cell Biol. 14 (1) (2013) 25–37, https://doi.org/10.1038/nrm3494.
[10] J. Almaliti, A.A. Al-Hamashi, A.T. Negmeldin, C.L. Hanigan, L. Perera, M. Kay, H. Pflum, R.A. ⊥ Casero, L.M. Viranga Tillekeratne, Largazole Analogues Embodying Radical Changes in the Depsipeptide Ring: Development of a More Selective and Highly Potent Analogue, (n.d.).
[11] W.K. Kelly, O.A. O'Connor, L.M. Krug, J.H. Chiao, M. Heaney, T. Curley, B. MacGregore-Cortelli, W. Tong, J.P. Secrist, L. Schwartz, S. Richardson, E. Chu, S. Olgac, P.A. Marks, H. Scher, V.M. Richon, Phase I Study of an Oral Histone Deacetylase Inhibitor, Suberoylanilide Hydroxamic Acid, in Patients With Advanced Cancer, J. Clin. Oncol. 23 (17) (2005) 3923–3931, https://doi.org/10.1200/JCO.2005.14.167.
[12] K.M. VanderMolen, W. McCulloch, C.J. Pearce, N.H. Oberlies, Romidepsin (Istodax, NSC 630176, FR901228, FK228, depsipeptide): a natural product recently approved for cutaneous T-cell lymphoma, J. Antibiot. (Tokyo) 64 (8) (2011) 525–531, https://doi.org/10.1038/ja.2011.35.
[13] P. Campbell, C.M. Thomas, Belinostat for the treatment of relapsed or refractory peripheral T-cell lymphoma, J. Oncol. Pharm. Pract. 23 (2) (2017) 143–147, https://doi.org/10.1177/1078155216634178.
[14] K.P. Garnock-Jones, Panobinostat: First Global Approval, Drugs. 75 (6) (2015) 695–704, https://doi.org/10.1007/s40265-015-0388-8.
[15] B.E. Gryder, Q.H. Sodji, A.K. Oyelere, Targeted cancer therapy: giving histone deacetylase inhibitors all they need to succeed, Futur. Med Chem. 4 (4) (2012) 505–524, https://doi.org/10.4155/fmc.12.3.
[16] A. Saito, T. Yamashita, Y. Mariko, Y. Nosaka, K. Tsuchiya, T. Ando, T. Suzuki, T. Tsuruo, O. Nakanishi, A synthetic inhibitor of histone deacetylase, MS-27-275, with marked in vivo antitumor activity against human tumors, Proc. Natl. Acad. Sci. U. S. A. 96 (8) (1999) 4592–4597, https://doi.org/10.1073/pnas.96.8.4592.
[17] Z.-Q. Ning, Z.-B. Li, M.J. Newman, S. Shan, X.-H. Wang, D.-S. Pan, J. Zhang, M. Dong, X. Du, X.-P. Lu, Chidamide (CS055/HBI-8000): a new histone deacetylase inhibitor of the benzamide class with antitumor activity and the ability to enhance immune cell-mediated tumor cell cytotoxicity, Cancer Chemother Pharmacol. 69 (4) (2012) 901–909, https://doi.org/10.1007/s00280-011-1766-x.
[18] A. Vasudevan, Z. Ji, R.R. Frey, C.K. Wada, D. Steinman, H.R. Heyman, Y. Guo, M. L. Curtin, J. Guo, J. Li, L. Pease, K.B. Glaser, P.A. Marcotte, J.J. Bouska, S. K. Davidsen, M.R. Michaelides, Heterocyclic ketones as inhibitors of histone deacetylase, Bioorganic Med. Chem. Lett. 13 (22) (2003) 3909–3913, https://doi.org/10.1016/j.bmcl.2003.09.007.
[19] C. Zhuang, W. Zhang, C. Sheng, W. Zhang, C. Xing, Z. Miao, Chalcone: A Privileged Structure in Medicinal Chemistry, Chem. Rev. 117 (12) (2017) 7762–7810, https://doi.org/10.1021/acs.chemrev.7b00020.
[20] M.L. Edwards, D.M. Stemerick, P.S. Sunkara, Chalcones: A New Class of Antimitotic Agents, J. Med. Chem. 33 (7) (1990) 1948–1954, https://doi.org/10.1021/jm00169a021.
[21] S. Ducki, R. Forrest, J.A. Hadfield, A. Kendall, N.J. Lawrence, A.T. McGown, D. Rennison, Potent antimitotic and cell growth inhibitory properties of substituted chalcones, Bioorganic Med. Chem. Lett. 8 (9) (1998) 1051–1056, https://doi.org/10.1016/S0960-894X(98)00162-0.
[22] N.J. Lawrence, R.P. Patterson, L.-L. Ooi, D. Cook, S. Ducki, Effects of α-substitutions on structure and biological activity of anticancer chalcones, Bioorganic Med. Chem. Lett. 16 (22) (2006) 5844–5848, https://doi.org/10.1016/j.bmcl.2006.08.065.
[23] N. Duchemin, E. Benedetti, L. Bethge, S. Vonhoff, S. Klussmann, J.-J. Vasseur, J. Cossy, M. Smietana, S. Arseniyadis, Expanding Biohybrid--Mediated Asymmetric Catalysis into the Realm of RNA, Chem. Commun. 52 (55) (2016) 8604–8607.
[24] A. Chakrabarti, I. Oehme, O. Witt, G. Oliveira, W. Sippl, C. Romier, R.J. Pierce, M. Jung, HDAC8: A multifaceted target for therapeutic interventions, Trends Pharmacol. Sci. 36 (7) (2015) 481–492, https://doi.org/10.1016/j.tips.2015.04.013.
[25] M.A. Deardorff, M. Bando, R. Nakato, E. Watrin, T. Itoh, M. Minamino, K. Saitoh, M. Komata, Y. Katou, D. Clark, K.E. Cole, E. De Baere, C. Decroos, N. Di Donato, S. Ernst, L.J. Francey, Y. Gyftodimou, K. Hirashima, M. Hullings, Y. Ishikawa, C. Jaulin, M. Kaur, T. Kiyono, P.M. Lombardi, L. Magnaghi-Jaulin, G.R. Mortier, N. Nozaki, M.B. Petersen, H. Seimiya, V.M. Siu, Y. Suzuki, K. Takagaki, J.J. Wilde, P.J. Willems, C. Prigent, G. Gillessen-Kaesbach, D.W. Christianson, F.J. Kaiser, L. G. Jackson, T. Hirota, I.D. Krantz, K. Shirahige, HDAC8 Mutations in Cornelia de Lange Syndrome Affect The Cohesin Acetylation Cycle, Nature. 489 (7415) (2012) 313–317, https://doi.org/10.1038/nature11316.
[26] R.H. Shoemaker, The NCI60 human tumour cell line anticancer drug screen, Nat Rev Cancer. 6 (10) (2006) 813–823, https://doi.org/10.1038/nrc1951.
[27] F.E. Stevens, H. Beamish, R. Warrener, B. Gabrielli, Histone deacetylase inhibitors induce mitotic slippage, Oncogene. 27 (10) (2008) 1345–1354, https://doi.org/10.1038/sj.onc.1210779.
[28] H.-J. Shin, K.-H. Baek, A.-H. Jeon, S.-J. Kim, K.-L. Jang, Y.-C. Sung, C.-M. Kim, C.-W. Lee, Inhibition of histone deacetylase activity increases chromosomal instability by the aberrant regulation of mitotic checkpoint activation, Oncogene. 22 (25) (2003) 3853–3858, https://doi.org/10.1038/sj.onc.1206502.
[29] L. Magnaghi-Jaulin, G. Eot-Houllier, G. Fulcrand, C. Jaulin, Histone Deacetylase Inhibitors Induce Premature Sister Chromatid Separation and Override the Mitotic Spindle Assembly Checkpoint, Cancer Res. 67 (13) (2007) 6360–6367, https://doi.org/10.1158/0008-5472.CAN-06-3012.
[30] M. Cornago, C. Garcia-Alberich, N. Blasco-Angulo, N. Vall-llaura, M. Nager, J. Herreros, J.X. Comella, D. Sanchis, M. Llovera, Histone deacetylase inhibitors promote glioma cell death by G2 checkpoint abrogation leading to mitotic catastrophe, Cell Death Dis. 5 (10) (2014) e1435, https://doi.org/10.1038/cddis.2014.412.
[31] A.T. Saurin, M.S. van der Waal, R.H. Medema, S.M.A. Lens, G.J.P.L. Kops, Aurora B potentiates Mps1 activation to ensure rapid checkpoint establishment at the onset of mitosis, Nat. Commun. 2 (1) (2011), https://doi.org/10.1038/ncomms1319.
[32] P.D. Andrews, Y. Ovechkina, N. Morrice, M. Wagenbach, K. Duncan, L. Wordeman, J.R. Swedlow, Aurora B Regulates MCAK at the Mitotic Centromere, Dev. Cell. 6 (2) (2004) 253–268.
[33] L.U. Cassimeris, P. Wadsworth, E.D. Salmon, Dynamics of microtubule depolymerization in monocytes, J. Cell Biol. 102 (1986) 2023–2032, https://doi.org/10.1083/jcb.102.6.2023.
[34] P.B. Schiff, S.B. Horwitz, Taxol Stabilizes Microtubules in Mouse Fibroblast Cells, Proc. Natl. Acad. Sci. U. S. A. 77 (3) (1980) 1561–1565.
[35] R.B.G. Ravelli, B. Gigant, P.A. Curmi, I. Jourdain, S. Lachkar, A. Sobel, M. Knossow, Insight Into Tubulin Regulation From A Complex With Colchicine and A Stathmin-Like Domain, Nature. 428 (6979) (2004) 198–202, https://doi.org/10.1038/nature02393.
[36] Y. Lu, J. Chen, M. Xiao, W. Li, D.D. Miller, An Overview of Tubulin Inhibitors That Interact With The Colchicine Binding Site, Pharm. Res. 29 (11) (2012) 2943–2971, https://doi.org/10.1007/s11095-012-0828-z.
[37] A. Fedoriw, S.R. Rajapurkar, S. O'Brien, S.V. Gerhart, L.H. Mitchell, N.D. Adams, N. Rioux, T. Lingaraj, S.A. Ribich, M.B. Pappalardi, N. Shah, J. Laraio, Y. Liu, M. Butticello, C.L. Carpenter, C. Creasy, S. Korenchuk, M.T. McCabe, C.F. McHugh, R. Nagarajan, C. Wagner, F. Zappacosta, R. Annan, N.O. Concha, R.A. Thomas, T. K. Hart, J.J. Smith, R.A. Copeland, M.P. Moyer, J. Campbell, K. Stickland, J. Mills, S. Jacques-O'Hagan, C. Allain, D. Johnston, A. Raimondi, M. Porter Scott, N. Waters, K. Swinger, A. Boriack-Sjodin, T. Riera, G. Shapiro, R. Chesworth, R. K. Prinjha, R.G. Kruger, O. Barbash, H.P. Mohammad, Anti-tumor Activity of the Type I PRMT Inhibitor, GSK3368715, Synergizes with PRMT5 Inhibition through MTAP Loss, Cancer Cell. 36 (1) (2019) 100–114.e25, https://doi.org/10.1016/j.ccell.2019.05.014.
[38] M.J. Lai, R. Ojha, M.H. Lin, Y.M. Liu, H.Y. Lee, T.E. Lin, K.C. Hsu, C.Y. Chang, M. C. Chen, K. Nepali, J.Y. Chang, J.P. Liou, 1-Arylsulfonyl indoline-benzamides as a

new antitubulin agents, with inhibition of histone deacetylase, Eur. J. Med. Chem. 162 (2019) 612–630, https://doi.org/10.1016/j.ejmech.2018.10.066.

[39] X. Peng, J. Chen, L. Li, Z. Sun, J. Liu, Y. Ren, J. Huang, J. Chen, Efficient Synthesis and Bioevaluation of Novel Dual Tubulin/Histone Deacetylase 3 Inhibitors as Potential Anticancer Agents, J. Med. Chem. 64 (12) (2021) 8447–8473, https://doi.org/10.1021/acs.jmedchem.1c0041310.1021/acs.jmedchem.1c00413.s00110.1021/acs.jmedchem.1c00413.s00210.1021/acs.jmedchem.1c00413.s00310.1021/acs.jmedchem.1c00413.s004.

[40] Y.W. Wu, K.C. Hsu, H.Y. Lee, T.C. Huang, T.E. Lin, Y.L. Chen, T.Y. Sung, J.P. Liou, W.W. Hwang-Verslues, S.L. Pan, W.C. HuangFu, A novel dual HDAC6 and tubulin inhibitor, MPT0B451, displays anti-tumor ability in human cancer cells in vitro and in vivo, Front. Pharmacol. 9 (2018) 1–16, https://doi.org/10.3389/fphar.2018.00205.

[41] L. Zhang, J. Zhang, Q. Jiang, L.i. Zhang, W. Song, Zinc binding groups for histone deacetylase inhibitors, J. Enzyme Inhib. Med. Chem. 33 (1) (2018) 714–721, https://doi.org/10.1080/14756366.2017.1417274.

[42] M.P. Phelps, J.N. Bailey, T. Vleeshouwer-Neumann, E.Y. Chen, CRISPR screen identifies the NCOR / HDAC3 complex as a major suppressor of differentiation in rhabdomyosarcoma, PNAS. 113 (52) (2016) 15090–15095, https://doi.org/10.1073/pnas.1610270114.